September 2019

Sequence-Defined Ionic Peptoid Block Copolymers: Synthesis and Solution Self-Assembly

Garrett Leigh Sternhagen
Louisiana State University and Agricultural and Mechanical College

SEQUENCE-DEFINED IONIC PEPTOID BLOCK COPOLYMERS: SYNTHESIS AND SOLUTION SELF-ASSEMBLY

A Dissertation

Submitted to the Graduate Faculty of the
Louisiana State University and
Agricultural and Mechanical College
in partial fulfillment of the
requirements for the degree of
Doctor of Philosophy

in

The Department of Chemistry

by
Garrett L Sternhagen
B.S., University of Wisconsin – Stevens Point, 2012
December 2019

ACKNOWLEDGMENTS

I gratefully acknowledge my family and friends. Without their support, I could not have completed my Ph.D.

I would like to thank Rafael Cueto, Doug Greer, Sunting Xuan, Ron Zuckermann and Jing Sun and for helpful conversations and instruction, as well as Ted Gauthier and Dong Liu. This work is supported by the U.S. Department of Energy (DOE) under EPSCoR Grant No. DE-SC0012432 with additional support from the Louisiana Board of Regents, and by NSF (1609447). Work at the Molecular Foundry was supported by the Office of Science, Office of Basic Energy Sciences, of the U.S. Department of Energy under Contract No. DE-AC02-05CH11231. This research used resources at the High Flux Isotope Reactor and Spallation Neutron Source, a DOE Office of Science User Facility operated by the Oak Ridge National Laboratory.

TABLE OF CONTENTS

LIST OF ACRONYMS

BCP – Block Copolymer

CMC – Critical Micelle Concentration

DCM – Dichloromethane

DIC – *N*,*N*-diisopropylcarbodiimide

DLS – Dynamic Light Scattering

DMF – *N*,*N*-dimethylformamide

DP – Number Average Degree of Polymerization

DRI – Differential Refractive Index

FTIR – Fourier Transform Infrared Spectroscopy

GPC – Gel Permeation Chromatography

HPLC – High Performance Liquid Chromatography

MALDI-TOF MS – Matrix Assisted Laser Desorption – Time of Flight Mass Spectroscopy

MALS – Multi-Angle Light Scattering

MEM – Maximum Entropy Method

MWCO – Molecular Weight Cutoff

NAM – Normal Amine Mechanism

Nce – *N*-2-carboxyethyl

Ndc – *N*-decyl

Nme – *N*-2-methoxyethyl

NMR – Nuclear Magnetic Resonance

PDI – Polydispersity Index

SANS – Small-Angle Neutron Scattering

SAS – Small-Angle Scattering

SAXS – Small-Angle X-ray Scattering

SPSS – Solid-phase Submonomer Synthesis

R-NCA – *N*-substituted glycine derived *N*-carboxyanhydride

ROP – Ring-Opening Polymerization

TEM – Transmission Electron Microscopy

TFA – Trifluoroacetic acid

THF – Tetrahydrofuran

ABSTRACT

This work covers efforts to develop a peptoid-based model system for systematically studying the role of ionic functional groups in determining the structure of ionic block copolymer (BCP) self-assemblies in water. A key challenge in the study of polyelectrolytes is the lack of synthetic control over the location of ionic monomers along a polymer chain. We developed a model system based on sequence-defined ionic peptoid BCPs having discrete chain length and precisely positioned ionic monomers along the chain to specifically address this issue. In Chapter 1, synthetic strategies to access well-defined polypeptoids and their application in BCP synthesis are reviewed.

Chapter 2 covers the design of a library of sequence-defined ionic peptoid BCPs and the characterization of their self-assembly in aqueous media. The library of materials with discrete chain length and precisely positioned ionic monomers (one or three) along the peptoid chain were obtained by SPPS. By systematically varying the location of ionic monomers along the peptoid BCP chains, the effect of ionic group location on self-assembled micelles can be studied.

In chapter 3, the response of self-assemblies of sequence-defined peptoid BCPs having discrete chain length to varying pH is studied. The weakly acidic nature of the carboxylic acid group used in the design of the library of sequence-defined ionic peptoid BCPs gives rise to stimuli-responsive behavior as the solution pH is varied.

Chapter 4 covers the synthesis of an R-NCA monomer bearing *N*-2-carboxyethyl that mimics the ionic sidechain used in the above sequence-defined ionic peptoid BCPs. The availability of this new NCA monomer allows the sequence-defined ionic peptoid BCPs to be accessed by polymerization methods.

CHAPTER 1. INTRODUCTION TO POLYPEPTOIDS

1.1. Background and Significance

Invented in the late 1980's by Zuckermann and coworkers at Chiron Corp.,[1] peptoids continue to gain popularity due to their many attractive chemical and physical properties. Similar to polypeptides, polypeptoids exhibit a polyglycine backbone with sidechains on each repeat-unit, defining the polymer primary structure. In contrast to peptides, which feature their sidechains attached to the α-carbon, the peptoid sidechain is attached to the nitrogen atom (Figure 1.1), which leads to the difference in properties observed between peptides and peptoids. This simple physical distinction confers important physical and

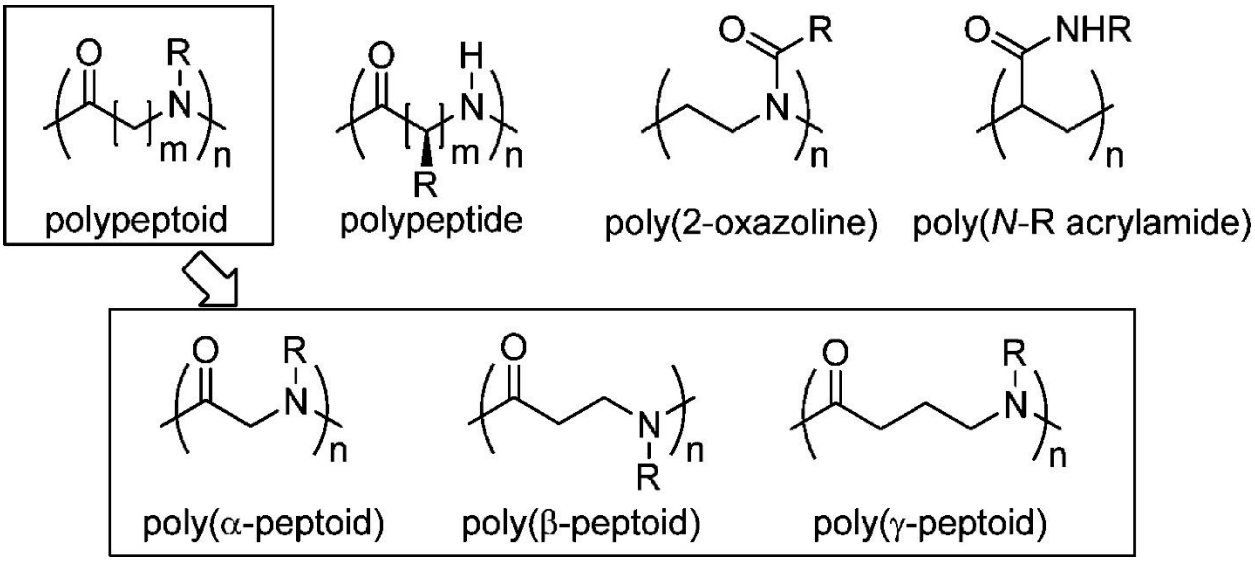

Figure 1.1. Common biopolymer chemical structures. Reprinted with permission from reference.[2] Copyright (2012) American Chemical Society.

chemical differences in polypeptoids, relative to peptides. *N*-substitution along the peptoid backbone results in a loss of the main chain stereogenic centers and the hydrogen bond donating characteristic normally seen in peptide backbones. The lack of main chain stereogenic centers and

decreased ability to hydrogen bond effectively eliminate the formation of common secondary structures (α-helix, β-sheet) observed in polypeptides. This leads predominantly to a random coil structure in solution, although well-defined secondary structure can be induced by careful selection of sidechains.[1] The earliest example is work by Zuckermann in reintroducing helical character into the peptoid solution structure.[3] By incorporating chirality into the peptoid sidechains, in the form of a bulky *N*-methylbenzyl group, the researchers were able to observe α-helical character in the solution structure of the synthesized peptoid. Polypeptoids can exhibit a fairly wide range of both chemical and physical properties due to the growing library of sidechains reported in the literature.[1] The available chemical variety of peptoid sidechains is owed to well-established and easily adaptable synthetic routes. Modular synthetic methods to synthesize both polypeptoids by ROP of NCA monomers and sequence-defined peptoids by SPSS allow direct incorporation of C1-C14[4-6] alkyl groups, aromatic groups,[3, 5, 7] oligo(ethylene glycol) groups,[8-9] and a host of other moieties through both direct synthesis[10] and post-polymerization modification.[11-12]

1.2. Synthesis of Polypeptoids through ROP of NCAs

Polypeptoids ranging from low to high (>30,000 g/mol) molecular weight can be synthesized by the ROP of appropriate NCA monomers. In a typical preparation, *N*-substituted glycines are synthesized by either the Gibbs glyoxylic acid reductive amination method[13] or reaction of a primary amine with bromoacetate esters.[9] The Gibbs method involves imine formation from glyoxylic acid and the desired primary amine, followed by reductive amination by an additional equivalent of glyoxylic acid and hydrolysis of an *N*-formyl group under acidic conditions (Figure 1.2 A). In the second method, nucleophilic displacement of the bromide ion, from a bromoacetate ester, followed by hydrolysis of the glycine ester, under either acidic or basic

conditions, yields the desired *N*-substituted glycine (Figure 1.2 B). The secondary amine group of the *N*-substituted glycine is then further functionalized towards the final, desired R-NCA.

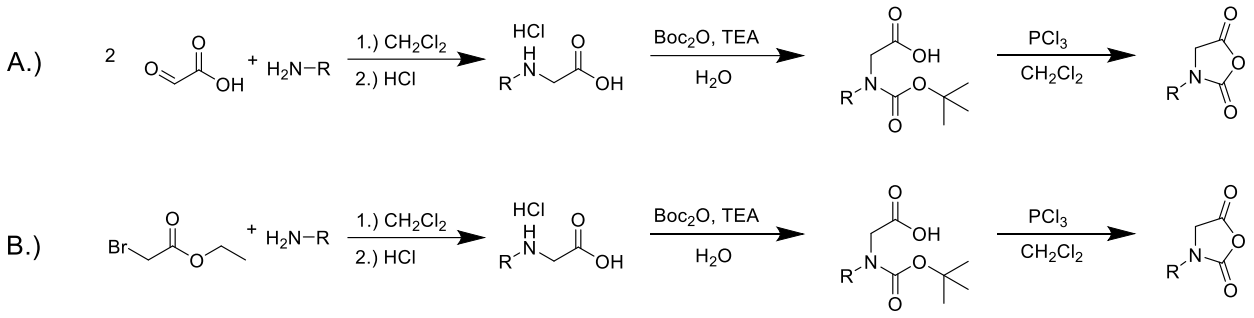

Figure 1.2. Synthesis of *N*-substituted glycine derived *N*-carboxyanhydride monomers (R-NCA). A.) Gibbs glyoxylic acid reductive amination method. B.) Nucleophilic displacement of haloacetate.

The Leuchs method[14] was adapted to directly cyclize an *N*-substituted glycine precursor into the desired NCA using diphosgene.[15] In the Fuchs-Farthing[16] method the secondary amine is *N*-Boc, or less frequently *N*-carboxybenzyl or carboxyethyl protected, before cyclization by appropriate activation of the carboxylic acid by phosphorous trihalide, thionyl or oxalyl chloride, or acetic anhydride/acetyl chloride to yield the desired R-NCA monomer.[12] The harsh conditions used in these synthetic routes have generally limited the sidechains used in R-NCA synthesis to simple alkyl and aromatic groups (Figure 1.3).

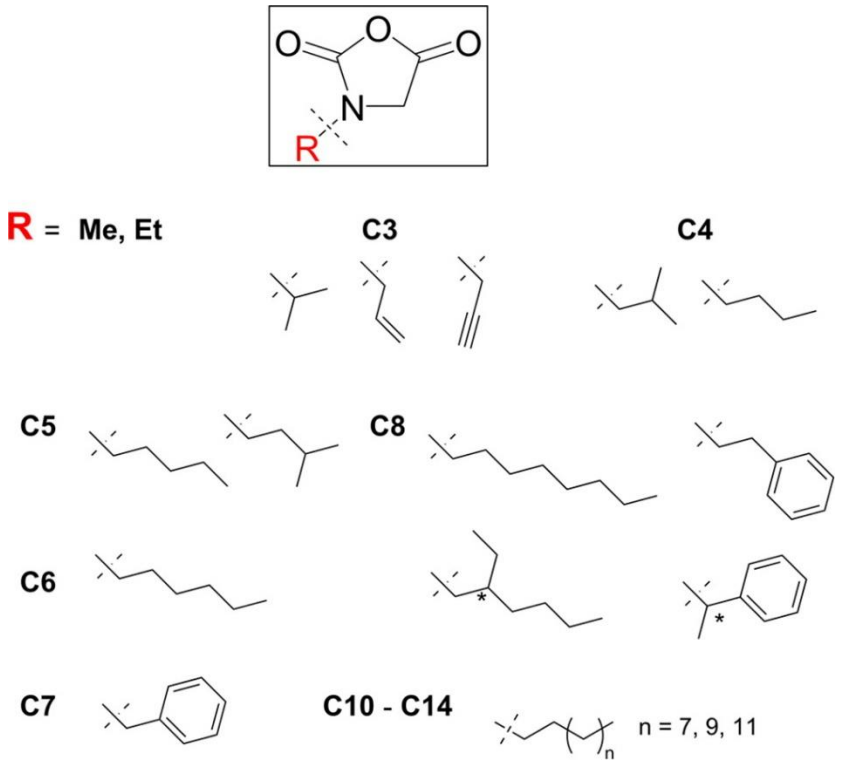

Figure 1.3. Common *N*-substituted NCA (R-NCA) used in polymerization to produce polypeptoids bearing various sidechains. Reprinted with permission from reference.[17] Copyright (2016) American Chemical Society.

Polymerization of R-NCA monomers to yield polypeptoids is most commonly effected through the normal amine mechanism (NAM). Addition of a primary or secondary amine initiator to a solution of NCA monomers results in attack of the C5 carbonyl on the R-NCA by the initiator and ring-opening of the R-NCA. Upon loss of CO2, yielding a secondary amine chain end, the growing polymer chain is free to propagate by attack of another R-NCA monomer by the propagating chain end (Figure 1.4).

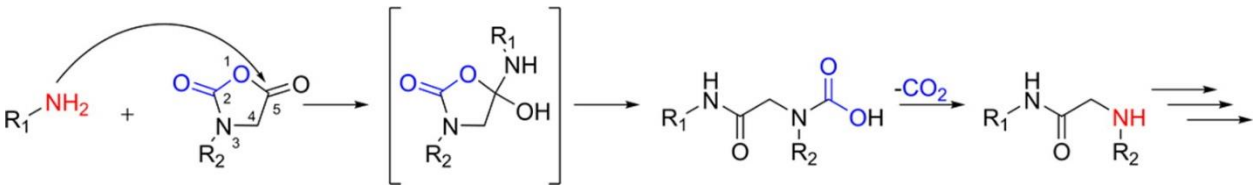

Figure 1.4. Polymerization of R-NCA by NAM. Reprinted with permission from reference.[17] Copyright (2016) American Chemical Society.

Polymerization of R-NCA monomers by the normal amine mechanism is a pseudo-living process, yielding polypeptoids with predictable molecular weight, low polydispersity, and living chain ends.[6] Several other initiator systems have been reported, including TMG/alcohol by Zhang et al.,[18] and rare earth metal borohydrides by Ling et al.[19] While these systems succeed in polymerizing R-NCAs in a well-defined and controlled manner, they lack the simplicity and versatility of a simple primary amine initiator which allows a variety of end-group structures to be introduced in a quantitative fashion.

1.3. Preparation of Polypeptoids via SPSS

Synthesis of sequence-defined peptoids is accomplished via the solid-phase submonomer synthesis method developed by Zuckermann and coworkers.[20-21] SPSS is an iterative synthetic method, involving repeated discrete reactions performed on a solid support. The original method was first popularized by Merrifield reporting the synthesis of a sequence-defined tetrapeptide utilizing Fmoc-protected amino acids.[22] This method, involving the repeated acylation of a solid support with an Fmoc-amino acid and subsequent deprotection of the Fmoc group was first adapted to the synthesis of sequence-defined peptoids by Zuckermann and coworkers utilizing the same chemistry.[20] The method was further refined into the submonomer method,[23] splitting a single monomer addition into two steps and eliminating the need for a deprotection step. In the current and most commonly used form of SPSS, alternating bromoacylation and nucleophilic displacement steps are used to build up a peptoid chain in discrete reaction steps. Starting from a functionalized polystyrene resin (commonly R-NH2), the first step involves bromoacylation of the resin by bromoacetic acid activated by DIC. The acylated resin is purified of excess reagents by solvent washes before a primary amine is added to conduct a nucleophilic displacement of the bromide, thus completing synthesis of one peptoid repeat unit in two discrete reaction steps. The

chain length is then built up by running successive bromoacylation and nucleophilic displacements from the terminal secondary amine (Figure 1.5).

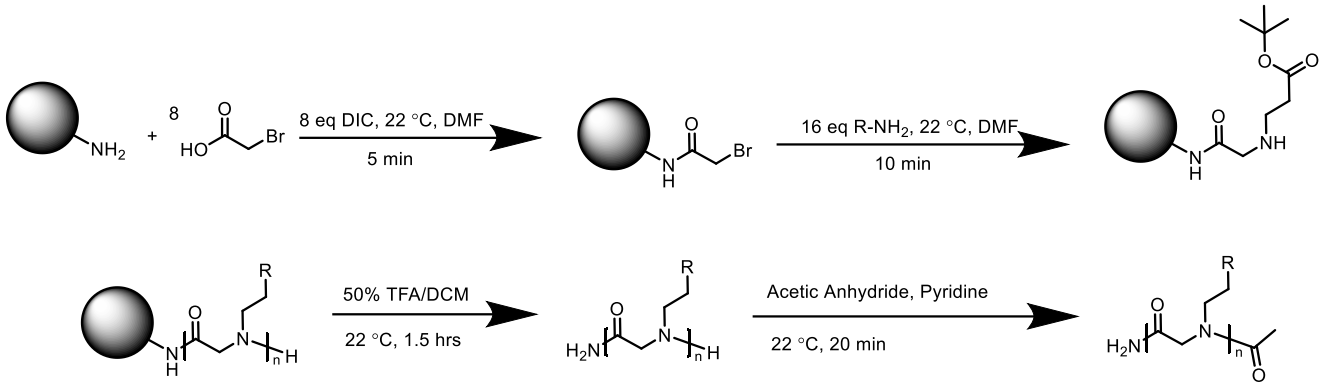

Figure 1.5. Synthesis of sequence-defined peptoids by SPSS.

Upon reaching the desired chain length the peptoids are cleaved from the solid support under mildly acidic conditions to yield the sequence-defined peptoid in solution. Although SPSS offers the major advantage of complete control over monomer sequence, this is only achieved using large excess of reagents, as well as time and solvent consuming washing steps. Purity of the final peptoid is also limited by the coupling efficiency of each step,[1] which limits the technique, in general, to chains with 50 or fewer monomers.

1.4. BCP Solution Self-Assemblies

Block copolymers have drawn seemingly endless fascination from chemists, polymer scientists, and material scientists for decades. The intrigue in this class of materials stems from the covalent attachment of two or more chemically dissimilar homopolymers in an end-to-end fashion. Covalent linking of the materials prevents a complete macroscopic phase separation, leading to microscopic phase separations and a range of morphologies (spheres in a cubic lattice, hexagonally packed cylinders, gyroid, lamellar, *etc*.) which can be tuned to specific desired properties and applications[24-25] (Figure 1.6).

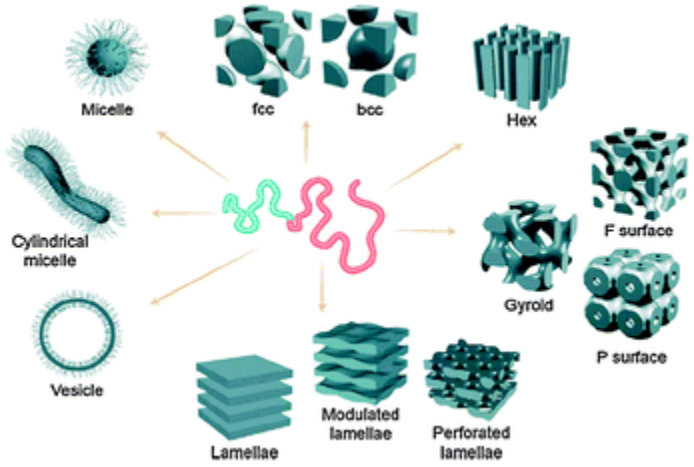

Figure 1.6. Block copolymer morphologies. Reproduced with permission from reference[26] from the Royal Society of Chemistry.

Examples of BCP in the literature are so extensive and varied "that to attempt to discuss every publication on this would be foolish."[27] This section will attempt to highlight only examples in solution deemed particularly relevant to the presently described work. For the remainder of this text, block copolymer will refer only to BCP with one solvophilic and one solvophobic block.

In dilute solution, and in a solvent which is selective for only one block, block copolymers tend to associate into self-assembled structures above a certain concentration (the critical micelle concentration, CMC). Above the CMC, assembly is driven entropically by the exclusion of solvent from the solvophobic polymer block. While the mixing of different chemical species is generally entropically preferred, in the case of an amphiphile (i.e., a BCP with a hydrophobic alkyl chain and a hydrophilic block) in water, the water molecules must align along the alkyl chain in a highly ordered fashion to solvate the alkyl chain. The entropy gained by the water molecules releasing into the bulk solution as the alkyl chain condenses into an oil phase with other alkyl chains outweighs the enthalpic penalty for demixing, thus driving assembly of the BCP in solution. This leads to condensed regions of the solvophobic block, which is connected to the extended and

solvated solvophilic block dispersed in the bulk solvent. The morphology of structures from self-assembled structures in dilute solution is controlled by the relative volume of the two polymer blocks, which can be roughly described by the packing parameter[28] (Figure 1.7).

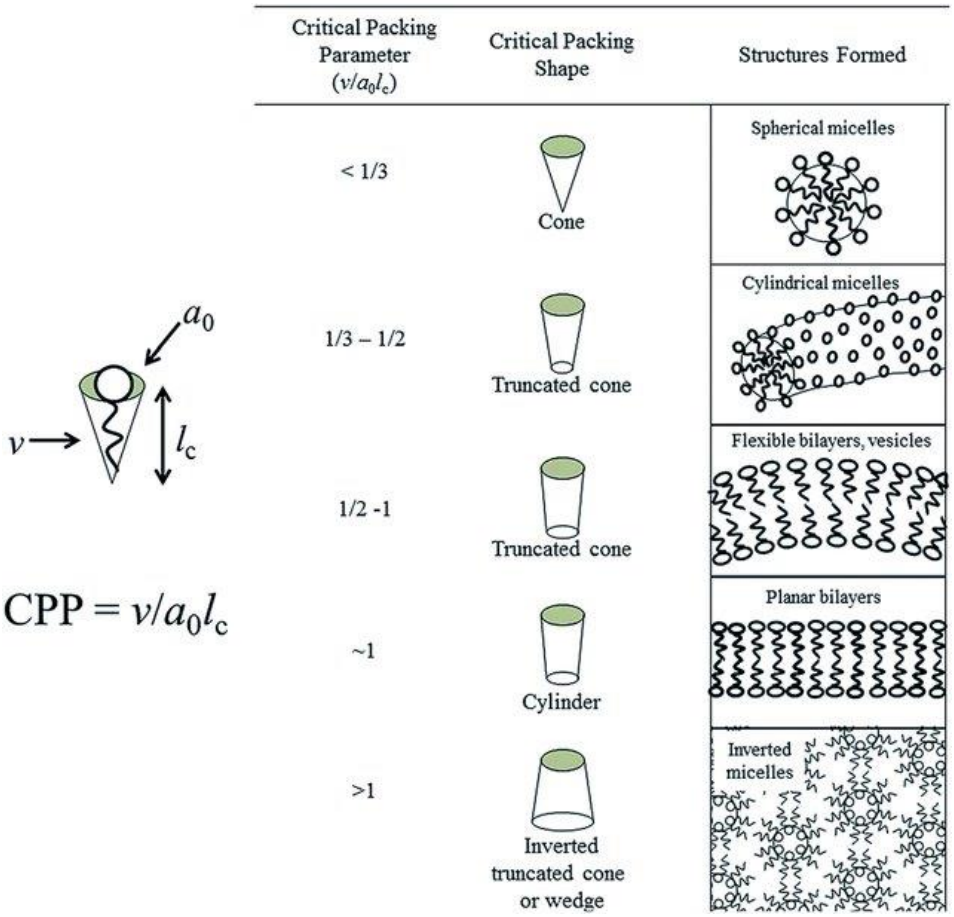

Figure 1.7. Packing Parameter Morphologies. Reproduced with permission from reference[29] from the Royal Society of Chemistry.

In cases where the volume of the solvophobic block is much less than the product of the area occupied by the solvophilic block multiplied by the length of the solvophobic block ($p < 1/3$), the resulting assembled structure will exhibit an interface with high surface curvature, e.g. a spherical interface. For intermediate values of the packing parameter ($1/3 < p < ½$), the resulting interface will be somewhat less curved, leading to worm-like, more extended structures. Packing

parameter values > ½ lead to assembled bilayer interfaces that are minimally curved, or even flat. Vesicles can result from materials with a packing parameter between ½ and 1, and flat bilayers are obtained when p ~ 1.

Spherical micelles resulting from block copolymer self-assembly have been studied extensively in the literature. Some of the oldest and most well studied systems are block copolymers comprised of two neutral blocks, such as the family of Pluronics, featuring PEO and PPO blocks,[30-31] PEO-PBO,[32] and many others.[30] These types of materials behave as surfactants, partitioning to an interface (i.e. air-water) until they reach the CMC. Upon exceeding the CMC they form self-assembled micelles in dilute solution. The size and structure of non-ionic micelles is governed exclusively by the length of each block and the quality of the chosen solvent for each block. There have been countless experimental studies, many of which have been collected in reviews[30-31], as well as proposed structural models[33-34] and theoretical predictions to explain and predict experimental results[35].

The structure of micellar self-assemblies from polyelectrolyte block copolymers depends on several parameters including the block length, charge fraction, type of charged group, and the amount of salt present in the solution. The effects of each of these parameters have been studied extensively in the literature. The size and aggregation number of polyelectrolyte BCP micelles have been predicted to scale with $R_{core} \sim N_B^{5/9} N_A^{-1/3} \alpha^{-4/9}$, $R_{corona} \sim N_B^{2/9} N_A^{2/3} \alpha^{2/9}$, and $N_{agg} \sim N_B^{2/3} N_A^{-1} \alpha^{-4/3}$ (where R_{core} is the micelle core radius, R_{corona} is the radius of the micelle corona, N_{agg} is the aggregation number of the micelle, N_B is the number of repeat units in the solvophobic block, N_A of the number of repeat units in the solvophilic block, and α is the fraction of charged monomers in the solvophilic block), respectively, which differs from BCP polymer micelles that are completely neutral. The charge fraction can be tuned either by copolymerization of a charged and

a neutral monomer,[36] or by the deprotection of a fraction of monomers which yield a charged functional group upon loss of the protecting group.[37-39] The fraction of charged monomers can be further modified by changing either the pH or the salt concentration in solution.[40-45] Changing pH or adding salt to the solution can affect the effective number of charged groups for annealed polyelectrolytes (polyelectrolytes in which the ionization depends on the environment, e.g. for weak acids, such as carboxylic acids), while quenched polyelectrolytes (polyelectrolytes in which the ionization of charged groups is insensitive to environmental conditions, e.g. strong acids such as sulfonic acids) are generally insensitive to these environmental conditions.

1.5. Peptoids as a Model System

As briefly mentioned previously, peptoids have been found to be important model compounds for detailed studies of macromolecular solution assembly. Using sequence defined peptoids of high purity, physical experiments can be conducted on discrete molecules (PDI ~ 1), rather than the collection of molecules (PDI > 1) afforded by traditional polymerization, which at best contain a well-defined block sequence smeared by polydispersity, and at worst contain a statistical distribution of monomers with ambiguous primary structure. The known primary structure of sequence-defined peptoids offers computational chemists the opportunity to describe a macromolecule in intricate detail (similar to modeling of small molecules in solution), and use coarse-graining techniques with improved accuracy, leading to more powerful models of peptoid solution behavior.[46]

The earliest examples of peptoids used as model systems for studying biomolecule solution behavior include Zuckermann's work reintroducing α-helical character into a peptoid via bulky chiral *N*-substituents proved the utility of peptoids in these structure-property or structure-function studies. Since these reports, peptoids have been used with regularity to probe various biomolecule

solution properties, and to gain insight into the biological systems from which they were inspired. Efforts have included the design of peptoids to mimic biological binding of metals, as in the zinc binding peptoids in a "two-helix bundle" to mimic the binding in the zinc finger motif,[47] and the use of short peptoids (> 7 monomers) to coordinate Co_4O_4 clusters in tetra or hexadentate orientations.[48] Peptoid systems have been developed to study assembly in solution with diblock systems of *N*-2-carboxyethyl and *N*-2-phenylethyl sidechains forming nanosheets which assemble into superhelices over time,[49] amphiphilic peptoids containing *N*-methyl and *N*-2-carboxyethyl sidechains for the study of the coil-to-globule transition in water/acetonitrile solution,[50] as well as the study of the mechanistic aspects of peptoid assembly and folding.[51-52]

Polypeptides, being more direct synthetic mimics of biological polymers, and accessible through similar synthetic methods have drawn interest as systems for studying solution self-assemblies. The Tirrell group has put significant effort into the development of sequence-defined peptide amphiphiles with an alkyl chain attached to the *N*-terminus. The hydrophobic alkyl chain allows the peptides to self-assemble in water into well-defined aggregates. The complication of using peptides in the study of more fundamental aspects of polymer solution self-assembly arises from the presence of the secondary amide group along the peptide backbone. The amide -NH- can act as a hydrogen bond donor, introducing additional chemical interactions which can complicate the understanding of experimental results. Hydrogen bonding along the peptide backbone can introduce β-sheet like interactions and twisted fibrous bundles, which can then further assemble into micelles.[53] In an aqueous solution the hydrogen bonding interaction is approximately 1.5 kcal/mol, which can quickly compete with or overwhelm other intermolecular interactions, such as dipole-dipole (1 – 6 kcal/mol), van der Waals (~1 kcal/mol), or electrostatic (~ 4 kcal/mol), particularly when multiple hydrogen bonds are present in a system.

Peptoids containing functional groups bearing ionic groups have been gaining attention recently. The unique ability of peptoids to incorporate a wide variety of chemical functionalities along a common polymer backbone make them an attractive material for simplifying the study of polyelectrolyte behavior. The addition of ionic groups into a polymeric system greatly increases the complexity of the system being studied and the difficulty in understanding that system. The strength of electrostatic interactions depends on a wide range of factors, many of which are also dependent on other environmental factors in the system. The proximity of two ionic groups in solution is affected both by the number and position of charged groups along any given polymer chain, as well as by the concentration of polymer in solution. The magnitude of the electrostatic interaction is further affected by the dielectric properties of the medium, salt content and pH of the solution, and the overall ionic strength.[43-44] A complete and accurate description of all of these properties quickly becomes a difficult task. The ability to synthesize peptoids in high purity as discrete molecules eliminates the complication of ambiguous monomer location (each monomer is placed discretely in a known sequence) and polydispersity (for highly pure sequence defined peptoids each synthesized chain is the same length, with PDI ~ 1). Polyelectrolyte systems based on peptoids have been used in several structure-property studies, including precise determination of the persistence length of sequence defined peptoids containing *N*-2-methoxyethyl and *N*-2-carboxyethyl sidechains,[54] the ability of phosphonated peptoid block copolymers to conduct protons,[55] and a recent study of the assembly of sequence-defined lipopeptoids containing both charged *N*-2-carboxyethyl and hydrophobic *N*-2-phenylethyl sidechains in the solvophilic block.[56]

In view of this work, we chose the peptoid as a platform to investigate to role of sequence-encoded charges on the solution self-assemblies of ionic peptoid BCPs.

CHAPTER 2. SELF-ASSEMBLIES OF SEQUENCE-DEFINED IONIC PEPTOID AMPHIPHILES[1]

2.1. Introduction

Ubiquitous in nature and synthetic systems, electrostatic interactions have garnered much research interest for their importance in biological systems and their usefulness in the design of stimuli-responsive polymeric materials for various applications (*e.g.*, water purification, oil recovery, drug delivery, *etc.*). Biomacromolecules (*e.g.*, DNA/RNA, proteins, polysaccharide, proteoglycans) can be highly charged and use electrostatic interactions to maintain their structures and functions.[57] In particular, proteins have precise control over the location of charged monomers along the chain, enabling the fine-tuning of the electrostatic interactions to access various sophisticated and well-defined higher order structures. The study of ionic macromolecules is complicated by the presence of many different electrostatic phenomena, relative to the charge neutral system.[58] For example, as compared to neutral macromolecules in solution, ionic macromolecules can be affected by electrostatic repulsion, osmotic swelling, counter-ion condensation, as well as external effects such as changes in solution pH or salt content that confers charge screening.[40-43, 45, 59]

Ionic block copolymer (BCP) micelles are an intriguing class of nano-colloids due to the combination of their highly tunable structure and the ability to respond to external stimuli such as change in solvent pH or ionic strength.[40-43, 45] Similar to neutral micelles the exclusion of solvent by the hydrophobic segments of the polymer in the micellar core provides the driving force for their self-assembly into micelles in solution. While the equilibrium micellar structures in dilute

This chapter was previously published as Sternhagen, G. L.; Gupta, S.; Zhang, Y.; John, V.; Schneider, G. J.; Zhang, D., Solution Self-Assemblies of Sequence-Defined Ionic Peptoid Block Copolymers. *Journal of the American Chemical Society* **2018**, *140* (11), 4100-4109. Reprinted by permission of the American Chemical Society.

solution are dependent on the degree of polymerization of the hydrophilic (N_A), hydrophobic segments (N_B), the fraction of charged monomers in the corona segment (α) and the solution salt concentration (C_s),[58,40, 60,61,62] kinetically trapped micellar assembly can lead to a diverse range of non-equilibrium morphologies.[62-63]

There have been theoretical studies on the scaling relationships for ionic BCP micelles in dilute solution.[35, 58] Under salt-free conditions, for star-like BCP micelles with sufficiently large fraction of charged monomers, the long-range Columbic repulsive interactions dominate over the short-range excluded volume interaction in the micellar corona. When the aggregation number of the micelle is small, the counter ions are mobile and distributed evenly throughout the entire micellar solution. In this so-called unscreened regime, the scaling theories predict that the power-law dependence of the micellar aggregation number (N_{agg}), the radius of the micellar core (R_{core}) and the radius of the micellar corona (R_{corona}) on N_A, N_B and α in the following relationship: $N_{agg} \sim N_B^{2/3} N_A^{-1} \alpha^{-4/3}$, $R_{core} \sim N_B^{5/9} N_A^{-1/3} \alpha^{-4/9}$and $R_{corona} \sim N_B^{2/9} N_A^{2/3} \alpha^{2/9}$. By contrast, for ionic BCP micelles with large aggregation number, the majority of the counter ions are concentrated in the micellar corona, resulting in increased osmotic pressure in the micellar corona and the stretching of the corona chains.[60] In this so-called osmotic regime, the following scaling relationships have been predicted: $N_{agg} \sim N_B^2 N_A^{-3} \alpha^{-3}$, $R_{core} \sim N_B N_A^{-1} \alpha^{-1}$and $R_{corona} \sim N_A \alpha^{1/2}$. In addition, star-like ionic BCP micelles with a small hydrophobic core can also be considered similarly as star-like ionic polymers with f number of arms and α fraction of charged monomers per arm.[64] In this model, the aggregation number of the micelle is equivalent to the number of arms (f) in the star-like polymer, whereas the degree of polymerization of the micellar corona segment is equivalent to the degree of polymerization of individual arm (N) in a star-like polymer. The theoretical study has predicted that the radius of the ionic star polymers [$R(f)$] to scale with N, α and f in the following relationship:

$R(f) \sim N\alpha^{2/3}f^{1/3}$ in the unscreened regime and $R(f) \sim N\alpha^{1/2}$ in the osmotic regime. There are currently no theoretical efforts that systematically address the effect of the location of charged monomers along the chain on the micellar structures, which is the unique and key aspect of the current study.

In conventional ionic BCP micelles, the charge fraction in the micellar corona is typically controlled by copolymerization of ionic and neutral monomers,[36] post polymerization modification to install ionic groups,[37-39] and by changing the pH or ionic strength of the solution.[40-43, 45] These approaches are limited in the control over the spatial arrangement of the ionic monomers along the chain or in the micelle. There is currently no experimental or theoretical study on whether and how charges arranged in a spatially-defined manner along the BCP chain will affect the micellar structure. This is mainly due to the lack of suitable synthetic platforms that enable the systematic tuning of the location and number of ionic monomer along the chain. While polypeptides can be obtained in a sequence-defined manner, the hydrogen bonding and hydrophobic interaction often dominate and can induce the formation of secondary structures (*e.g.*, helix or sheet),[53, 65] which introduces additional complexity towards the understanding of the electrostatic effects on the micellar structure.

Peptoid polymers featuring *N*-substituted polyglycine backbones are structural mimic of polypeptides.[2, 17] Because of *N*-substitution, peptoid polymers do not have stereogenic centers along the backbone and inter- or intramolecular hydrogen bonding relative to polypeptides. This allows various molecular interactions in the peptoid polymers to be systematically adjusted by controlling the *N*-substituent structure. The advent of the sub-monomer method has enabled access to peptoid polymers where the monomer sequence is precisely defined.[66-68] With far-reaching applications ranging from biomaterials to energy[17] to more fundamental structure-property

investigations,[5, 50, 69-73] sequence-defined peptoid polymers represent a versatile platform for the study of a variety of nanoscale self-assembly processes.[55, 73-75]

In view of the synthetic ease, structure tunability and absence of secondary structures, we reason that sequence-defined peptoid polymers represent an idea model to investigate the effect of sequence-defined charges on the ionic BCP self-assembly and structure in solution. Herein we design and synthesize a series of sequence-defined peptoid block copolymers where the number and position of ionic monomers along the polymer chain are precisely controlled. We have observed a significant effect of the position of ionic monomers on the micellar structure (*e.g.*, aggregation number and micellar size). This study underscores the potential to precisely control and tailor the ionic micellar structure via the control of monomer sequence.

2.2. Materials and Methods

2.2.1. Materials

Solvents used were HPLC grade or comparable and used as received. *N*,*N*'-Dimethylformamide (Omnisolv, HPLC grade) and Deuterium Oxide (99.9%) were purchased from EMD Millipore. *N*-methylpyrrolidone was purchased from BDH (>99.0%). All reagents were used as received. Piperidine (20% in DMF) was purchased from Protein Technologies. Bromoacetic acid (99%) and *N*-decylamine (99%) were purchased from Acros Organics. Diisopropylcarbodiimide (99.51%) and β-alanine *t*-butyl ester hydrochloride (99.25%) were purchased from ChemImpex Intl. Acetic acid (ACS grade) was purchased from Fisher Scientific. Trifluoroacetic acid (99%) was purchased from Alfa Aesar. Sodium hydroxide (ACS) was purchased from VWR.

2.2.2. Synthesis of Peptoid Block Copolymers

Peptoid block copolymers were synthesized by solid-phase submonomer synthesis (SPSS), using an adapted reported procedure,[21] on an AAPPTEc Apex 396 at the Molecular Foundry. In a general synthesis, 50 μmol Rink amide resin (0.57 meq/g) was deprotected in 20% 4-methylpiperidine in *N*,*N*'-Dimethylformamide (DMF) for 12 min. The resulting amine functionalized resin was acylated with 1 mL of 0.4 M bromoacetic acid in DMF with 1 eq of *N*,*N*'-diisopropylcarbodiimide (DIC) for 20 min. The resin was then washed 5 × 1 mL with DMF. The bromoacylated resin was then treated with 1 mL of the proper amine (either 2-methoxyethylamine, β-alanine OtBu ester, or *n*-decylamine) as a 1 M solution in *N*-methylpyrrolidone for 2 hours. The resin was again washed with 5 × 1 mL DMF. The acylation and displacement steps were repeated until the desired peptoid chain length was achieved. The peptoids polymers on the resin were then acylated with acetic acid/DIC to cap the terminal secondary amine. Crude peptoid polymers were cleaved from the resin in 95% TFA/H_2O for 20 min. The solution was evaporated under nitrogen and the peptoid polymers were dissolved in water and lyophilized to produce a white fluffy powder.

2.2.3. Matrix-assisted laser desorption ionization-time-of-flight (MALDI-TOF) mass spectrometry

MALDI-TOF MS measurements were conducted on a Bruker ultrafleXtreme tandem time-of-flight (TOF) mass spectrometer equipped with a smartbeam-II ™ 1000 Hz laser (Bruker Daltonics, Billerica, MA). The instrument was calibrated with Peptide Calibration Standard II (Bruker Daltonics, Billerica, MA). A saturated solution of α-cyano-4-hydroxycinnamic acid (CHCA) in THF was used as the matrix in all measurements. The polymer solution samples (10 mg/mL in THF:TFA) were mixed with the saturated matrix solutions at 1:1 volume ratio mixed thoroughly. The mixtures (1 μL) were deposited onto a 384-well ground-steel sample plate and

were allowed to dry in air prior to measurement using positive reflector mode. Data analysis was carried out using FlexAnalysis software and results are presented in Figure S2.1.

2.2.4. High-Performance Liquid Chromatography (HPLC)

HPLC analysis was performed with a Waters 616 pump, Waters 2707 Autosampler, and 996 Photodiode Assay Detector which are controlled by Waters Empower 2 software. The separation was performed on an Agilent Waters XSelect-HSS Cyano column (3.5 μm, 75 x 3.0 mm) by a gradient resulting from mixing eluents A (0.1% TFA in water) and B (0.1% TFA in acetonitrile). The gradient started from 50% B to 95% B in 30 min. The flow rate was 0.4 mL/min and detected wavelength was 215 nm. A representative HPLC chromatogram is presented in Figure S2.2. The purity levels of peptoids polymer samples (Table S2.1) are determined by integrating the HPLC peak corresponding to the targeted sequence versus the integration of all peaks due to the targeted sequence as well as the deletion sequences.

2.2.5. Cryo-Transmission Electron Microscopy

CryoTEM imaging was done on an FEI G2 F30 Tecnai TEM operated at 100 kV. Samples were prepared at 5 mg/mL by direct dissolution in ultrapure water, adjusted to pH=9 with NaOH. 10 μl of the sample solution was applied on a 200-mesh lacey carbon grid (Electron Microscopy Sciences) mounted on the FEI Vitrobot. The excess liquid was removed by blotting the grid by filter papers for 2.5 seconds to form a thin sample film. The film was then vitrified extremely fast by plunging into liquid ethane. The vitrified sample was finally transferred onto a single tilt cryo specimen holder for imaging. The mean micellar radii (R_m, Table S2.2) are determined by measuring n=50 particles in the CryoTEM micrographs.

2.2.6. Critical Micelle Concentration (CMC) Determination[76]

The CMC of each peptoid block copolymer sample was measured by fluorescence spectroscopy on a Perkin Elmer LS50B Luminescence spectrometer. Data was collected and analyzed in FL WinLab. Peptoid block copolymers were dissolved in a saturated aqueous solution of pyrene-1-carboxaldyhyde at various concentrations. Pyrene-1-carboxaldehyde, which is sensitive to solvent polarity was excited at 380 nm and emission was measured from 400-500 nm. The wavelength at maximum intensity (λ_{max}) was plotted versus concentration. CMC was determined as the intersection of curve fits to the low and high concentration regimes, as shown in Figure S2.3. Reported values are the average of three separate concentration series.

2.2.7. Dynamic light Scattering (DLS)

DLS measurements were conducted on a Malvern Zetasizer Nano ZS using a laser wavelength of 633 nm at a temperature of 25 °C. Peptoid block copolymers were dissolved in ultrapure water (5 mg/mL) adjusted to pH= 9 with NaOH, and then filtered through cellulose acetate syringe filters (0.45 μm) into clean cuvettes before measurement. The correlation functions were fitted using the maximum entropy method (MEM)[77] to calculate the diffusion coefficient and hydrodynamic radius (R_h) and polydispersity. Maximum Entropy analysis was performed using the Clementine (v1.2) package for Igor Pro (v6.37) and results are shown in Figure S2.4. The fitting resulted in a distribution of decay times (Eq. 2.1) which were converted to diffusion coefficients using Eq. 2.2 and hydrodynamic radii using the Stokes-Einstein relationship (Eq. 2.3). The hydrodynamic size distribution was fitted with a lognormal distribution function and sizes were reported as the distribution mean with standard deviation. The polydispersity index (PDI) to describe the distribution width is reported as the standard deviation squared over the mean squared.

$$g_1(t) = exp^{-\Gamma t} \quad \text{Eq. 2.1}$$

$$D = \left(\frac{\Gamma}{q^2}\right) \quad \text{Eq. 2.2}$$

$$R_h = \frac{k_B T}{6\pi\eta D} \quad \text{Eq. 2.3}$$

$$PDI = \left(\frac{\sigma}{\mu}\right)^2 \quad \text{Eq. 2.4}$$

2.2.8. Zeta Potential

Zeta potential was measured on a Malvern Zetasizer Nano ZS using a laser wavelength of 633 nm at a temperature of 25 °C. Peptoid block copolymers were dissolved in ultrapure water (5 mg/mL) adjusted to pH= 9 with NaOH, and filtered through cellulose acetate syringe filters (0.45 μm) into clean folded capillary cells before measurement. Measurements are reported as the average of three measurements for each sample.

2.2.9. SANS Modeling Considerations

Samples were prepared by direct dissolution of peptoids polymers in D_2O adjusted to pH=9 with NaOH. Solutions were filtered through 0.22 μm cellulose acetate syringe filters into clean 2 mm Hellma cells. Measurements were collected at 25 °C, at EQ-SANS and Bio-SANS. Data reduction was conducted employing the Igor Pro platform or Mantid.[78] A typical SANS data reduction protocol, consisting of subtracting scattering contributions from the empty cell (2 mm Hellma cells), background scattering, and sorting data collected from two different detector distances was used to yield normalized scattering intensities, I(Q) (cm^{-1}) *a.k.a.* the macroscopic scattering cross-section ($d\Sigma/d\Omega$) as a function of the momentum transfer, Q ($Å^{-1}$). The SANS scattering cross ($d\Sigma/d\Omega$) in absolute units [cm^{-1}] following core-shell model in dilute solution is given by:[79]

$$\frac{d\Sigma}{d\Omega} = \frac{\phi}{V_m}[I_{core}(Q) + I^b_{corona}(Q) + I_{inter}(Q) + I_{blob}(Q)] \quad \text{Eq. S5}$$

Here V_m and ϕ are the volume and the volume fraction of the micelles. The terms, $I_{core}(Q)$ and $I^b_{corona}(Q)$ corresponds to the scattering contribution from the micellar core and corona respectively. The third contribution, $I_{inter}(Q)$, comes from the interference term between the core and the corona and the blob scattering, $I_{blob}(Q)$, from swollen corona is implemented following Svaneborg and Pedersen.[80]

2.3. Results and Discussion

2.3.1. Synthesis and Characterization of the Sequence-defined Ionic Peptoid BCPs

To achieve control over the monomer sequence, we have adopted the sub-monomer method in the synthesis of a series of sequence-defined amphiphilic peptoid block copolymers (BCPs) with precisely located ionic monomers in the hydrophilic segment.[21] This series of peptoid BCPs are comprised of a total of twenty-five monomer units (DP=25) with three different types of *N*-substituents: *n*-decyl (hydrophobic), 2-methoxyethyl (neutral) and 2-carboxyethyl (ionic) (Figure 2.1A). The hydrophobic segment in each polypeptoid chain is conserved with five *N*-*n*-decyl-glycine (N_{dc}) monomers, whereas the hydrophilic segment has a total of twenty monomer units comprised of a single *N*-2-carboxyethyl-glycine (N_{ce}) and nineteen *N*-2-methoxyethyl-glycine (N_{me}) residues in the singly charged series or three N_{ce} and seventeen N_{me} for the triply charged series. The monomer sequence in the hydrophilic segment is systematically varied to enable precise control of the ionic monomer position along the chain. In the singly charged series, the single ionic monomer is placed progressively towards the junction of the hydrophilic and hydrophobic segments (Sequence 1-5, Figure 2.1B). In the triply charged series, the three ionic monomers are spaced apart by a neutral monomer, and are placed increasingly close to the junction

of the hydrophilic and hydrophobic segments (Sequence 6-8, Figure 2.1B). A charge-neutral sequence (Sequence 9, Figure 2.1B) has also been synthesized as a control sample for comparison with the singly and triply charged series. MALDI-TOF MS analysis of all peptoid samples revealed the presence of a major mass ion that corresponds to the molecular mass of targeted peptoid structures (Figure S2.1). In addition, several low intensity mass ions that are separated by 115 m/z can also be seen, corresponding to some monomer deletion impurities. HPLC analysis revealed purity levels in 82%-95% range for all peptoid samples (Figure S2.2).

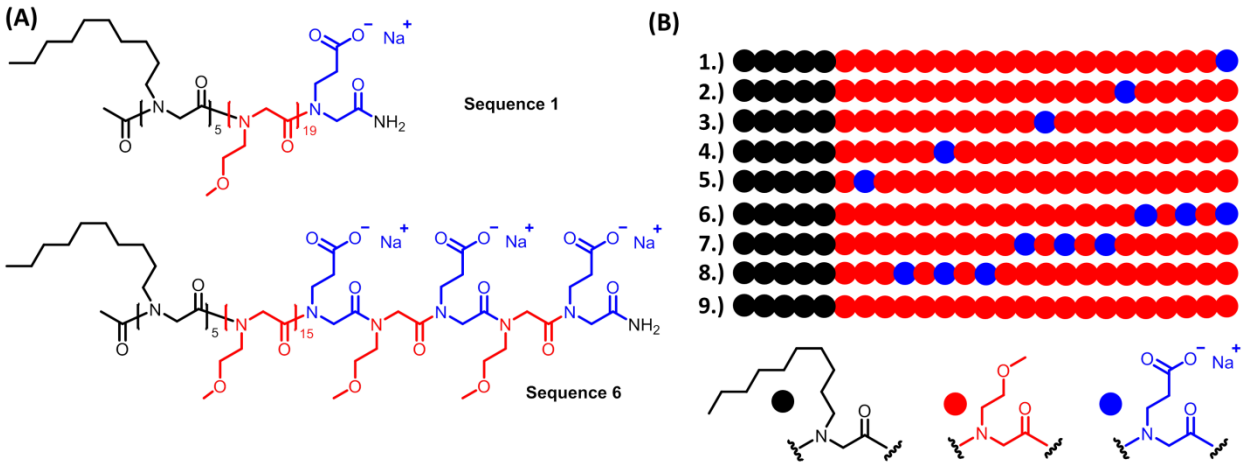

Figure 2.1. (A) Chemical structures of representative sequences of ionic peptoid block copolymers (1 or 6) and (B) the sequence library showing the singly charged (1-5), triply charged series (6-8) and the charge-neutral sequence (9).

2.3.2. Characterization of the Dilute Solution Structure of Sequence-defined Peptoid BCPs

All peptoid block copolymers shown in Figure 2.1 can be readily dissolved in aqueous solution in the 1×10^{-4}–13 mg/mL concentration range. The aqueous solution was adjusted with 4 equivalents of NaOH per equivalent of COOH groups to ensure full deprotonation of the carboxylic acid and the reaching of pH 9.[54] The peptoid block copolymers form micelles with

critical micelle concentration (CMC) in the 0.034-0.094 mg/mL (*i.e.*, 9.9×10^{-6} – 2.8×10^{-5} M) range as determined by pyrene-1-carboxaldehyde fluorescence method (Figure S2.3-S2.4 and Table 2.1).[76] At pH 9, all carboxyl groups are expected to be fully deprotonated. While association of polymers can cause a shift in pKa of ionizable groups, this effect is expected to be relatively small based on reported literature.[81] The zeta potential (ζ) measurement of the peptoids polymer solutions revealed that the micellar particles are negatively charged with ζ = -26 – -29 mV for the singly charged series and ζ = -33 – -40 mV for the triply charged series, consistent with the triply charged series bearing more negative charges than that singly charged series (Table 2.1 and Figure S2.4). No significant difference of zeta potential was seen for different sequences that have the same total number of ionic monomers. In comparison, the charge-neutral peptoid polymer (Sequence 9, Figure 2.1) exhibited a small positive zeta potential of 2.7 mV, which is attributed to association of proton or hydronium ion to the polymer.

Table 2.1. CMC, micellar radius (R_m) determined by CryoTEM image analysis, hydrodynamic radius of the micelles (R_h) and polydispersity determined by DLS analysis, and zeta potential (ζ) of various sequence-defined peptoid block copolymers (Sequence 1-9, Figure 2.1B) in dilute aqueous solution (pH 9)

Sequence #	CMC (mg/mL)	R_m (nm, CryoTEM)	R_h (nm, DLS MEM)	PDI (DLS MEM)	Zeta Potential (ζ, mV)
1	0.072±0.005	3.4±0.6	7±2	0.07±0.02	-27±2
2	0.069±0.009	3.9±0.3	5±2	0.10±0.05	-27.9±0.6
3	0.070±0.005	3.4±0.3	8±2	0.07±0.02	-29±1
4	0.05±0.02	3.4±0.3	5±2	0.11±0.04	-26.5±0.7
5	0.094±0.005	4.2±0.6	9±2	0.05±0.01	-28±3
6	0.034±0.004	3.0±0.4	7±2	0.07±0.02	-35±3
7	0.037±0.007	3.2±0.3	7±2	0.07±0.03	-40±3
8	0.036±0.002	2.9±0.3	7±2	0.07±0.02	-33.5±0.9
9	0.09±0.01	4.1±0.5	11±2	0.03±0.01	2.7±0.1

Dynamic light scattering (DLS) analysis of a dilute aqueous solution of all peptoid polymer samples (5 mg/mL, pH 9) revealed a bimodal distribution with a major peak corresponding to hydrodynamic radius (R_h) of ~5 – 11 nm and low polydispersity (PDI = 0.05 – 0.11) (Figure S2.5 and Table 2.1), consistent with the formation of micelles. The minor peaks correspond to much larger aggregates. The correlation data were fitted using the maximum entropy method (MEM)[77] to enable estimation of the size and relative abundance of larger particles. MEM analysis revealed the larger aggregate size (R_h) to be between 50-100 nm for ionic peptoid samples and ~115 nm for the charge-neutral sample. As the intensity of scattered light scales as $I \alpha r^6$ (r = particle radius), the molar ratio of micellar particles to larger aggregates is estimated at ~1×10^6 : 1 for these samples. This indicates that the peptoid BCP series mainly form well-defined micelles at 0.5 wt% aqueous solution (pH = 9) with negligible amounts of larger aggregates. While DLS analysis unambiguously confirmed the aggregation of the peptoid BCP series in aqueous solution, no significant difference in hydrodynamic size of the micelles was observed for these samples with varying sequences (Table 2.1).

CryoTEM analysis of the ionic peptoid polymers in dilute aqueous solution (0.5 wt%) revealed the predominant presence of spherical micelles (Figure 2.2). The spherical micelles are fairly uniform in size with the singly charged series having mean radii in the 3.4 – 4.2 nm range (n = 50) and triply charged series having slightly smaller mean radii in the 2.9 – 3.2 nm range (n = 50) (Table 2.1). For the neutral peptoid sample, spherical micelles having a 4.1 nm mean radius (Sequence 9, Table 2.1) were observed to be the main species with occasional short worm-like nanostructures (Figure S2.6).

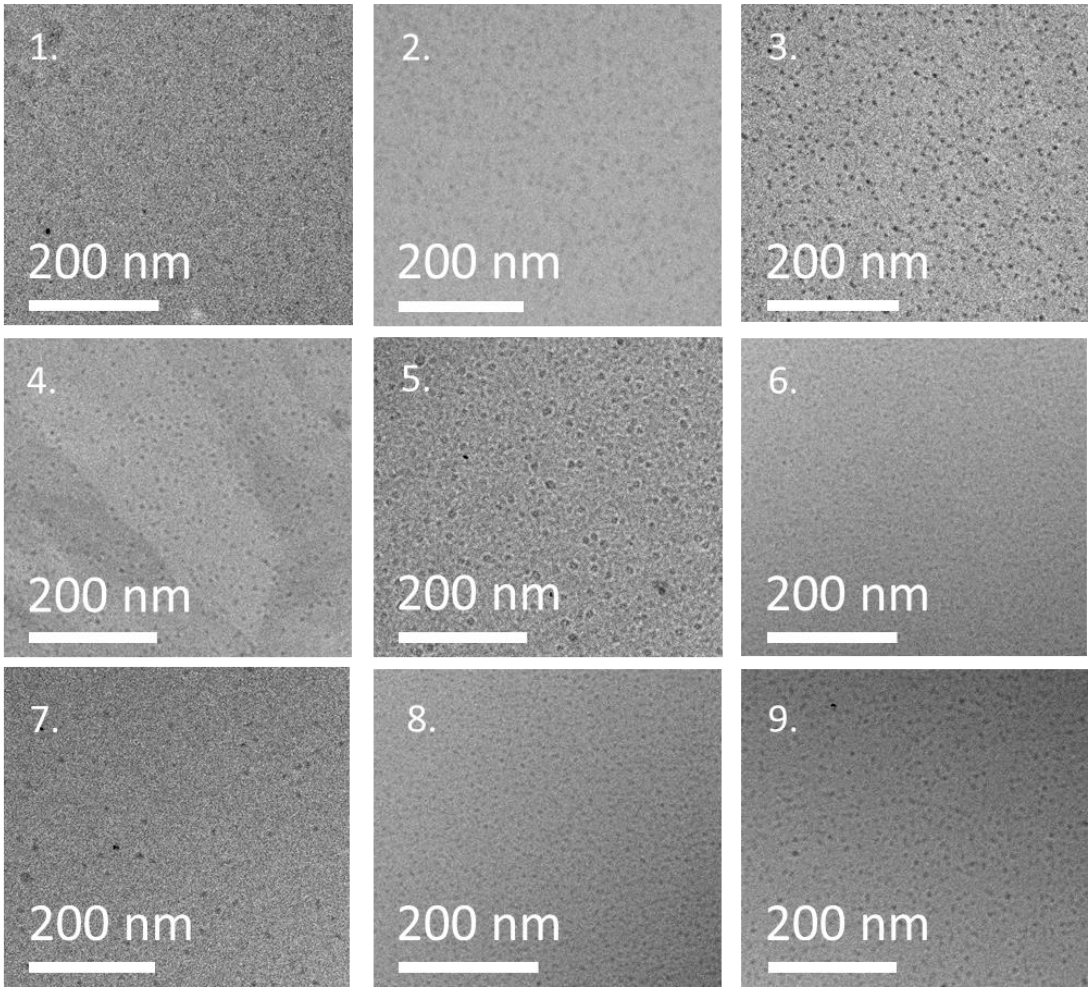

Figure 2.2. CryoTEM images of various sequence-defined ionic peptoid block copolymers (Sequence 1-9, Figure 2.1) in dilute aqueous solution (5 mg/mL, pH 9).

2.3.3. Small-Angle Neutron Scattering (SANS) Analysis of the Micellar Structure in Dilute Aqueous Solution

To further investigate the detailed structure of the micelles, SANS experiments were conducted on the series of sequence-defined peptoid micellar solutions (Entry 1-9, Table 2.2) at a concentration of 0.45 vol% (0.5 wt%) and pH = 9 in D_2O. Measurements were conducted at the Spallation Neutron Source (EQ-SANS) and the High-Flux Isotope Reactor (Bio-SANS). For SANS analysis the neutron scattering length densities (SLDs) for each of the hydrophobic (N_{dc} monomers) and hydrophilic moiety (N_{ce} + N_{me} monomers) are calculated from the corresponding

mass density following Murnen *et al.*[54] For the SANS analysis the corresponding SLDs are kept constant for each of singly or triply charged system. All SANS data exhibited a Guinier-like low *q* region, suggesting that the inter-particle interactions arising from the structure factor can be neglected at this concentration (Figure 2.3, S2.7 and S2.8). For the singly charged series shown in Figure 2.3, as the ionic monomer position along the peptoid polymer chain are shifted further from the junction of hydrophilic and hydrophobic segments, there is a notable increase in scattering intensity at low *q*, indicating an increase in aggregation number (N_{agg}). A horizontal shift of the scattering curve toward the low *q* region was also observed in the corresponding SANS plot indicating an increase in micellar radius (R_m). A similar trend was also observed for the micellar solution based on the triply charged peptoid polymer series (Figure S2.7).

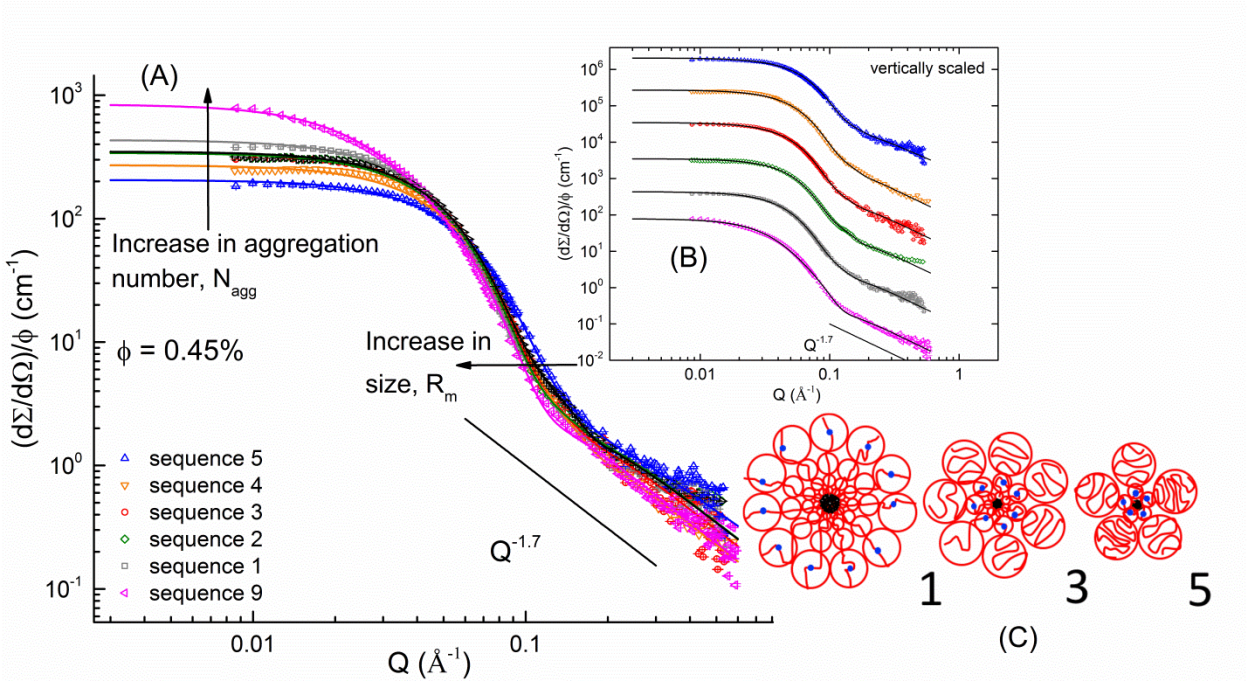

Figure 2.3. SANS scattering intensity, normalized by the polymer volume fraction, and analysis of the micellar solutions of sequence-defined peptoid block copolymers bearing a single ionic monomer (Sequence 1-5, Figure 2.1) in 0.45 vol% D_2O (pH 9). Pictured are the fitted data for the singly charged peptoid polymer series (A) and the data vertically scaled by a constant for clarity (caption cont'd.)

(B). The solid lines correspond to fits using the core-shell model.[82] At low q an increase of scattering intensity corresponding to an increase in aggregation number is observed, while the general shift of the curves to lower q indicates an overall increase in size as the ionic monomer is moved further away alone the chain from the junction of the hydrophilic and hydrophobic segments. (C) A cartoon representation of the micellar structure with respect to the ionic monomer position along the peptoid polymer chain.

At high q, the scattering intensity exhibited a power law dependence on q with a -1.7 exponent, suggesting a swollen coil in the micellar corona. This is in contrast to ionic block copolymer micelles with a highly charged corona segment, which were reported to exhibit a more rod-like or highly extended behavior where the exponent is close to -1 at the high q region.[60-61, 83] The SANS data can be well-fitted with a core-shell form factor, using a neutral star-like micelle density profile, which was previously reported[82] and briefly described in the Supporting Information. The micellar aggregation number (N_{agg}) and micellar size (R_m) were obtained from the fitting. The micellar radius of gyration (R_g) was determined from the Guinier analysis of the SANS data (Figure S2.9-S2.10). The q range was selected with the criteria of $R_g \cdot q_{max} << 1$. The core radius of the micelle (R_c), the corona thickness (R_m-R_c), the core-corona interfacial area per polymer chain (σ) and the corona volume occupied per polymer chain (v) were calculated from the N_{agg} and R_m, which will be further discussed (*vide infra*). All structural parameters of the micelles obtained from SANS analysis are summarized in Table 2.1 for different sequence-defined polypeptoids.

Table 2.2. Structural parameters of the micelles based on the sequence-defined ionic peptoid block copolymers (Sequence 1-9, Figure 2.1) as determined by SANS data analysis. The parameters include the particle aggregation number (N_{agg}), the micellar radius (R_m), the micellar radius of gyration (R_g), the core radius (R_c), the corona thickness (R_m-R_c), the core-corona interfacial area per polymer chain (σ) and the corona volume occupied per polymer chain (v)

Sequence #	Ionic monomer Position #	N_{agg}	R_m (nm)	R_c (nm)	R_m-R_c (nm)	R_g (nm)	σ (nm^2)	v (nm^3)
1.	20	28±2	5.70±0.05	2.30±0.05	3.40±0.08	4.02±0.04	2.4±0.2	26±2
2.	15	25±1	5.65±0.09	2.12±0.06	3.53±0.11	3.70±0.07	2.3±0.1	29±1
3.	11	23±1	5.35±0.05	2.13±0.03	3.22±0.05	3.56±0.05	2.5±0.1	26±1
4.	6	18±1	5.08±0.07	1.96±0.03	3.12±0.06	3.24±0.05	2.7±0.2	29±2
5.	2	13±1	4.47±0.04	1.80±0.04	2.67±0.06	2.88±0.03	3.1±0.3	27±2
6.	16,18,20	18±1	4.50±0.03	1.95±0.03	2.55±0.04	3.19±0.03	2.7±0.2	20±1
7.	10,12,14	17±2	4.41±0.04	1.93±0.07	2.48±0.09	3.15±0.03	2.8±0.4	19±2
8.	4,6,8	12±1	4.24±0.03	1.71±0.04	2.53±0.06	2.88±0.04	3.1±0.3	25±2
9.	n/a	52±2	6.42±0.05	2.80±0.09	3.62±0.12	4.52±0.04	1.9±0.1	19±1

The micelles based on the charge-neutral peptoid BCP (Table 2.2) have a significantly higher aggregation number (N_{agg} =52±2) relative to the singly (N_{agg} =13±1 – 28±2) or triply charged series (N_{agg} =12±1 – 18±1), while the micellar radius (R_m = 6.42±0.05 nm) is moderately larger than those of the charged micelles (R_m = 4.47±0.04–5.70±0.05 nm for the singly charged series and R_m = 4.24±0.03 – 4.50±0.03 nm for the triply charged series) (Table 2.2). These results are consistent with an early SANS study of the polystyrene-polyisoprene (PS-PI) micelle having a single charge monomer per chain residing at the core-corona interface of the micelles.[84] The PS-PI micelles having the charged monomers were shown to have significantly smaller aggregation number (N_{agg}= 47) and moderately reduced micellar size (R_m = 10 nm) than the charge-neutral micellar analogs (N_{agg}= 90, R_m = 13.2 nm). The radius of gyration (R_g) follows the similar trend as that of R_m with the neutral micelles being larger (R_g = 4.52±0.04 nm) than those of the charged micelles (R_g = 2.88±0.03 – 4.02±0.04 nm for the singly charged series and R_g = 2.88±0.04 –

3.19±0.03 nm for the triply charged series) (Table 2.2). The dimensionless shape parameter defined as the ratio of R_g to R_h is in the 0.3±0.1 – 0.7±0.2 range for all micelles. They are lower than the theoretical prediction for a hard sphere (0.77). This could be due to the difference in solvent penetration into the micellar core and corona or the segmental density difference in the micelles, resulting in more complex hydrodynamic interactions, as previously reported on microgels or porous spheres.[44, 85-89]

Assuming all micelles form a dense core, the micellar core radius can be calculated by using $R_c = (3N_{agg}M_{w,core}/4\pi\rho_{core}N_a)^{1/3}$ and N_{agg} values obtained from SANS analysis. The micellar corona thickness defined as R_m-R_c can also be calculated. It was found that the neutral micelles have larger core radius (R_c =2.80±0.09 nm) and corona thickness (R_m-R_c =3.62±0.12 nm) relative to the singly charged (R_c = 1.80±0.04 – 2.30±0.05 nm, R_m-R_c =2.67±0.06 – 3.53±0.11 nm) or triply charged micelles (R_c = 1.71±0.04 – 1.95±0.03 nm, R_m-R_c =2.48±0.09 – 2.55±0.04 nm) (Table 2.2, Figure 2.5A-2.5B). To assess the aerial density of polymer chains at the core-corona interface, the packing area per chain at the core-shell interface (σ) was calculated using $\sigma = 4\pi R_c^2/N_{agg}$. The neutral micelle has a smaller σ (1.9±0.1 nm^2) than the singly (σ =2.3±0.1 – 3.1±0.3 nm^2) or triply charged micelles (σ =2.7±0.2 – 3.1±0.3 nm^2) (Figure 2.5C). The corona volume occupied per polymer chain (v) has also been calculated using $v = N_{agg}/(4/3\pi R_m^3 - 4/3\pi R_c^3)$ to allow for assessment of the volume density of polymer chains in the micellar corona. The neutral micelles have a much smaller v (= 19±1 nm^3) than all singly charged micelles (v = 26±2 – 29±2 nm^3) and the triply charged micelles (Sequence 8, Figure 2.1) with the ionic monomers positioned closest to the block junction along the chain (v = 25±2 nm^3) (Figure 2.5D). Interestingly, the other two triply charged micelles with the ionic monomers positioned further away from the block junction (Sequence 7 and 6, Figure 2.1) has comparable volume chain density (v =19±2 and 20±1 nm^2) as

the neutral micelles. These results clearly suggest a significant role of electrostatic interactions in the micellar corona in the solution assemblies of ionic block copolymer even in a weakly charged system, and that the position and total number of ionic monomers along the hydrophilic segment (*i.e.*, the monomer sequence) can be manipulated to precisely tailor the structure details of ionic micelles.

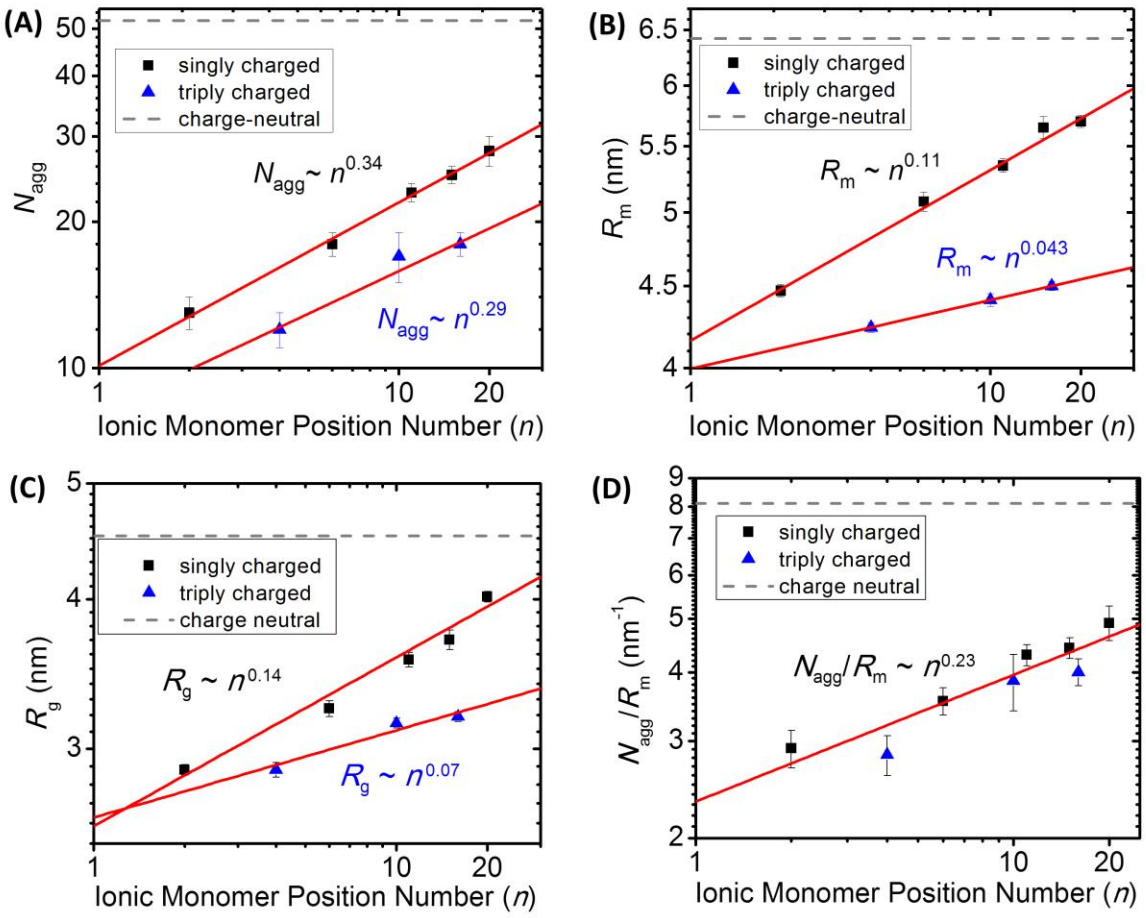

Figure 2.4. (A) Plots of the micellar aggregation number (N_{agg}), (B) the micellar radius (R_m), and (C) the radius of gyration of the micelles (R_g), and (D) the N_{agg}/R_m ratio versus the position number of the ionic monomer (n) in the sequence-defined peptoid polymer chain with a single charge (■) or triple charges (▲). The data for the neutral peptoid micelles are plotted as a dash line (---) in the respective figures for comparison. The position number is defined as the ionic monomer number along the hydrophilic segment counted by starting from the junction of the hydrophilic and hydrophobic segments. For the triply charged series, the position number in these plots is taken

(caption cont'd.)

for the innermost ionic monomer. N_{agg}, R_m and R_g are all determined from the fitting of SANS data with a core-shell model using a neutral star-like micelle density profile.[82]

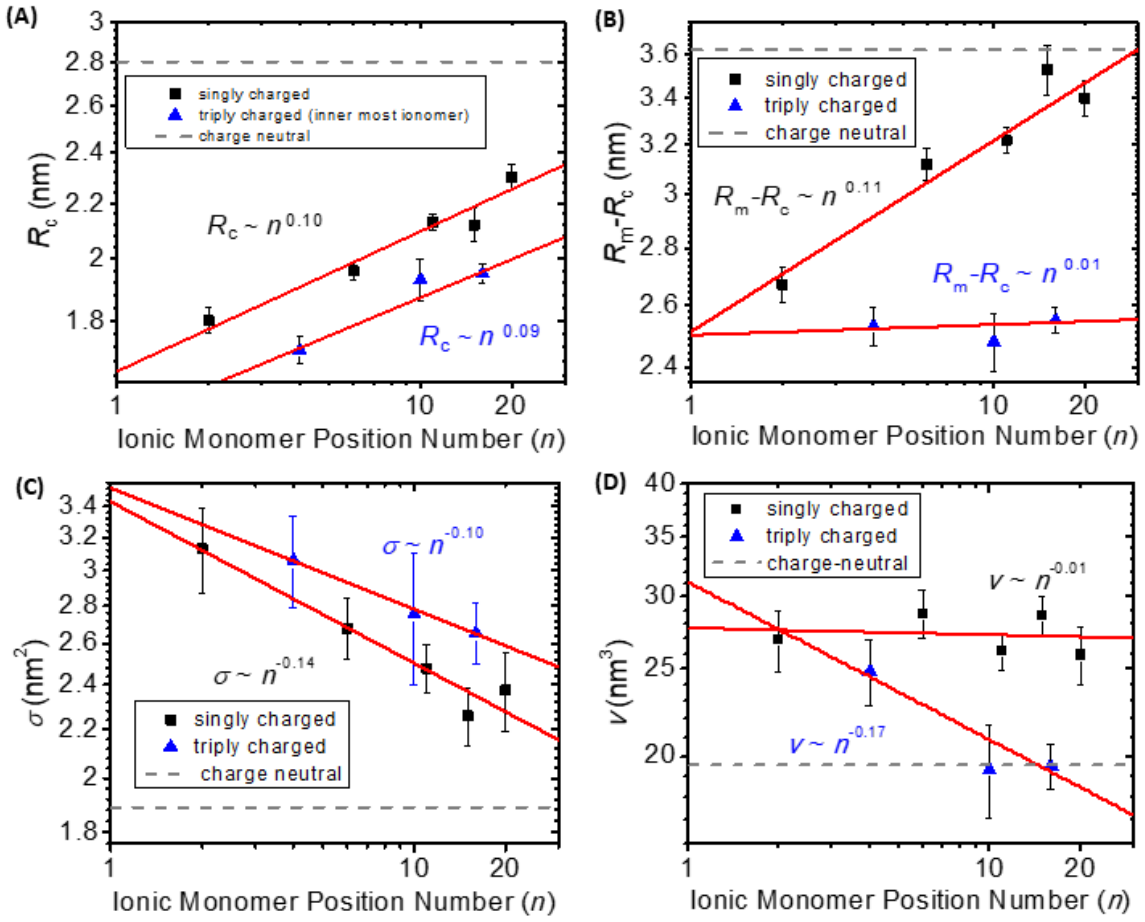

Figure 2.5. (A) Plots of the micellar core radius (R_c), (B) the micellar corona thickness (R_m -R_c), (C) the core-corona interfacial area per polymer chain (σ), and (D) the corona volume occupied per polymer chain (v) versus the position number of the ionic monomer (n) in the sequence-defined peptoids polymer chain with a single charge (■) or triple charges (▲). The data for the neutral peptoid micelles are plotted as a dash line (---) in the respective figures for comparison. The position number is defined as the ionic monomer number along the hydrophilic segment counted by starting from the junction of the hydrophilic and hydrophobic segments. For the triply charged series, the position number in these plots is taken for the innermost ionic monomer.

2.3.4. Investigation of the Sequence Effect on the Micellar Structure by Scaling Analysis

The sequence-defined nature of the peptoid block copolymers allows for precise description of each monomer's position along the chain. Considering the hydrophobic monomers as part of a compact core, the hydrophilic monomers in the micellar corona were numbered from 1 to 20, starting from the first hydrophilic monomer residue at the junction of the hydrophilic and hydrophobic segments (Table 2.2 and Figure 2.1). The effect of ionic monomer position on the micellar structure has been assessed through the scaling relationship analysis of different structural parameters of micelles (*i.e.*, N_{agg}, R_m, R_g, R_c, R_m-R_c, σ and ν) versus the ionic monomer position number (n). For the triply charged micellar series, the analysis was conducted using the innermost, middle or outermost ionic monomer position number (n), respectively. The results are summarized in Table 2.3.

Table 2.3. The prefactors and exponents for the power law relationship between various structural parameters (N_{agg}, R_m, R_g, N_{agg}/R_m, R_c, R_m-R_c, σ and ν) of the sequence-defined peptoid block copolymer micelles (Sequence 1-9, Figure 2.1) and the ionic monomer position number (n). The error bars of the prefactors and exponents were obtained from the data fitting using the power law function ($y=ax^b$). For the triply charged series, the innermost, middle and outermost ionic monomer position are separately considered in the data fitting using the power law function.

	Singly charged series		**Triply charged series**					
			Innermost		**Middle**		**Outermost**	
	Prefactor	Exponent	Prefactor	Exponent	Prefactor	Exponent	Prefactor	Exponent
N_{agg}	10.1±0.4	0.34±0.01	8.1±0.9	0.29±0.04	6±1	0.37±0.06	5±1	0.44±0.08
R_m	4.15±0.04	0.107±0.004	3.9950±0.0002	0.04293±0.00002	3.85±0.01	0.054±0.002	3.70±0.03	0.065±0.003
R_g	2.58±0.07	0.14±0.01	2.6±0.1	0.07±0.02	2.5±0.2	0.09±0.03	2.3±0.2	0.11±0.04
N_{agg}/R_m	2.4±0.1	0.23±0.02	2.0±0.2	0.25±0.04	1.6±0.3	0.31±0.06	1.3±0.3	0.37±0.08
R_c	1.65±0.05	0.10±0.01	1.51±0.06	0.09±0.02	1.39±0.09	0.12±0.02	1.3±0.1	0.14±0.03
R_m-R_c	2.51±0.09	0.11±0.02	2.50±0.08	0.01±0.01	2.5±0.1	0.01±0.02	2.5±0.1	0.01±0.02
σ	3.4±0.1	-0.14±0.02	3.53±0.06	-0.10±0.01	3.9±0.1	-0.13±0.01	4.2±0.2	-0.15±0.02
ν	28±3	-0.01±0.04	31±4	-0.17±0.05	36±7	-0.22±0.07	40±10	-0.26±0.09

Plotting of the aggregation number (N_{agg}) versus the ionic monomer position number (n) for the singly charged micellar series revealed an intriguing and unprecedented power-law relationship with an exponent of 0.34±0.01 (Figure 2.4A, Table 2.3). The error bar of the exponent reflects the quality of the data fitting with the power- law function. A similar scaling relationship was also observed for the triply charged series with an exponent of 0.29±0.04 using the position number of the innermost ionic monomer (which is closest to the junction of the hydrophilic and hydrophobic segments) in the analysis (Figure 2.4A). When the position number of the middle or outermost ionic monomer in the triply charged series is used, the exponent increased to 0.37±0.06 and 0.44±0.08 respectively (Figure S2.11-A). The micellar size (R_m) determined by SANS analysis was also found to exhibit a power-law dependence on n but much weakly with an exponent of 0.107±0.004 for the singly charged series, 0.04293±0.00002, 0.054±0.002 and 0.065±0.003 for the triply charged series using the respective innermost, middle or outermost ionic monomer position number (Figure 2.4B and S2.11-B, Table 2.3). The radius of gyration of the micelles (R_g) also increases with n similar to that of R_m with a power-law exponent of 0.14±0.01 for the singly charged series (Figure 2.4C, Table 2.3). The R_g of the triply charged series scales more weakly with n relative to the singly charged series, evidenced by the exponent of 0.07±0.02, 0.09±0.03, 0.11±0.04 (Figure 2.4C and S2.11-C) for the former using the respective innermost, middle and outermost ionic monomer position number. It is noteworthy that when the N_{agg}/R_m ratio is plotted versus n for the singly charged series or the triply charged series using the innermost ionic monomer position number, the two series can be collapsed into a master curve with the experimental accuracy and be described by a power-law function with an exponent of 0.23±0.04 and a prefactor of 2.3±0.2 (Figure 2.4D).

The micellar core radius (R_c) calculated from the N_{agg} using $R_c = (3N_{agg}M_{w,core}/4\pi\rho_{core}N_a)^{1/3}$ was found to increase with n in a power-law relationship (Figure 2.5A). The exponent (0.10±0.01) for the singly charged series is comparable to that the triply charged series (0.09±0.02, 0.12±0.02, 0.14±0.03 using the respective innermost, middle or outermost ionic monomer position number in the scaling analysis) (Figure S2.11-E, Table 2.3). The micellar corona thickness (R_m-R_c) also exhibited a power-law dependence on the ionic monomer position number with an exponent of 0.11±0.02 for the singly charged series (Figure 2.5B, Table 2.3). By contrast, the micellar corona size of the triply charged series is essentially independent on n with a close-to-zero exponent (0.01±0.01, 0.01±0.02, 0.01±0.02) (Figure 2.5B and S2.11-F, Table 2.2).

The core-corona interfacial area per polymer chain (σ) was found to decrease with increasing ionic monomer position number for both the singly and triply charged micellar series with comparable power-law exponents (-0.14±0.02 for the former, -0.10±0.01, -0.13±0.01 and -0.15±0.02 for the latter) (Figure 2.5C and S2.11-G, Table 2.3). The volume occupied per polymer chain in the corona (v) were shown to remain nearly invariant with the change of the ionic monomer position for the singly charged micelles, evidenced by a close-to-zero exponent (-0.01±0.04) in the scaling analysis (Figure 2.5D). By contrast, v appears to be more sensitive to the ionic monomer position for the triply charged series. Increasing the position number resulted in a decrease of v in a power-law relationship with exponents of -0.17±0.05, -0.22±0.07 and -0.26±0.09 using the innermost, middle or outermost ionic monomer position, respectively (Figure 2.5D and S11-H, Table 2.3).

To better understand the electrostatic effect on the ionic peptoid micellar structure, we conducted additional scaling analysis in the framework of an ionic star-like polymer model.[64] It was found that the micellar radius (R_m) and the micellar corona size (R_m-R_c) both increases with

increasing aggregation number (N_{agg}) in a power law relationship with an exponent that is approximately 1/3 [*i.e.*, $R_m=(1.9\pm0.1)\times N_{agg}^{0.32\pm0.02}$; R_m-R_c= $(1.2\pm0.2)\times N_{agg}^{0.31\pm0.06}$] for the singly charged polypeptoid series (Figure 2.6). This scaling relationship is consistent with the theoretical prediction on the dependence of polymer radius [$R(f)$] on the number of arms (f) for ionic star-like polymers [*i.e.*, $R(f) \sim f^{1/3}$] in unscreened regime where the equilibrium polymer size is obtained by balancing the electrostatic repulsion with the conformational free energy penalty due to the extension of the polymer arms.[64] In this regime, the electrostatic interaction within the corona is considered unscreened with an infinite Debye screening length, which can be satisfied when the polymer arm is weakly charged (*i.e.*, low fraction of ionic monomers) in dilute solution of ionic star-like polymers. By comparison, for neutral star-like polymers with f arms, the polymer radius is more weakly dependent on f with a $R(f) \sim f^{1/4}$ (θ solvent) or $f^{1/5}$ (good solvent) power law relationship.[64] This indicates that the long-range electrostatic repulsion can cause stronger chain extension than the short-range non-electrostatic repulsion (*i.e.*, excluded volume interaction). The singly charged sequence-defined peptoid block copolymers containing a 5% molar fraction of the ionic monomers in the hydrophilic segments in dilute aqueous solution (0.5 wt %, pH = 9) effectively behave like an ionic star-like polymer in the unscreened regime. In addition, the low fraction of the ionic monomer content in the hydrophilic segments does not significantly perturb the global chain conformation in the corona, thus giving rise to $I \sim q^{-1.7}$ scaling relationship at the high q region in the SANS profile which is typically observed for star-like micelles of neutral block copolymers or neutral star-shape polymers in good solvent.[82, 90-92]

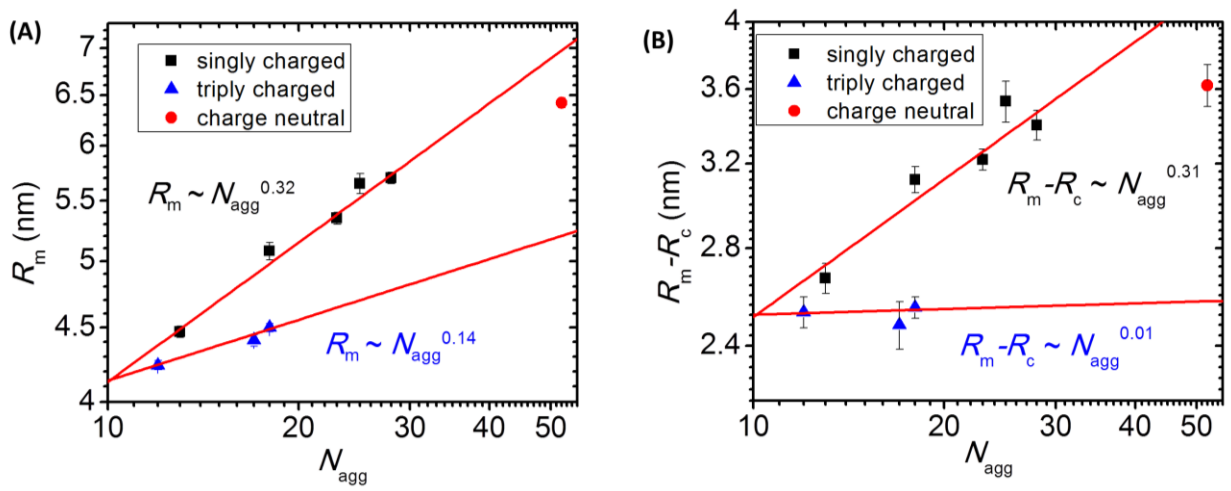

Figure 2.6. (A) Plots of the micellar radius (R_m) or (B) the micellar corona thickness (R_m-R_c) versus the aggregation number (N_{agg}) for the micelles based on the singly and triply charged peptoid block copolymer series (Table 2.2).

For the triply charged peptoid BCP series, the micellar radius is exhibits a weaker dependence on the aggregation number in a power law relationship [*i.e.*, $R_m = (3.0\pm0.2)\times N_{agg}^{0.14\pm0.03}$] with an exponent of 0.14±0.03 relative to the singly charged series (exponent=0.32±0.02) (Figure 2.6). Interestingly, the micellar corona size exhibited an even weaker power-law dependence on N_{agg} [*i.e.*, R_m-$R_c = (2.4\pm0.3)\times N_{agg}^{0.01\pm0.05}$]with an exponent of 0.01±0.05 as compared to that of the singly charged series (exponent=0.31±0.06). This is most likely due to the increased charge content in the hydrophilic segment in the triply charged series (*i.e.*, 15 % molar fraction), resulting in increased trapping of the counter ions inside the micellar corona and screening of the electrostatic repulsion among the ionic monomers. The increased counter-ion concentration inside the corona will cause the corona chain to stretch through osmotic force. In this so-called osmotic regime, the equilibrium micellar size of ionic star-like polymers has been theoretically considered by balancing the free energy contribution of the osmotic force with the conformational free energy of stretched polymer chains, and predicted to be virtually independent on the number of arms in the ionic star-like polymers. Hence, the weak power law

dependence of the micellar size (R_m) and corona size (R_m-R_c) on the N_{agg} for the triply charged peptoid series may represent a transition from the unscreened regime to the osmotic regime for this class of ionic star-like micelles. To fully understand the scaling relationship for the triply charged series, additional samples with different sequences needs to be analyzed.

It is clear that the electrostatic interaction encoded in the position and total number of the ionic monomers along the chain (*i.e.*, the sequence information) has a notable impact on the self-assembled structures of the ionic peptoid block copolymers in dilute solution. In the singly charged sequence-defined peptoid BCP micelles, the electrostatic repulsion in the corona is systematically enhanced due to increased proximity of ionic monomers at the core-corona interface of the micelles, as the ionic monomer is placed progressively closer to the junction of the hydrophilic and hydrophobic segments along the chain. This results in a systematic decrease of the aggregation number and the micellar size accordingly. Similarly, increasing the total number of ionic monomers in the polymer chain further enhances the electrostatic repulsion in the micellar corona, leading to additional reduction of the aggregation number and micellar size in the triply charged micellar series relative to the singly charged micelles (Figure 2.4B). In addition, as the charge fraction is relatively low in the singly and triply charged series (*i.e.*, 5 mol% and 15 mol%), the chain conformation is not significantly perturbed from the swollen coil conformation. The micellar structure based on these sequence-defined ionic peptoid block copolymers represents an intermediate between the neutral star-like micelles and ionic star-like micelles (strongly charged). One can manipulate the position and number of ionic monomers along the chain to control the ionic micellar structure.

2.4. Conclusions

We have demonstrated that the electrostatic interactions are very important to the self-assembled structures of sequence-defined peptoid block copolymers containing ionic monomers. By simply controlling the monomer sequence, *i.e.*, the positon and number of ionic monomers along the amphiphilic block copolymer chain, the resulting micellar structures (*e.g.*, aggregation number and micellar size) can be precisely tailored. By placing increasing amount of ionic monomers closer to the junction of hydrophilic and hydrophobic segments along the chain, the micellar structures reorganize in aqueous solution to minimize electrostatic repulsive interaction. This study has demonstrated a novel strategy to access small star-like micelles (*i.e.*, R_h in sub-10 nm) having identical chemical composition but differing structural details by controlling the monomer sequences. Furthermore, the study has revealed a general principle that is potentially applicable to a variety of weakly charged soft matter self-assemblies, *i.e.*, when the charge fraction is low in the system, the detailed structure of molecular assemblies can be tailored by the position and sequence of the ionic building blocks. This effect could be further explored towards the design of smart soft nano-colloids, tuning the fine structure of a drug carrier by the placement of a single well-chosen ionic functional group. Future efforts will be focused on investigating the effect of pH, salt, solvent polarity on the micellar structure, and unravelling the scaling relationship of micellar structure with non-spherical interfaces.

CHAPTER 3. pH DEPENDENCE OF SELF-ASSEMBLIES OF SEQUENCE-DEFINED IONIC PEPTOID BLOCK COPOLYMERS

3.1. Introduction

Stimuli responsive micelles have enjoyed significant research interest as the desire for "smart materials" grows. In a recent perspective, Kowalski et al. describe smart materials as those "that can be designed to adapt their chemical and mechanical properties in response to changes in physiological parameters and exogenous stimuli."[93] These materials are particularly sought after for applications such as drug delivery, tissue engineering, or other biological applications where changes in pH, salinity, concentration or other environmental factors are likely.[94-95] The environmental changes can be sensed by a well-designed material and affect a structural change. A change in the material structure, or even a triggered destruction of the material, can effect a desired outcome, such as the targeted release of an encapsulated drug.[94]

The interactions that make smart materials, such as pH responsive micelles, useful can also make a complete understanding of the material and its behavior more complex[35, 64, 96-99]. Ionic block copolymer micelle structure is not only governed by the polymer block lengths and the solvent quality as in neutral micelles, but also by the chemical nature of the ionic groups (pKa, strong vs weak acid or base), the solution pH,[36, 43-45, 83, 100-101] salinity,[40-42, 83] total ionic strength,[43-45]and as was recently reported the ionic monomer location.[102] Each of these factors has been demonstrated to play a significant role in the solution structure and interactions of ionic block copolymer micelles.

As discussed briefly in Chapter 2, ionic block copolymer micelles containing weak acid or base functional groups exhibit stimuli responsive behavior in response to changing environmental conditions. For example, the structure of an ionic BCP micelle in solution can be tuned by either changing the solution pH, or by increasing the solution salinity. Both adjusting pH and addition of

salt to the solution affect the micellar structure by changing the apparent charge fraction of the micelle. Adjusting the pH of a solution containing a weak acid (i.e., a carboxylic acid) shifts the equilibrium between protonated carboxylic acid groups (electrostatically neutral) and deprotonated carboxylate (electrostatically negative) groups. A carboxylic acid containing BCP micelle in a low pH solution will be expected to have a higher fraction of ionizable groups protonated, and thus more electrostatically neutral groups, than a than a BCP micelle in a high pH solution. At high pH a carboxylic acid group will be deprotonated and bear a negative charge. As the fraction of charged ionizable monomers increases, electrostatic interactions within the micelle become more significant. For static micelles, micelles in which the core is frozen and aggregation number is fixed, forces due to electrostatic repulsion along a single polymer chain will cause the chain to extend and rigidify. In a static micelle this effect causes a larger micellar structure due to the extended chain conformation. This general phenomenon is illustrated in Figure 3.1. Dynamic micelles, micelles in which the core is not frozen and the polymer chains show some measure of mobility, exhibit somewhat more complicated behavior. Electrostatic repulsion between polymer chains within a single micelle will cause an increased inter-chain distance, which can lead to a lower aggregation number. A lower aggregation number corresponds to less material in the micelle and leads to a smaller micellar radius. This effect is balanced against the increase in micellar radius due to the extension of the individual polymer chains.

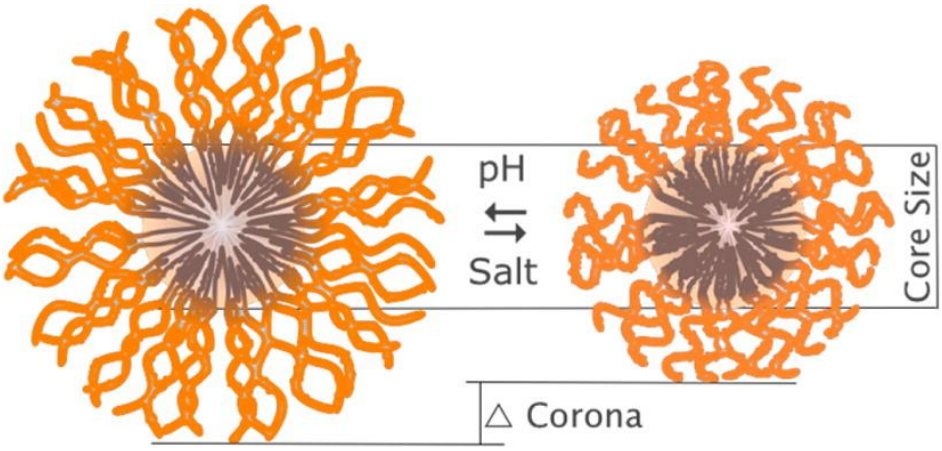

Figure 3.1. Cartoon illustrating generic ionic micelle response to changes in solution pH or salt concentration. Reprinted with permission from reference.[44] Copyright (2016) American Chemical Society.

pH responsive micelles have been demonstrated in the literature, a few of which will be highlighted here. Crichton and Bhatia synthesized poly(styrene)-b-poly(ethyl acrylate) copolymers, which when partially hydrolyzed form poly(styrene)-b-poly(acrylic acid - ethyl acrylate) and assembled into spherical micelles in water.[37] As the fraction of ethyl acrylate groups is decreased by base hydrolysis, forming ionic sodium acrylate groups (increasing charge fraction), the aggregation number of the micelles is significantly decreased from N_{agg} = 148 at a charge fraction f = 0.44, to N_{agg} = 63 and a charge fraction f = 0.97, where f = 1-(ethyl acrylate/ethyl acrylate + sodium acrylate). The increase in electrostatic repulsion between polymer chains in the micelle causes a structural change to increase the interchain distance, leading to a lower aggregation number. A corresponding decrease in the micellar radius was also observed, from R = 100.4±0.3 at f = 0.44, to R = 71.7±0.5 at f = 0.97.

Burkhardt et al. studied poly(isobutylene)-b-poly(sodium methacrylate) (PIB-b-PMAA) with multiple hydrophobic and hydrophilic block lengths under a range of salt and pH conditions.[103] For a PIB_{75}-$PMAA_{1600}$ polymer in 0.1 M NaCl a dramatic increase in R_h from ~ 50

nm up to ~100 nm was observed near the PMAA pKa of ~ 6 as the solution pH was increased. The increase in the micelle R_h was attributed to the extension of the hydrophilic PMAA arms as the increasing pH caused an increased fraction of ionized monomers along the polymer chain.

Stubenrauch et. al. in an effort to prepare more well-defined polymers for the study of polyelectrolyte block copolymer self-assembly used anionic polymerization to prepare block copolymers of poly[5,6-bis(ethoxymethyl)bicyclo[2.2.1]hept-2-ene]-b-poly[endo,exo[2.2.1]bicyclohept-5-ene-2,3-dicarboxyclic tert-butylester], or poly[endo,exo[2.2.1]bicyclohept-5-ene-2,3-diylbis(phenylmethanone)]-b-poly[endo,exo[2.2.1]bicyclohept-5-ene-2,3-dicarboxyclic tert-butylester], which were treated with acid to form the desired carboxylic acid in the hydrophilic ionizable block.[83] The relative block lengths were systematically varied and in all cases is was found that with increasing pH, from pH = 3 to pH = 10 the measured micelle R_h roughly doubled.

In Chapter 2 we reported on the size and structure of ionic micelles formed by the self-assembly of sequence defined ionic peptoid block copolymers. It was found that the micellar radius and aggregation number can be tuned by the precise placement of an ionic group along the peptoid polymer chain. These materials, singly charged series shown in Figure 3.2, based on the weakly acidic carboxylic acid functional group as the ionizable group, present an opportunity to further tune the micellar behavior in dilute aqueous solution.

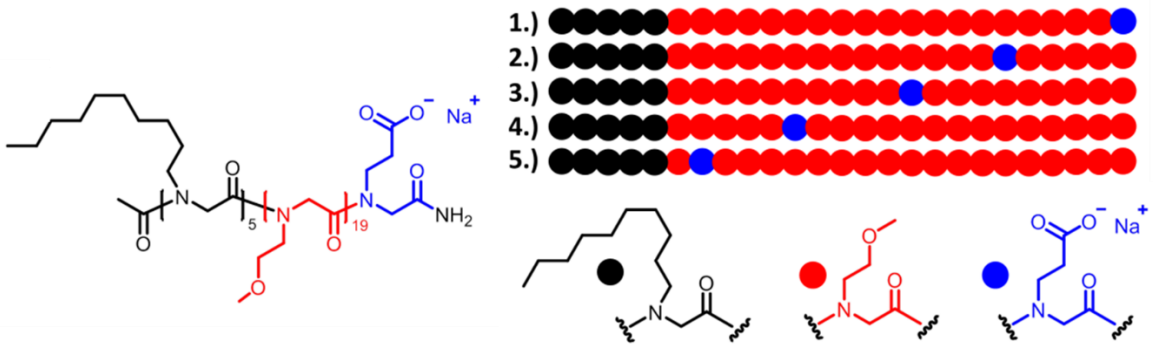

Figure 3.2. Sequence-defined ionic peptoid block copolymer singly charged series.

Given the strong relationship between the position of an ionic monomer along the sequence-defined ionic peptoid block copolymer and the structure of the resulting self-assembled micelle in solution, we propose further tunability of the micellar structure in response to changes in the solution pH. By lowering the pH of the micellar solution and shifting the protonation state of the carboxylate toward a neutral carboxylic acid, a micellar structure resembling the fully neutral state should be obtained.

3.2. Materials and Methods

3.2.1. Synthesis of Sequence-Defined Ionic Peptoid Block Copolymers

Sequence-defined ionic peptoid block copolymers were synthesized according to reported procedures.[102]

3.2.2. Measurement of Micelle solution pH

All samples were prepared in ultrapure water at 0.5 wt% and filtered through 0.22 μm PES syringe filter (Restek) before measurement. Solution pH was adjusted by successive addition of aq. NaOH solution (0.5 M) in increments of 1 eq NaOH relative to carboxylic acid groups. The solution pH was measured using a Mettler Toledo OrionStar A111 pH meter with an Orion Triode probe calibrated at 3 points (pH = 4.01, 7.00, 10.01).

3.2.2. Dynamic Light Scattering (DLS)

All samples were prepared in ultrapure water at 0.5 wt % and filtered through 0.22 μm PES syringe filter (Restek) before measurement. Sample measurements were performed on a Wyatt HELEOS II equipped with a GaAs laser at 658 nm and a QELS detector at 90 °. Data analysis and fitting were performed in Astra v. 7.1.0. Correlation functions were well fit by cumulants analysis (general Eq. 3.1) (R^2 = 0.999) and the decay rate (Γ) was converted into a diffusion coefficient (D) (Eq. 3.2). A representative correlation function is plotted in supplemental figure S3.1. The obtained diffusion coefficient can be converted to the hydrodynamic radius (R_h) using the Stokes-Einstein relationship (Eq. 3.3). Data from at least 10 scans were manually averaged to obtain the hydrodynamic radius with propagated error.

$$g_1(t) = \exp(-\Gamma\tau + \kappa_2\tau^2) \quad \text{Eq. 3.1}$$

$$D = \left(\frac{\Gamma}{q^2}\right) \quad \text{Eq. 3.2}$$

$$R_h = \frac{k_B T}{6\pi\eta D} \quad \text{Eq. 3.3}$$

3.3. Results and Discussion

In order to assess the ability of a micelle formed by self-assembly of a sequence-defined peptoid block copolymer to respond to changes in solution pH solutions were prepared at 0.5 wt% in water without adjusting the pH. The pH was then systematically raised by sequential addition of NaOH and measurement of the sample solution by DLS to obtain the hydrodynamic radius of the particle at each measured pH value. As a general consideration, as the number of additions of NaOH increased, the error associated with the measurement increased. This may be attributable to the repeated opening and closing of the sample vial, leading to introduced impurities. This might have been mitigated by re-filtering the samples after each successive addition.

The micellar hydrodynamic radius R_h is plotted vs the solution pH in Figure 3.3. It was observed that initially at low pH all samples were found to be in the range $6.9 < R_h < 9.0$ nm. The samples were generally in the order from samples 1 and 2 (Figure 3.2) being the smallest in size, 3 and 4 being intermediate in size, and 5 exhibiting the largest measured R_h. As the pH of the solution is increased samples 2, 3 and 4 all appear to remain relatively constant in size, within the observed experimental error. Sample 1 showed an increase in size from R_h = 7.2±0.3 nm at pH = 3.01, to R_h = 10.5±1.7 nm at pH = 8.34. Above pH 10, the correlation function baseline was not flat and the data was not analyzed. Sample 5 showed an overall decrease in size from R_h = 9.0±0.2 nm at pH = 2.98, to R_h = 6.9±1.0 nm at pH = 12.18. Individual plots of Rh vs solution pH for each sample are provided in Figures S3.2-S3.6.

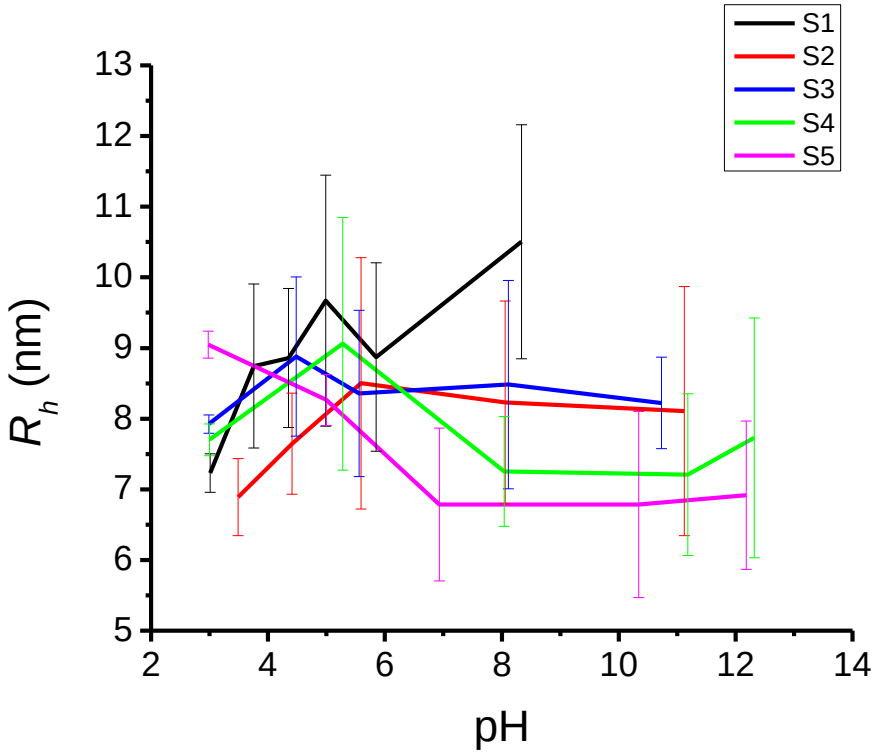

Figure 3.3. Plot of hydrodynamic radius (R_h) vs solution pH for sequence-defined ionic peptoid block copolymers (Figure 3.2) in aqueous solution.

Previously reported polyelectrolyte micelle systems have demonstrated an ability to increase or decrease the micellar radius and aggregation number with a change in pH, as well as some ability to tune the magnitude of the size change by controlling the polymer charge fraction by copolymerization or other methods. These systems always, however, exhibit a size change in a single direction, with respect to a given pH change. For a carboxylic acid based system, bearing negatively charged groups at high pH, the size of the micelle increases with an increase in pH.[37, 44, 103] In order to decrease the size of the micelle, the pH must be lowered. Current synthetic control over copolymerization does not allow sufficient control over monomer placement to change the micelle behavior in response to an increase in pH. Sequence defined ionic peptoid block copolymers do appear to show different behavior, with respect to the location of an ionic monomer, in response to increasing pH. As the ionic monomer is placed successively closer to the micelle core-shell interface the size change of the micelle shifts from an increase in radius with an increase in the solution pH, to a decrease in radius with an increase in pH. It is interesting to note that none of the samples measured approached the size of the neutral micelle analogue, previously reported in Chapter 2 (R_h = 11±2 nm).

In contrast to more traditional polymeric ionic micellar systems with a much larger charge fraction, the weakly charged peptoid BCPs exhibit a relatively small change in R_h in response to pH, with sample 5 even decreasing in R_h with increasing pH. This might be explained by the Gaussian coil conformation of the hydrophilic block of the peptoid BCPs, even in basic solution. Polyelectrolyte systems previously reported in the literature and discussed here change their radius and aggregation number along with a rigidifying and lengthening of the hydrophilic polymer block as the chain becomes increasingly ionized. In the case of the peptoid BCPs, the hydrophilic block still appears to be a random coil even when the charged monomer is ionized in basic solution. This

means the mechanism for changing the micellar radius and aggregation number must be different, at least in part, from that of a more highly charged polyelectrolyte micelle system. The presence of only a single ionizable group per peptoid chain ensures that there can be no contribution to the micellar structure from electrostatic interactions along a peptoid chain. The observed changes must be due to either interchain interactions, or an increased solubility of the carboxylate group as it is deprotonated and a tendency for the ionic group to be displayed near the surface of the micelle.

3.4. Conclusions

It was demonstrated that micellar self-assemblies of sequence-defined ionic peptoid block copolymers exhibit stimuli responsive behavior in response to varying solution pH. In contrast to previously reported carboxylate-based pH responsive micelles in the literature, which grow or contract with a corresponding increase or decrease in pH, respectively, the pH responsive behavior of sequence-defined ionic peptoid BCP depends on the location of an ionic monomer along the polymer chain. Placing an ionic monomer at the end of the polymer chain, furthest from the micelle core-shell interface caused an increase in the micellar radius with an increase in the solution pH. An ionic monomer placed close to the core-shell interface caused opposite behavior, with the micellar radius decreasing with an increase in pH. Intermediate placements of the ionic monomer appeared relatively insensitive to changes in pH.

CHAPTER 4. SYNTHESIS OF *N*-CARBOXYL ESTER *N*-CARBOXYANHYDRIDE (NCA) TOWARD ANIONIC POLYPEPTOIDS AND THEIR BLOCK COPOLYMERS

4.1. Introduction

Since their inception peptoids have enjoyed a diverse and increasing scope of applications, due to the wide variety of physiochemical properties available. Peptoids synthesized by the solid phase submonomer method are readily equipped with a range of functional chemical groups. From their conception in the 1980's the synthetic routes to peptoids were devised to be combinatorial in nature.[20-21] Efforts to speed up the synthesis of large libraries of new medical drug candidates, by Zuckermann and coworkers, to address the synthetic bottleneck in prodrug discovery yielded the modular SPSS route to sequence defined peptoids. The modular nature of the method adapted well to combinatorial chemistry. The first iteration of the library of chemical functionalities which can be incorporated into the peptoid chain was reported.[1] Since that time peptoids have been used in drug discovery and delivery, as building blocks for assembled nanostructures, and for fundamental structure-property studies. Zuckermann, Cohen, and Barron et al. used α-chiral sidechains to probe the formation of α-helix from peptoids which have achiral backbones.[3, 104-105] Kirschenbaum et al have used peptoids as transfection reagents[106], foldamers for enantioselective catalysis[107], and as antimicrobial agents.[108] Peptoids have also been used recently in the formation of self- assembled nanostructures and as model systems to gain insight into polymeric assemblies. Peptoid amphiphiles were recently shown to form well-defined spherical structures when incorporating phenylethyl groups in alternating fashion into the hydrophilic segment of the amphiphile.[56] Zhang et al reported the tunability of the aggregation and radius of micellar self-assemblies in which the location of ionic functional groups was systematically varied.[102]

While sequence defined peptoids have received much research attention and applicability across a wide range of disciplines, polypeptoids, polymeric versions of peptoids derived from the ring opening polymerization of NCA monomers, have faced difficulty matching the diverse physiochemical properties of sequence-defined peptoids. Polypeptoids address many of the shortcomings that face sequence defined peptoids: they are easily scalable from milligram to multi gram scales, polymerizations can achieve high molecular weight (>30,000 g/mol) without joining two or more shorter chains together, and the synthetic methods are not as wasteful in reagent, equipment, and time costs. While synthetic routes to polypeptoids are also modular in nature, they do not share the same freedom and simplicity of sequence-defined peptoids in varying the polymer side chains. Traditional routes to NCA monomers for later polymerization into polypeptoids begin with either the Gibbs glyoxylic acid reduction method[13] or amination of a haloacetate ester with the desired primary amine.[9] Both routes employ relatively harsh conditions during synthesis which can preclude reactive sidechains, even when reactive functional groups are protected. This has generally limited the scope of available chemistries of polypeptoid sidechains to simple alkyl and aromatic groups, with limited exceptions.[2, 12] Allyl and propargyl sidechains have been used for post-polymerization modification to increase the functionality of the parent polypeptoid.[11]

In chapter 2 we reported the synthesis and characterization of a library of sequence-defined ionic peptoid block copolymers, in which the position of an ionic monomer is precisely located along the polymer chain.[102] The precise placement of ionic monomers allows for a unique ability to tune the radius and aggregation number of micelles formed by these peptoids in aqueous solution. A significant limitation of this system is the synthetic limit to the length of the polymer chain. In general the SPSS method is limited to polymer chains with <50 monomers, due to an increase in impurities as the chain is grown longer.

In an effort to increase sidechain diversity and further investigate the effect of charged monomers on the solution-assembly of sequence-defined peptoid block copolymers (Chapter 2) with longer chain length, we proposed to investigate the synthesis of new *N*-carboxyl-containing monomers that are amenable to ring-opening polymerization and their use for the synthesis of polymeric analogs of previously reported sequence-defined peptoid block copolymers (Chapter 2).[54, 102] While polypeptoids obtained by polymerization methods do not offer the atomistic level of control over the monomer sequence that was afforded by SPSS, sequential polymerization of NCA monomers can be used to mimic sequence-defined ionic peptoid block copolymers having longer chain length. We propose the synthesis of a new NCA monomer **M1** (Scheme 4.1) with a *t*-butyl ester functionality on the side chain. When deprotected by treatment

Scheme 4.1. General synthesis of COE-NCA (**M1**).

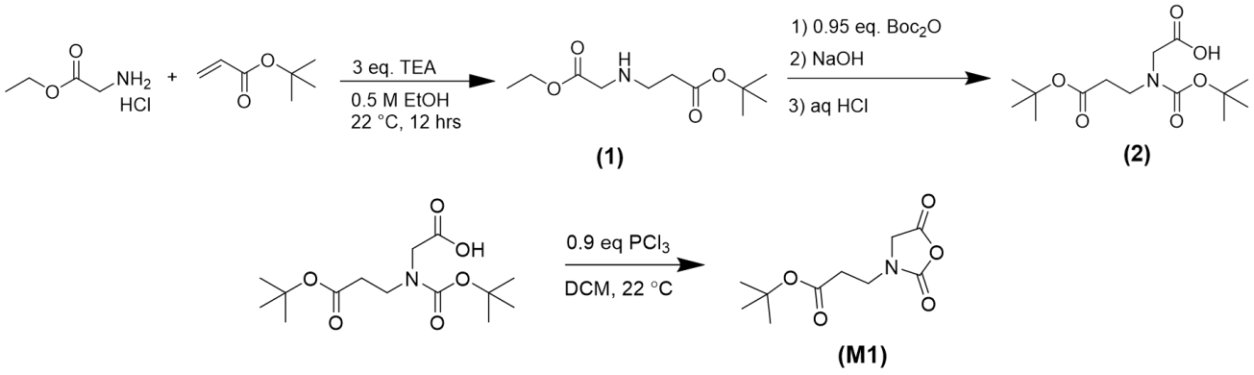

with acid the resulting carboxylic acid will mimic the carboxylate containing monomer used in the sequence-defined ionic peptoid block copolymers (Chapter 2). Utilizing sequential polymerization approach (Scheme 4.2) with appropriate co-monomers (**M2** and **M3**), we propose the synthesis of a 50olypeptoids block copolymer containing each of the three chemical functionalities present in the sequence-defined ionic peptoid block copolymers previously discussed in Chapter 2.

Scheme 4.2. Synthesis of *N*-carboxylic acid-containing polypeptoid block copolymer by sequential ring-opening polymerization approach.

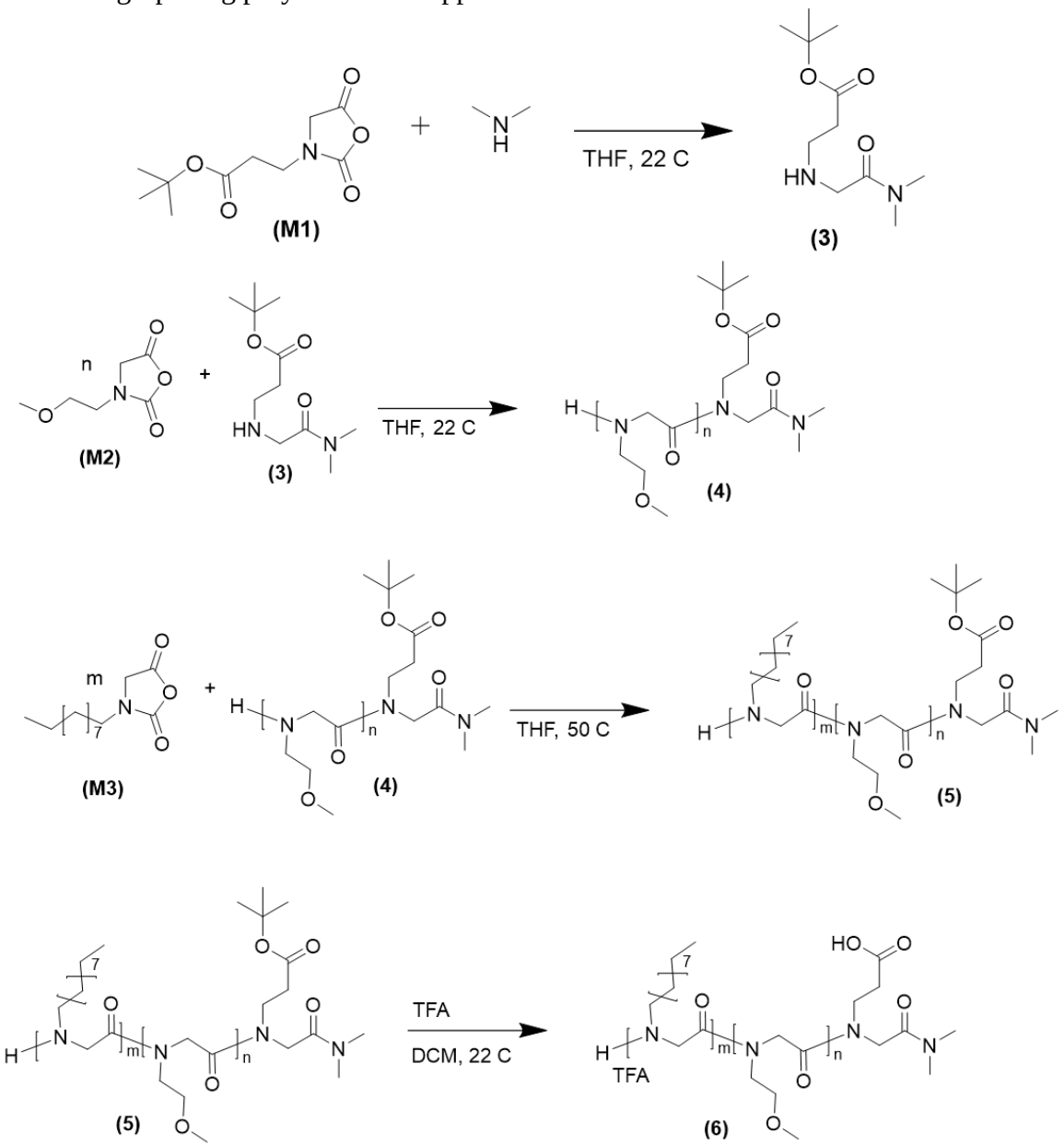

Herein we report the synthesis of a new NCA monomer, *N*-2-*t*-butoxycarboxyethyl-NCA (**M1**), the controlled polymerization of **M1** to form the corresponding poly(*N*-2-*t*-butoxycarboxyethyl glycine) polymer, and the well-controlled synthesis of block copolypeptoids

mimicking the monomer sequence of previously reported sequence-defined ionic peptoid block copolymers synthesized by SPSS methods.

4.2. Materials and Methods

4.2.1. Materials

Solvents used were HPLC grade or comparable and used as received. Dichloromethane, ethyl acetate, methanol, THF, and toluene were purchased from Fisher Chemical. Hexanes were purchased from Macron Fine Chemicals. Acetic acid (ACS gr) was purchased form Fisher Chemical. Glycine ethyl ester HCl (99%), and triethylamine (99+ %) were purchased from Alfa Aesar. Decylamine (>98.0 %) and tert-butyl acrylate (>98.0 %) were purchased from TCI. Di-tert-butyl pyrocarbonate (99.5 %) was purchased from Chem-Impex Int'l Inc. Hydrochloric acid aq. (37 %) and sodium hydroxide (ACS gr) were purchased from VWR. Phosphorous trichloride (98 %) was purchased from Beantown Chemical. Benzylamine and dimethylamine (2.0 M in THF), and 2-methoxyethylamine (99 %) were purchased from Sigma Aldrich.

4.2.2. Nuclear Magnetic Resonance Spectroscopy (NMR)

^{1}H and $^{13}C\{^{1}H\}$ NMR spectra were obtained using a Bruker AV-400 Nanobay spectrometer (400 MHz for ^{1}H NMR and 100 MHz for $^{13}C\{^{1}H\}$ NMR) and a Bruker AV-500 spectrometer (500 MHz for ^{1}H NMR and 125 MHz for $^{13}C\{^{1}H\}$ NMR) at 298 K. Chemical shifts (δ) given in parts per million (ppm) were referenced to protio impurities or the ^{13}C isotopes of deuterated solvents.

4.2.3. Fourier Transform Infrared Spectroscopy (FTIR)

FTIR spectra and polymerization monitoring were recorded on a Bruker ALPHA II FTIR spectrometer equipped with Platinum ATR. Data were processed using OPUS v7.2 software.

4.2.4. Gel Permeation Chromatography – Multi-Angle Light Scattering (GPC-MALS)

GPC of the polypeptoids was performed using an Agilent 1200 system (Agilent 1200 series degasser, isocratic pump, autosampler, and column heater) equipped with two (100 Å and 1000 Å) or three (100 Å, 1000 Å, and Linear(2)) Phenomenex 5 μm, 300 × 7.8 mm columns, a Wyatt OptilabrEX differential refractive index (DRI) detector with a 690 nm light source, and a Wyatt DAWN EOS multiangle light scattering (MALS) detector (GaAs 30mWlaser at $\lambda = 690$ nm). DMF with 0.1MLiBr was used as the eluent at a flow rate of 0.5 $mL \cdot min^{-1}$. The column and detector temperatures were set at 25 °C. All data analysis was performed using Wyatt Astra V 5.3 software. Polymer molecular weight (M_n) and molecular weight distribution (PDI) were obtained by the Zimm model fit of the MALS-DRI data. The absolute polymer molecular weight (M_n) was determined using the refractive index increment dn/dc value calculated from the Astra mass recovery template. The refractive index increment (dn/dc) of the polymer was determined to be 0.040 mL/g in DMF with 0.1 M LiBr.

4.2.5. Electrospray Ionization – Time of Flight Mass Spectrometry (ESI-TOF MS)

High Performance liquid chromatography (HPLC) coupled to accurate mass electrospray ionization (ESI) mass spectrometry was utilized in this analysis. Specifically, an Agilent 1260 Infinity II quaternary liquid chromatograph coupled to an Agilent 6230 Electrospray Time-of-Flight mass spectrometer was used for detection of analytes. The samples were run in positive mode ionization with a capillary voltage of 4000v. Drying gas (nitrogen) temperature was 325oC delivered at 10l/min and the fragmentor voltage was set to 150v. No LC column was used for sample delivery, only flow through injection was utilized (direct injection from LC to mass

spectrometer). Mobile phases used were A: 30% LCMS grade water with 0.1% formic acid and B: 70% LCMS grade acetonitrile with 0.1% formic acid with a flow rate of 0.4ml/min.

4.2.6. Dynamic Light Scattering (DLS)

All samples were prepared in ultrapure water at 0.5 wt % and filtered through 0.22 μm PES syringe filter (Restek) before measurement. Sample measurements were performed on a Wyatt HELEOS II equipped with a GaAs laser at 658 nm and a QELS detector at 90 °. Correlation functions were fit by cumulants analysis and data from at least 10 scans were averaged to obtain the hydrodynamic radius by using the Einstein-Stokes equation (Eq. 4.1), where R_h is the hydrodynamic radius, k_B is the Boltzmann constant, T is the temperature, η is the solution viscosity and D is the measured diffusion coefficient.

$$R_h = \frac{k_B T}{6\pi\eta D} \qquad \text{Eq. 4.1}$$

4.2.7. Synthesis of *N*-ethoxycarbonylmethyl-β-alanine *t*-butyl ester (1)

In a typical synthesis glycine ethyl ester HCl (14.53 g, 62.74 mmol) was dissolved in ethanol (0.5 M) with tert-butyl acrylate (9.10 mL, 62.4 mmol) and triethylamine (26 mL, 190 mmol). Reaction was allowed to stir for 12 h and was concentrated. Residue was mixed with hexane and filtered. Filtrate was concentrated to yield the product as a colorless to pale yellow oil (12.24 g, 52.92 mmol, 85 %).

^{1}H-NMR (Figure S4.1) (δ in $CDCl_3$, ppm): 1.27 (t, -$COCH_2CH_3$); 1.45 (s, $(CH_3)_3CCOOCH_2CH_2$-); 1.99 (s, -N*H*-); 2.43 (t, $(CH_3)_3CCOOCH_2CH_2$-); 2.88 (t, $(CH_3)_3CCOOCH_2CH_2$-); 3.40 (s, -$COCH_2$-); 4.19 (q, -$COCH_2CH_3$)

^{13}C-NMR (Figure S4.2) (δ in $CDCl_3$, ppm): 14.36 (-$COCH_2CH_3$); 28.24 ($(CH_3)_3CCOOCH_2CH_2$-); 36.11 ($(CH_3)_3CCOOCH_2CH_2$-); 45.11 ($(CH_3)_3CCOOCH_2CH_2$-); 51.04 (-$COCH_2$-); 60.86 (-$COCH_2CH_3$); 80.73 ($(CH_3)_3CCOOCH_2CH_2$-); 171.9 ($(CH_3)_3CCOOCH_2CH_2$-); 172.3 (-$COCH_2$-)

4.2.8. Synthesis of 2-[*N*-(*tert*-butoxycarbonyl)-*N*-[3-(*tert*-butoxy)-3-oxopropyl] amino] acetic acid (2)

Compound **1** (12.24 g, 52.92 mmol) was stirred in DI water (1 M) with triethylamine and di-tert-butyl dicarbonate (10.99 g, 50.4 mmol) for 12 h. Mixture was acidified to pH 2 with 4 M HCl aq. and extracted with ethyl acetate (3 x 150 mL). Organic extracts were concentrated to yield the product as a colorless oil. The oil was stirred with NaOH (2.22 g, 55.5 mmol) in MeOH:DI H_2O for 2 h. Solution was acidified to pH 2 with 4 M HCl aq. and extracted with ethyl acetate (3 x 150 mL). Organic extracts were combined and concentrated to yield the product as a colorless oil (11.71 g, 38.6 mmol, 73%).

^{1}H-NMR (Figure S4.3) (δ in $CDCl_3$, ppm): 1.44 (s, (CH_3)$_3$CCOOCH$_2$CH$_2$-); 1.48 (s, -NCOOC(CH_3)$_3$); 2.53 (t, (CH_3)$_3$CCOOCH$_2$CH_2-); 3.52 (t, (CH_3)$_3$CCOOCH_2CH$_2$-); 4.01 and 4.07 (s, -COCH_2-); 9.64 (s, -COO*H*)

^{13}C-NMR (Figure S4.4) (δ in $CDCl_3$, ppm): 28.23 ((*C*H$_3$)$_3$CCOOCH$_2$CH$_2$- and (*C*H$_3$)$_3$CCOON-); 35.23 ((CH$_3$)$_3$CCOOCH$_2$*C*H$_2$-); 44.98 ((CH$_3$)$_3$CCOO*C*H$_2$CH$_2$-); 50.33 (-CO*C*H$_2$-); 81.04 ((CH$_3$)$_3$*C*COOCH$_2$CH$_2$- and (CH$_3$)$_3$*C*COON-); 155.56 ((CH$_3$)$_3$C*C*OON-); 171.9 ((CH$_3$)$_3$C*C*OOCH$_2$CH$_2$); 175.6 (-*C*OOH)

4.2.9. Synthesis of *N*-2-t-butoxycarboxyethyl NCA (COE-NCA, M1)

Compound **2** (11.71 g, 38.60 mmol) was dissolved in dry DCM (0.25 M) with PCl_3 (3.0 mL, 34 mmol) and was allowed to stir for 14 h. The solution was concentrated under vacuum and residue was filtered through a silica plug with DCM. The filtrate was concentrated to yield the product as a pale yellow oil (2.8861 g, 12.590 mmol, 33 %). The monomer was used in the polymerization without further purification.

^{1}H-NMR (Figure S4.5) (δ in $CDCl_3$, ppm): 1.45 (s, $(CH_3)_3CCOOCH_2CH_2$-); 2.60 (t, $(CH_3)_3CCOOCH_2CH_2$-); 3.64 (t, $(CH_3)_3CCOOCH_2CH_2$-); 4.25 (s, -$COCH_2$-)

^{13}C-NMR (Figure S4.6) (δ in $CDCl_3$, ppm): 28.19 ($(CH_3)_3CCOOCH_2CH_2$-); 33.94 ($(CH_3)_3CCOOCH_2CH_2$-); 39.84 ($(CH_3)_3CCOOCH_2CH_2$-); 50.34 (-$COCH_2$-); 82.03 ($(CH_3)_3CCOOCH_2CH_2$-); 152.3 (-N*C*OO-); 165.7 (-*C*OCH_2-); 170.7 ($(CH_3)_3CCOOCH_2CH_2$-)

4.2.10. Synthesis of poly(*N*-2-*t*-butoxycarboxyethyl glycine)

In a typical polymerization, **M1** (56.1 mg, 0.245 mmol) was dissolved in toluene (0.5 M). Benzylamine in toluene (0.2 M, 6.2 µL, 1.2 umol) was added for the target [M]:[I] ratio 200:1. Solution was stirred at 23 °C and conversion was monitored by FTIR spectroscopy (Figure S4.7). Solution was concentrated under vacuum to yield a sticky, viscous oil (41.8 mg, 1.23 umol, 92%). Polymer samples were freeze dried from DMSO to remove residual toluene before NMR end group analysis.

4.2.11. Synthesis of *N*-Methoxyethyl NCA (M2)

N-Methoxyethyl NCA (MeOEt-NCA) was prepared according to reported procedures.[9]

4.2.12. Synthesis of *N*-Decyl NCA (M3)

N-Deyl NCA (De-NCA) was prepared according to reported procedures.[109]

4.2.13. Synthesis of poly(*N*-2-carboxyethyl glycine)-*b*-poly(*N*-2-methoxyethyl glycine)-*b*-poly(*N*-decyl glycine) (7)

To a solution of **M1** (152.3 mg, 0.6644 mmol) was added dimethylamine in THF (2.0 M) (332.2 µL, 0.6644 mmol). Solution was allowed to stir overnight and was concentrated to yield a white residue **3** (115.2 mg, 0.4990 mmol, 75 %). The residue was characterized by ESI-MS and used as the initiator for polymerization of **M2** (Figure S4.8). To a solution of **M2** (271.5 mg, 1.706 mmol) was added of compound **3** (20.7 mg, 89.6 µmol). The solution was allowed to stir overnight and was then concentrated to yield a slightly yellow powder **4** (161.9 mg, 42.6 µmol, 77 %). A

portion was taken for analysis by GPC. Compound **4** (96.3 mg, 25.3 μmol) was dissolved in THF (0.5 M). To the solution was added **M3** (34.6 mg, 0.143 mmol). The solution was allowed to stir overnight before being concentrated to yield a slight yellow powder **5**. Peptoid was stirred in TFA, evaporated, and freeze dried from water to yield **6**. The peptoid was then dissolved in THF and to the solution was added acetic anhydride and triethylamine (5 eq). Polymer was precipitated by pouring into hexane to yield a waxy residue **7** (113.4 mg, 22.8 μmol, 96%).

4.2.14. Measurement of Polymerization Kinetics

In a typical polymerization, **M1** (63.6 mg, 0.277 mmol) was dissolved in toluene-d8 (0.55 mL) under a nitrogen atmosphere. To the vial was added *n*-butylamine (0.199 M in toluene-d8) for an initial $[M]_0$:$[I]_0$ ratio of 100:1 (14.0 uL, 2.79 umol) and the time was recorded as t=0. The solution was transferred to an NMR tube and ^{1}H spectra were recorded at preset time intervals (either 5 or 15 min). Polymerizations were conducted with initial $[M]_0$:$[I]_0$ ratios of 50:1 and 25:1 by adjusting the amount of *n*-butylamine added. The observed reaction rate constant k_{obs} was taken as the slope of the plot of $\ln(M_o/M) = k_{obs}(t)$, where M_o is the initial monomer concentration and M is the monomer concentration at time t. Error on k_{obs} was obtained from two measurements.

4.3. Results and Discussion

4.3.1. Synthesis of *N*-2-*t*-butoxycarboxyethyl-NCA (COE-NCA)

Several considerations went into the design of an appropriate monomer to ultimately yield the desired N-substituted glycine polymer with a carboxylic acid-bearing sidechain. Due to the use of a carboxylic acid activating agent during the monomer cyclization step, an ester was chosen as the protecting group for the sidechain. Esters can be easily deprotected under either acidic or basic conditions. The length of the sidechain was initially chosen to include the same number of non-hydrogen atoms, four, as the sidechain in poly(*N*-methoxyethyl glycine) (Scheme 4.3).

Scheme 4.3. Chemical structures of poly(*N*-substituted glycine)s considered in monomer design. The methoxyethyl and carboxymethyl sidechains both contain four non-hydrogen atoms, while the carboxyethyl sidechain contains five non-hydrogen atoms.

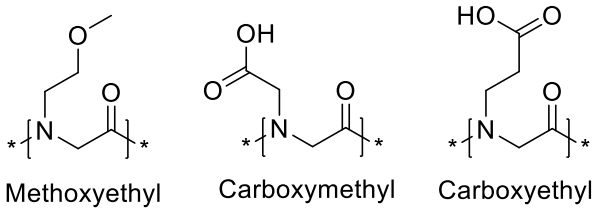

Several generations of ester containing NCAs or NCA precursors were synthesized (Scheme 4.4), but most proved difficult to polymerize in a well-controlled manner. Under polymerization conditions initiated by a primary amine, monomer **G1** quickly formed diketopiperazine structures as observed in ESI-MS (Figure S4.13). The propagating chain end reacted with the sidechain of the previously added monomer, terminating the chain and polymerization. A t-butyl ester was chosen for monomer G2 to mitigate the chain termination affecting G1, but no significant improvement in polymerization efficiency was observed. To avoid the formation of the six membered diketopiperazine ring, the sidechain was lengthened by 1 carbon atom for **G3** and **M1**, leaving only the opportunity for backbiting with a sidechain to form a 7-membered ring which should be disfavored. **G3** was designed as a latent NCA monomer for improved stability. Doriti et al. have previously shown that an *N*-phenoxycarbonyl protected *N*-substituted glycine can be used to generate an NCA and polymerize in-situ in the presence of an initiator, tertiary amine base and heat.[110] While this approach works well for short alkyl sidechains, the bulky **G3** does not polymerize and decomposes when heated above 50 °C.

Scheme 4.4. Synthesized *N*-carboxyl ester-containing NCAs and related precursors.

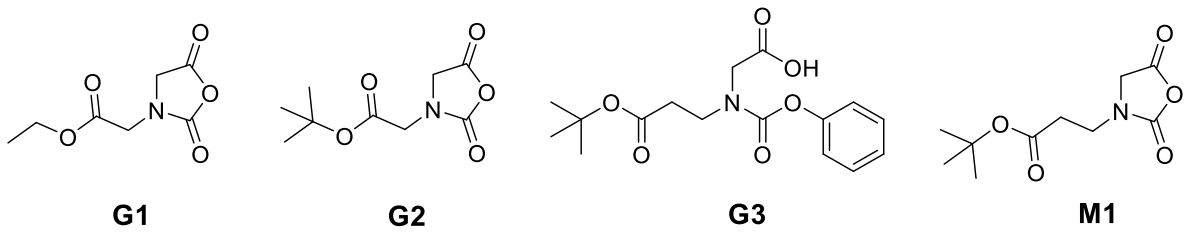

The synthesis of an NCA monomer containing a deprotectable ester (**M1**) was accomplished by the synthesis of an asymmetric diester with orthogonal ester deprotection chemistries, followed by Boc protection of the amine, deprotection of the glycine ester, and finally ring closure (Scheme 4.1). The synthesis of a suitable asymmetric diester, compound **1**, involves Michael addition utilizing glycine ethyl ester and t-butyl acrylate to provide ethyl and t-butyl esters which can be selectively deprotected under basic and acidic conditions, respectively. Boc protection of the amine, followed by treatment with base to hydrolyze the ethyl ester to form **2**, provides the necessary carboxy functionalities used in typical NCA cyclization. Treatment of **2** with a carboxylic acid activating agent, such as PCl_3 yields **M1**.

4.3.2. Polymerization Kinetics

Polymerizations of N-substituted NCAs are well known to proceed in a pseudo living manner via pseudo first order kinetics.[17] It is important to check whether this remains true for bulky, and especially functional, sidechains. Polymerization of **M1** was studied extensively in toluene, as well as briefly in DCM, THF, and MeCN. Initial tests synthesizing low MW poly(**M1**) confirmed ability of **M1** to be ring-opened by primary amine and propagate via primary amine mechanism. To investigate the kinetics of the polymerization, **M1** was weighed into a vial and dissolved in dry toluene-d8 at 0.5 M under a nitrogen atmosphere. The vial was stirred to dissolve the monomer before the appropriate amount of butylamine in toluene-d8 was then injected into the

vial to initiate the polymerization. While the monomer concentration was kept constant, the initiator (butylamine) loading was varied from 5.1 mM, to 9.7 mM, to 19.9 mM, in order to target [M]:[I] ratios of 100:1, 50:1, and 25:1, respectively. Reaction conversion was followed by ^{1}H-NMR at ambient pressure and 23 °C in Tol-d8. By monitoring the conversion of a characteristic monomer peak (δ = 2.04 ppm) into polymer (δ = 2.88-2.31 ppm), both the monomer conversion over time and the polymerization kinetics can be tracked (Figure S4.16). In the case of COE-NCA, it was found that the polymerization also follows first-order kinetics in the concentration range of initiator studied. When the $\ln(M_o/M)$ is plotted vs time (t) the plots all remain linear, even at high monomer conversion (>95 %). The linearity of this data is indicative of a pseudo-first order kinetic and is expected of typical *N*-substituted NCA polymerizations. The rate of polymerization of *N*-substituted NCA monomers have been studied in the literature with respect to the solvent quality (polarity), N-substituents, and pressure.[17] In less polar solvents, the reaction kinetics are enhanced relative to more polar solvent systems, while *N*-substituents were found to decrease the rate of polymerization as the bulkiness of the substituent increased. When polymerizing *N*-substituted NCA monomers under reduced pressure no dependence of reaction kinetics on the pressure was found.[6] The kinetic result is consistent with a polymerization of a *N*-substituted NCA monomer by the normal amine mechanism. The polymerization proceeded relatively rapidly, reaching quantitative or near quantitative conversion in approximately 6 h for the slowest set of samples measured ($[M]_o:[I]_o$ = 100:1). The observed rate constant increased systematically from 0.6±0.2, to 2.08±0.05, to 3.22±0.05 h^{-1} as the concentration of initiator was increased from 5.1 mM, to 9.7 mM, to 19.9 mM (Figure 4.1A, Table 4.1).

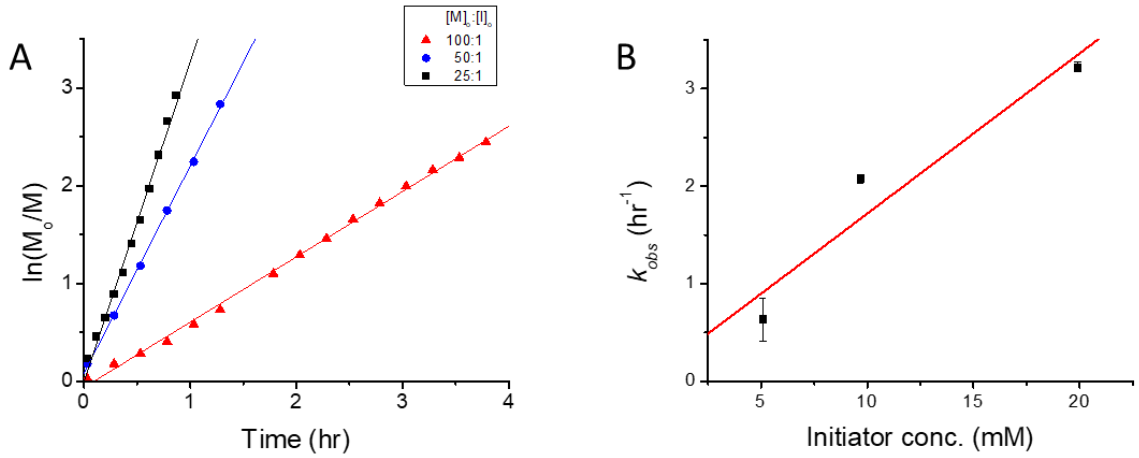

Figure 4.1. A.) Representative kinetic study of COE-NCA polymerization in toluene initiated by *n*-butylamine. M_o = 0.5 M, T = 23 °C, I_o = 5.1 mM (▲), 9.7 mM (●), 19.9 mM (■) with linear fits (R2 = 0.99, 0.99, 0.99). Data were fit using the equation $\ln(M_o/M) = k_{obs}(t)$. k_{obs} = 0.6±0.2; 2.08±0.05; 3.22±0.05 h^{-1}. B.) Plot of k_{obs} vs I_o for N-2-t-butoxycarboxyethyl-NCA. From the linear fitting of the data a k_p = 160±50 $M^{-1}hr^{-1}$ was obtained.

Table 4.1. Observed rate constant (k_{obs}) of COE-NCA polymerization in toluene initiated by *n*-butylamine.

$[M]_o/[I]_o$	k_{obs} (h^{-1})	Conv. (%)
25	3.22±0.05	>99
50	2.08±0.05	>99
100	0.6±0.2	>99

The polymerization rate constant k_p was obtained by the linear fitting of k_{obs} vs I_o (R^2 = 0.92) (Figure 4.1B). The polymerization rate constant was found to be 160±50 $M^{-1}hr^{-1}$ at a concentration of 0.5 M in toluene at 23 °C. This rate constant is approximately twice that found for Sarcosine NCA under a range of experimental conditions.[5]

4.3.3. Polymer Characterization

Several polymerizations were conducted in toluene with varying initial $[M]_0:[I]_0$ ratios to assess polymerization control over molecular weight and dispersity. The monomer to initiator ratio was systematically varied between 25 and 400, to target molecular weights between 4700 and

74,000 g/mol. It was found that for all $[M]_0$:$[I]_0$ ratios studied, the resulting molecular weights are all higher than the theoretical molecular weights based on living polymerization initiated by primary amine. Specifically, with increasing $[M]_0$:$[I]_0$ ratio, DP calculated from GPC chromatograms (45, 77, 124, 259, and 388) was found to increase accordingly, despite they are all higher than targeted DP of 24, 48, 101, 197 and 371, respectively (Figure 4.2, Table 4.2). All obtained chromatograms showed narrow, monomodal peaks with a slight tail skewed toward low molecular weight (Figure 4.3B). The PDI for all samples was narrow, and decreased slightly with increasing $[M]_0$:$[I]_0$ ratio from 1.04 to 1.01 (Figure 4.2A). Molecular weights determined by GPC agree reasonably with those obtained by end-group analysis using ^{1}H-NMR. Specifically, end group analysis by ^{1}H-NMR in CD_2Cl_2 was performed by comparison of integration values for the end group phenyl protons at 7.18-7.37 ppm with the polymer sidechain t-butyl protons at 1.31-1.53 ppm (Figure S4.15). Degree of polymerization by NMR for each sample was found to be 30, 55, 76 and 208, which deviates somewhat form the targeted DPs of 24, 48, 101, and 197 (Figure 4.2A, Table 4.2). End-group analysis of the largest polymer ($[M]_0$:$[I]_0$ = 371) was deemed less reliable and were not reported, due to overlap of the phenyl group protons with residual solvent.

Table 4.2. Polymerization data for COE-NCA initiated by *n*-benzylamine, M_o = 0.5 M, T = 23 °C.

Target $[M]_0$:$[I]_0$	Targeted DP	M_n (Theor.)	DP (NMR)	M_n (NMR)	DP (GPC)	M_n (GPC)	PDI (GPC)
25	24.2	4580	29.8	5630	45	8400	1.04
50	48.4	9060	55.3	10400	77	14300	1.03
100	101	18900	76.3	14200	124	23100	1.01
200	197	36700	208	38700	259	48100	1.01
400	371	68900	--	--	388	71900	1.01

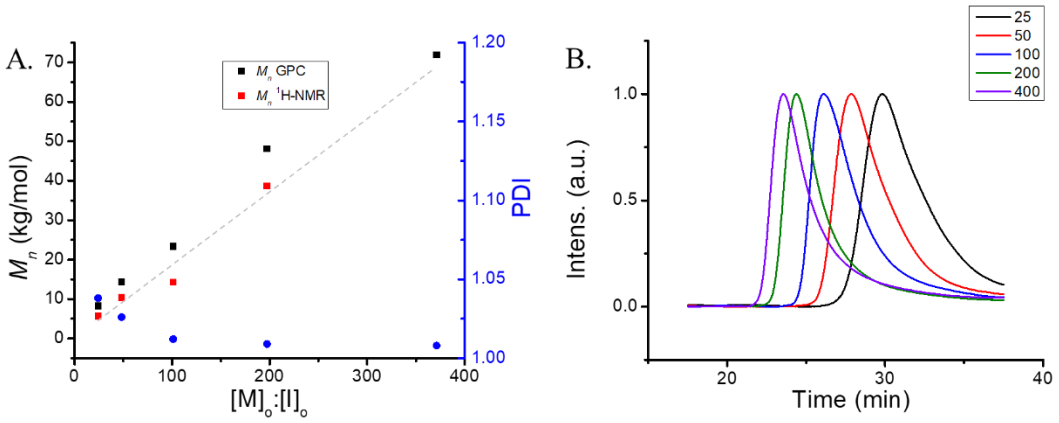

Figure 4.2. A) Plots of M_n obtained by ^{1}H NMR and GPC analysis vs $[M]_o$:$[I]_o$ (left axis) and PDI vs $[M]_o$:$[I]_o$ (right axis). B) GPC chromatograms of polypeptoids obtained by polymerization of COE-NCA with *n*-benzylmine. $[M]_o$:$[I]_o$ was varied from 25, 50, 100, 200, 400.

4.3.4. Synthesis of Block Copolypeptoids containing *N*-2-Carboxyethyl Sidechains.

Synthesis of a polymeric analogue of the sequence-defined peptoid block copolymers (Chapter 2, sequence 1) has been investigated by sequential ring-opening polymerization of the corresponding *N*-substituted NCA monomers (Scheme 4.2). The ring opening addition of **M1** can be affected with a stoichiometric amount of *N*,*N*-dimethylamine to yield the *tert*-butyl 3-[[2-(dimethylamino)-2-oxoethyl]amino]propanoate (**3)**. The synthesis of **3** was confirmed by ESI-MS, which showed only major peaks corresponding to the H^+ and Na^+ adducts at 231.172 and 253.153 m/z, as well as a peak corresponding to the deprotected ester at 175.108 m/z, likely induced by the formic acid used in the ESI-MS measurement (Figure S4.8). Compound **3** can be used as an initiator for the polymerization of *N*-methoxyethyl NCA, yielding the polypeptoid **4** with a *t*-butyl ester group at one terminus, allowing for late-stage deprotection to yield a carboxylic acid. Polymer **4** was analyzed by ^{1}H NMR and GPC methods. End group analysis by ^{1}H NMR method revealed a DP of 22 (Figure S4.9). Analysis by GPC showed a monomodal peak corresponding to M_n = 3800 g/mol and a DP = 31 with PDI = 1.07 (Figure S4.10).

Further chain extension utilizing the polymer **4** as a macroinitiator and *N*-decyl NCA monomers was performed to form the amphiphilic polypeptoid block copolymer **5** (Figure S4.11). Treatment of **5** with trifluoroacetic acid afforded polypeptoid block copolymer **6** bearing a carboxylic acid functional group (Figure S4.12). ^{1}H NMR end-group analysis revealed a final polypeptoid composition with n=23 and m=4. Acylation of the terminal *N*-decyl secondary amine was performed by using acetic anhydride and triethylamine in THF, yielding the desired end-acylated polypeptoid block copolymer **7**. Analysis of the final polypeptoid **7** by ^{1}H NMR was not sufficient to assess the quantitative acylation of the peptoid, and insolubility in DMF and THF prevented analysis by GPC.

Scheme 4.3. Acylation of *N*-carboxylic acid containing block copolymer **7**.

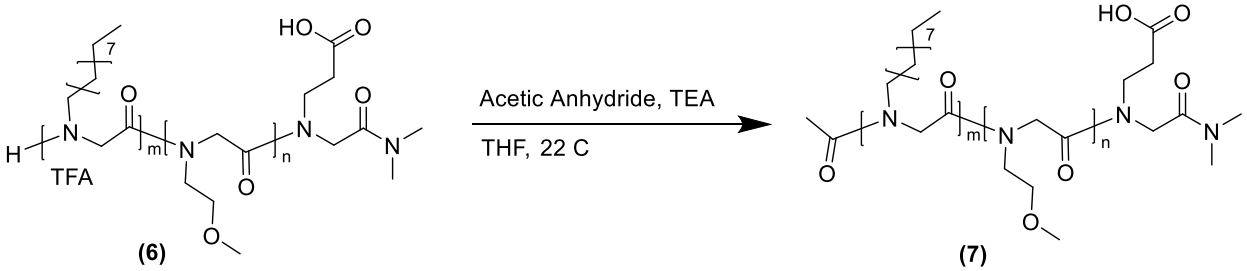

To assess whether the final polypeptoids block copolymer **7** can assemble into a micelle in water and mimic the behavior of the previously reported sequence defined ionic peptoid amphiphile (sequence 2, chapter 2), the polymer **7** was dissolved in nanopure water at 5 mg/mL and the pH of the solution was adjusted to pH 9, which is to ensure the majority of the carboxylic acid groups remain in the ionized state. The block copolymer solution was analyzed by DLS to characterize the size of the solution aggregates (Figure S4.14). The polypeptoids were found to form well-defined and stable aggregates with a measured R_h = 32±2 nm. This value is much larger than the

analogous sequence-defined peptoid block copolymer having a discrete chain length of 25 (R_h = 7±2 nm, Chapter 2).

4.4. Conclusions

A new *N*-substituted *N*-carboxyanhydride monomer bearing a deprotectable t-butyl ester (COE-NCA) on the side chain was synthesized. It was demonstrated that the ring-opening polymerization of COE-NCA can be efficiently initiated by primary amine and secondary amines (*i.e.*, *N*,*N*-dimethylamine), and the polymerization occurred by the normal amine mechanism. Polymerization of COE-NCA conducted in toluene was found to proceed rapidly and is in the range expected for polymerization of *N*-substituted NCAs with bulky sidechains in a low polarity solvent. Kinetic studies revealed a first-order dependence on the monomer concentration, consistent with the polymerization occurring by the normal amine mechanism.

The polymerization of COE-NCA was further investigated to assess the control over the polymerization with respect to molecular weight and polydispersity. A range of molecular weights from 5 to 70 kg/mol as determined by ^{1}H NMR and GPC analysis can be obtained by systematically varying the monomer-to-initiator loading. Polydispersity remained low for all investigated polymerizations and decreased with increasing $[M]_0$:$[I]_0$ ratio, as is expected of a living polymerization.

An amphiphilic polypeptoids block copolymer containing the *N*-2-carboxyethyl sidechains, a polymeric analog of the sequence-defined ionic peptoid amphiphile discussed in Chapter 2, has been synthesized by sequential ring-opening polymerization of COE-NCA, MeOEt-NCA, and De-NCA using *N*,*N*-dimethylamine initiators and post-polymerization deprotection to reveal the *N*-2-carboxylethyl sidechains. The resulting polymer was shown to self-assemble into well-defined aggregate in DI water (pH = 9), evidenced by DLS analysis.

CHAPTER 5. CONCLUSION

This work focused on the synthesis and characterization of well-defined materials to further the fundamental understanding and application of ionic block copolymer self-assemblies and more specifically those comprised of peptidomimetic polymers. In chapter 2, SPSS methods were adapted to synthesize a library of sequence-defined ionic peptoid block copolymers containing an ionic carboxylate-containing monomer, a hydrophilic neutral, and a hydrophobic monomer. The block lengths of the hydrophilic and hydrophobic blocks were conserved. The location of a single, or cluster of three ionic monomers, was systematically varied along the polymer hydrophilic block. Upon dissolution in water at pH = 9 the sequence-defined ionic peptoid block copolymers formed well-defined aggregates in solution. Utilizing SANS it was observed that the micellar radius and aggregation number depended significantly on the location of the ionic monomers along the polymer chain. As the ionic monomer was placed successively closer to the micelle core-shell interface, the radius and aggregation number systematically decreased. This observation demonstrated the importance of the location of ionic monomers in polyelectrolyte complexes and introduced a new mechanism to tune the physical properties of assemblies of ionic block copolymers.

To further explore the tunability of micellar self-assemblies of sequence-defined ionic peptoid block copolymers, the dependence of the hydrodynamic radius on the solution pH was studied in chapter 3. Sequence-defined ionic peptoid block copolymers were dissolved in water and the micelle hydrodynamic radius was measured as the solution pH was systematically raised. Due to the carboxylic acid functionality, the unadjusted pH of the micelle solution was ~ pH = 3. By adding sodium hydroxide to the solution the acid groups were deprotonated, leading to an increase in the charge fraction of the micelles with increasing pH. As the pH was increased, the

library of sequence defined ionic peptoid block copolymers showed unique behavior. The sample with the ionic group furthest from the micelle core-shell interface increased in radius, while the sample with the ionic monomer closest to the core-shell interface showed a decrease in its measured hydrodynamic radius. Samples with an intermediate placement of the ionic monomer appeared relatively insensitive to changes in the solution pH.

In chapter 4, as an extension of the work on sequence-defined ionic peptoid block copolymers, a polymeric analogue was developed. Polypeptoids are commonly accessed by polymerization of N-carboxyanhydride monomers. NCA monomers to access the hydrophilic neutral and hydrophobic moieties used in chapters 2 and 3 have been reported in the literature. A suitable monomer to yield the ionic sidechain has not been previously reported. An NCA bearing a t-butyl ester on the sidechain was synthesized and its ability to polymerize in a well-controlled manner was assessed, as well as the ability to be incorporated into a BCP utilizing sequential polymerization techniques. It was found that the monomer (N-2-t-butoxycarboxyethyl-NCA) polymerized in a pseudo living manner. A BCP prepared by sequential polymerization of N-2-t-butoxycarboxyethyl-NCA, N-methoxyethyl-NCA, and N-decyl-NCA, and deprotection of the t-butyl ester, formed aggregates when dissolved in a basic aqueous solution, although formed aggregates were much larger than expected.

Biological molecules such as proteins and DNA utilize sequence specific patterning of monomers, especially ionic monomers, to stabilize a desired structure or affect a specific structural change to drive a particular function.[57] While this use of sequence specificity is well known, there is still a limited understanding of how to harness this tool for synthetic systems.[111] Both polyelectrolyte complexes and synthetic sequence specific molecules, despite decades of research, still seem to be in their infancy with respect to their utility.

Overall this work serves to demonstrate the utility of sequence-defined peptoids and polypeptoids to be used as model systems for fundamental material property studies, as well as their potential application as highly tunable biomaterials. Micelles have found abundant use as drug carriers with a range of targets including cancer[112]. There is still a need for better control over material structure and the resulting properties, and this work affords a highly tunable, biocompatible platform for further development. Additionally this work may serve as a springboard for more fundamental studies into solution self-assemblies. Of interest are larger, more extended structures, such as worms or fibrils, and vesicles. These structures may be accessed by tuning the length and volume fraction of the hydrophilic and hydrophobic blocks, with the possibility of precisely controlling the size and structure of these much larger assemblies. Currently these types of structures face the same obstacles to a complete level of control over the structure and tunability of the material as spherical micelles, namely a lack of synthetic control during polymer synthesis.[99] Patterning ionic monomers within these structures may offer a new level of control over their assembly and structures.

REFERENCES

1. Zuckermann, R. N., Peptoid origins. *Peptide Science* **2011,** *96* (5), 545-555.

2. Zhang, D.; Lahasky, S. H.; Guo, L.; Lee, C.-U.; Lavan, M., Polypeptoid Materials: Current Status and Future Perspectives. *Macromolecules* **2012,** *45* (15), 5833-5841.

3. Armand, P.; Kirshenbaum, K.; Falicov, A.; Dunbrack, R. L.; Dill, K. A.; Zuckermann, R. N.; Cohen, F. E., Chiral N-substituted glycines can form stable helical conformations. *Folding and Design* **1997,** *2* (6), 369-375.

4. Lee, C.-U.; Li, A.; Ghale, K.; Zhang, D., Crystallization and Melting Behaviors of Cyclic and Linear Polypeptoids with Alkyl Side Chains. *Macromolecules* **2013,** *46* (20), 8213-8223.

5. Fetsch, C.; Gaitzsch, J.; Messager, L.; Battaglia, G.; Luxenhofer, R., Self-Assembly of Amphiphilic Block Copolypeptoids – Micelles, Worms and Polymersomes. *Scientific Reports* **2016,** *6*, 33491.

6. Fetsch, C.; Grossmann, A.; Holz, L.; Nawroth, J. F.; Luxenhofer, R., Polypeptoids from N-Substituted Glycine N-Carboxyanhydrides: Hydrophilic, Hydrophobic, and Amphiphilic Polymers with Poisson Distribution. *Macromolecules* **2011,** *44* (17), 6746-6758.

7. Guo, L.; Li, J.; Brown, Z.; Ghale, K.; Zhang, D., Synthesis and characterization of cyclic and linear helical poly(α-peptoid)s by N-heterocyclic carbene-mediated ring-opening polymerizations of N-substituted N-carboxyanhydrides. *Peptide Science* **2011,** *96* (5), 596-603.

8. Sun, J.; Stone, G. M.; Balsara, N. P.; Zuckermann, R. N., Structure–Conductivity Relationship for Peptoid-Based PEO–Mimetic Polymer Electrolytes. *Macromolecules* **2012,** *45* (12), 5151-5156.

9. Xuan, S.; Gupta, S.; Li, X.; Bleuel, M.; Schneider, G. J.; Zhang, D., Synthesis and Characterization of Well-Defined PEGylated Polypeptoids as Protein-Resistant Polymers. *Biomacromolecules* **2017,** *18* (3), 951-964.

10. Luxenhofer, R.; Fetsch, C.; Grossmann, A., Polypeptoids: A perfect match for molecular definition and macromolecular engineering? *Journal of Polymer Science Part A: Polymer Chemistry* **2013,** *51* (13), 2731-2752.

11. Zhu, L.; Simpson, J. M.; Xu, X.; He, H.; Zhang, D.; Yin, L., Cationic Polypeptoids with Optimized Molecular Characteristics toward Efficient Nonviral Gene Delivery. *ACS applied materials & interfaces* **2017,** *9* (28), 23476-23486.

12. Chan, B. A.; Xuan, S.; Li, A.; Simpson, J. M.; Sternhagen, G. L.; Yu, T.; Darvish, O. A.; Jiang, N.; Zhang, D., Polypeptoid polymers: Synthesis, characterization, and properties. *Biopolymers* **2018,** *109* (1), e23070.

13. Gibbs, T. J. K.; Boomhoff, M.; Tomkinson, N. C. O., A Mild and Efficient Method for the One-Pot Monocarboxymethylation of Primary Amines. *Synlett* **2007,** *2007* (10), 1573-1576.
14. Leuchs, H., Ueber die Glycin-carbonsäure. *Berichte der deutschen chemischen Gesellschaft* **1906,** *39* (1), 857-861.

15. Birke, A.; Huesmann, D.; Kelsch, A.; Weilbächer, M.; Xie, J.; Bros, M.; Bopp, T.; Becker, C.; Landfester, K.; Barz, M., Polypeptoid-block-polypeptide Copolymers: Synthesis, Characterization, and Application of Amphiphilic Block Copolypept(o)ides in Drug Formulations and Miniemulsion Techniques. *Biomacromolecules* **2013,** *15* (2), 548-557.

16. Fuchs, F., Über N-Carbonsäure-anhydride. *Berichte der deutschen chemischen Gesellschaft (A and B Series)* **1922,** *55* (9), 2943-2943.

17. Gangloff, N.; Ulbricht, J.; Lorson, T.; Schlaad, H.; Luxenhofer, R., Peptoids and Polypeptoids at the Frontier of Supra- and Macromolecular Engineering. *Chemical reviews* **2016,** *116* (4), 1753-1802.

18. Chan, B. A.; Xuan, S.; Horton, M.; Zhang, D., 1,1,3,3-Tetramethylguanidine-Promoted Ring-Opening Polymerization of N-Butyl N-Carboxyanhydride Using Alcohol Initiators. *Macromolecules* **2016,** *49* (6), 2002-2012.

19. Tao, X.; Deng, Y.; Shen, Z.; Ling, J., Controlled Polymerization of N-Substituted Glycine N-Thiocarboxyanhydrides Initiated by Rare Earth Borohydrides toward Hydrophilic and Hydrophobic Polypeptoids. *Macromolecules* **2014,** *47* (18), 6173-6180.

20. Simon, R. J.; Kania, R. S.; Zuckermann, R. N.; Huebner, V. D.; Jewell, D. A.; Banville, S.; Ng, S.; Wang, L.; Rosenberg, S.; Marlowe, C. K., Peptoids: a modular approach to drug discovery. *Proceedings of the National Academy of Sciences* **1992,** *89* (20), 9367-9371.

21. Figliozzi, G. M.; Goldsmith, R.; Ng, S. C.; Banville, S. C.; Zuckermann, R. N., [25] Synthesis of N-substituted glycine peptoid libraries. *Methods in Enzymology* **1996,** *Volume 267*, 437-447.

22. Merrifield, R. B., Solid Phase Peptide Synthesis. I. The Synthesis of a Tetrapeptide. *Journal of the American Chemical Society* **1963,** *85* (14), 2149-2154.

23. Zuckermann, R. N.; Kerr, J. M.; Kent, S. B. H.; Moos, W. H., Efficient method for the preparation of peptoids [oligo(N-substituted glycines)] by submonomer solid-phase synthesis. *Journal of the American Chemical Society* **1992,** *114* (26), 10646-10647.

24. Jain, S.; Bates, F. S., On the Origins of Morphological Complexity in Block Copolymer Surfactants. *Science* **2003,** *300* (5618), 460.

25. Whitesides, G. M.; Mathias, J. P.; Seto, C. T., Molecular self-assembly and nanochemistry: a chemical strategy for the synthesis of nanostructures. *Science* **1991,** *254* (5036), 1312.

26. Deng, Y.; Wei, J.; Sun, Z.; Zhao, D., Large-pore ordered mesoporous materials templated from non-Pluronic amphiphilic block copolymers. *Chemical Society Reviews* **2013,** *42* (9), 4054-4070.

27. Hamley, I. W., Introduction. *Block Copolymers in Solution: Fundamentals and Applications* **2012**.

28. Discher, D. E.; Ahmed, F., POLYMERSOMES. *Annual Review of Biomedical Engineering* **2006,** *8* (1), 323-341.

29. Dutt, S.; Siril, P. F.; Remita, S., Swollen liquid crystals (SLCs): a versatile template for the synthesis of nano structured materials. *RSC Advances* **2017,** *7* (10), 5733-5750.

30. Hamley, I. W., Neutral Block Copolymers in Dilute Solution. *Block Copolymers in Solution: Fundamentals and Applications* **2012**, 7-104.

31. Booth, C.; Attwood, D., Effects of block architecture and composition on the association properties of poly(oxyalkylene) copolymers in aqueous solution. *Macromolecular Rapid Communications* **2000,** *21* (9), 501-527.

32. Yu, G.-E.; Yang, Y.-W.; Yang, Z.; Attwood, D.; Booth, C.; Nace, V. M., Association of Diblock and Triblock Copolymers of Ethylene Oxide and Butylene Oxide in Aqueous Solution. *Langmuir* **1996,** *12* (14), 3404-3412.

33. Svaneborg, C.; Pedersen, J. S., Block copolymer micelle coronas as quasi-two-dimensional dilute or semidilute polymer solutions. *Physical Review E* **2001,** *64* (1), 010802.

34. Pedersen, J. S.; Svaneborg, C.; Almdal, K.; Hamley, I. W.; Young, R. N., A Small-Angle Neutron and X-ray Contrast Variation Scattering Study of the Structure of Block Copolymer Micelles: Corona Shape and Excluded Volume Interactions. *Macromolecules* **2003,** *36* (2), 416-433.

35. Zhulina, E. B.; Borisov, O. V., Theory of Block Polymer Micelles: Recent Advances and Current Challenges. *Macromolecules* **2012,** *45* (11), 4429-4440.

36. Wright, D. B.; Patterson, J. P.; Pitto-Barry, A.; Cotanda, P.; Chassenieux, C.; Colombani, O.; O'Reilly, R. K., Tuning the aggregation behavior of pH-responsive micelles by copolymerization. *Polymer Chemistry* **2015,** *6* (14), 2761-2768.

37. Crichton, M. A.; Bhatia, S. R., Small-angle neutron scattering of poly(styrene)/poly(acrylic acid–ethyl acrylate) copolymers: The effect of the degree of hydrolysis of the poly(acrylic acid–ethyl acrylate) block. *Journal of Applied Polymer Science* **2004,** *93* (2), 490-497.

38. Kulebyakina, A. I.; Lysenko, E. A.; Chelushkin, P. S.; Kabanov, A. V.; Zezin, A. B., Self-assembly of an amphiphilic diblock copolymer in aqueous solutions: Effect of linear charge density of an ionogenic block. *Polymer Science Series A* **2010,** *52* (6), 574-585.

39. Lysenko, E. A.; Kulebyakina, A. I.; Chelushkin, P. S.; Rumyantsev, A. M.; Kramarenko, E. Y.; Zezin, A. B., Polymer Micelles with Hydrophobic Core and Ionic Amphiphilic Corona. 2. Starlike Distribution of Charged and Nonpolar Blocks in Corona. *Langmuir* **2012,** *28* (34), 12663-12670.

40. Förster, S.; Hermsdorf, N.; Böttcher, C.; Lindner, P., Structure of Polyelectrolyte Block Copolymer Micelles. *Macromolecules* **2002,** *35* (10), 4096-4105.

41. Guenoun, P.; Davis, H. T.; Tirrell, M.; Mays, J. W., Aqueous Micellar Solutions of Hydrophobically Modified Polyelectrolytes. *Macromolecules* **1996,** *29* (11), 3965-3969.

42. Khougaz, K.; Astafieva, I.; Eisenberg, A., Micellization in Block Polyelectrolyte Solutions. 3. Static Light Scattering Characterization. *Macromolecules* **1995,** *28* (21), 7135-7147.

43. Laaser, J. E.; Jiang, Y.; Sprouse, D.; Reineke, T. M.; Lodge, T. P., pH- and Ionic-Strength-Induced Contraction of Polybasic Micelles in Buffered Aqueous Solutions. *Macromolecules* **2015,** *48* (8), 2677-2685.

44. Sprouse, D.; Jiang, Y.; Laaser, J. E.; Lodge, T. P.; Reineke, T. M., Tuning Cationic Block Copolymer Micelle Size by pH and Ionic Strength. *Biomacromolecules* **2016,** *17* (9), 2849-2859.

45. Lee, A. S.; Bütün, V.; Vamvakaki, M.; Armes, S. P.; Pople, J. A.; Gast, A. P., Structure of pH-Dependent Block Copolymer Micelles: Charge and Ionic Strength Dependence. *Macromolecules* **2002,** *35* (22), 8540-8551.

46. Du, P.; Li, A.; Li, X.; Zhang, Y.; Do, C.; He, L.; Rick, S. W.; John, V. T.; Kumar, R.; Zhang, D., Aggregation of cyclic polypeptoids bearing zwitterionic end-groups with attractive dipole–dipole and solvophobic interactions: a study by small-angle neutron scattering and molecular dynamics simulation. *Physical Chemistry Chemical Physics* **2017,** *19* (22), 14388-14400.

47. Lee, B.-C.; Chu, T. K.; Dill, K. A.; Zuckermann, R. N., Biomimetic Nanostructures: Creating a High-Affinity Zinc-Binding Site in a Folded Nonbiological Polymer. *Journal of the American Chemical Society* **2008,** *130* (27), 8847-8855.

48. Nguyen, A. I.; Spencer, R. K.; Anderson, Christopher L.; Zuckermann, R. N., A bio-inspired approach to ligand design: folding single-chain peptoids to chelate a multimetallic cluster. *Chemical Science* **2018,** *9* (47), 8806-8813.

49. Murnen, H. K.; Rosales, A. M.; Jaworski, J. N.; Segalman, R. A.; Zuckermann, R. N., Hierarchical Self-Assembly of a Biomimetic Diblock Copolypeptoid into Homochiral Superhelices. *Journal of the American Chemical Society* **2010,** *132* (45), 16112-16119.

50. Murnen, H. K.; Khokhlov, A. R.; Khalatur, P. G.; Segalman, R. A.; Zuckermann, R. N., Impact of Hydrophobic Sequence Patterning on the Coil-to-Globule Transition of Protein-like Polymers. *Macromolecules* **2012,** *45* (12), 5229-5236.

51. Sanii, B.; Haxton, T. K.; Olivier, G. K.; Cho, A.; Barton, B.; Proulx, C.; Whitelam, S.; Zuckermann, R. N., Structure-Determining Step in the Hierarchical Assembly of Peptoid Nanosheets. *ACS Nano* **2014,** *8* (11), 11674-11684.

52. Guseva, E.; Zuckermann, R. N.; Dill, K. A., Foldamer hypothesis for the growth and sequence differentiation of prebiotic polymers. *Proceedings of the National Academy of Sciences* **2017,** *114* (36), E7460.

53. Trent, A.; Marullo, R.; Lin, B.; Black, M.; Tirrell, M., Structural properties of soluble peptide amphiphile micelles. *Soft Matter* **2011,** *7* (20), 9572-9582.

54. Murnen, H. K.; Rosales, A. M.; Dobrynin, A. V.; Zuckermann, R. N.; Segalman, R. A., Persistence length of polyelectrolytes with precisely located charges. *Soft Matter* **2013,** *9* (1), 90-98.

55. Sun, J.; Jiang, X.; Siegmund, A.; Connolly, M. D.; Downing, K. H.; Balsara, N. P.; Zuckermann, R. N., Morphology and Proton Transport in Humidified Phosphonated Peptoid Block Copolymers. *Macromolecules* **2016,** *49* (8), 3083-3090.

56. Lau, K. H. A.; Castelletto, V.; Kendall, T.; Sefcik, J.; Hamley, I. W.; Reza, M.; Ruokolainen, J., Self-assembly of ultra-small micelles from amphiphilic lipopeptoids. *Chemical Communications* **2017,** *53* (13), 2178-2181.

57. de Graff, Adam M. R.; Hazoglou, Michael J.; Dill, Ken A., Highly Charged Proteins: The Achilles' Heel of Aging Proteomes. *Structure* **2016,** *24* (2), 329-336.

58. Borisov, O. V.; Zhulina, E. B.; Leermakers, F. A. M.; Müller, A. H. E., Self-Assembled Structures of Amphiphilic Ionic Block Copolymers: Theory, Self-Consistent Field Modeling and Experiment. In *Self Organized Nanostructures of Amphiphilic Block Copolymers I*, Müller, A. H. E.; Borisov, O., Eds. Springer Berlin Heidelberg: Berlin, Heidelberg, 2011; pp 57-129.

59. Gupta, S.; Stellbrink, J.; Zaccarelli, E.; Likos, C. N.; Camargo, M.; Holmqvist, P.; Allgaier, J.; Willner, L.; Richter, D., Validity of the Stokes-Einstein Relation in Soft Colloids up to the Glass Transition. *Physical Review Letters* **2015,** *115* (12), 128302.

60. Guenoun, P.; Muller, F.; Delsanti, M.; Auvray, L.; Chen, Y. J.; Mays, J. W.; Tirrell, M., Rodlike Behavior of Polyelectrolyte Brushes. *Physical Review Letters* **1998,** *81* (18), 3872-3875.

61. Zhang, L.; Barlow, R. J.; Eisenberg, A., Scaling Relations and Coronal Dimensions in Aqueous Block Polyelectrolyte Micelles. *Macromolecules* **1995,** *28* (18), 6055-6066.

62. Moffitt, M.; Khougaz, K.; Eisenberg, A., Micellization of Ionic Block Copolymers. *Acc. Chem. Res.* **1996,** *29* (2), 95-102.

63. Zhang, L.; Eisenberg, A., Multiple Morphologies of "Crew-Cut" Aggregates of Polystyrene-b-poly(acrylic acid) Block Copolymers. *Science* **1995,** *268* (5218), 1728-1731.

64. Borisov, O. V.; Zhulina, E. B., Effects of ionic strength and charge annealing in star-branched polyelectrolytes. *The European Physical Journal B - Condensed Matter and Complex Systems* **1998,** *4* (2), 205-217.

65. Hamley, I. W., Self-assembly of amphiphilic peptides. *Soft Matter* **2011,** *7* (9), 4122-4138.

66. Knight, A. S.; Zhou, E. Y.; Francis, M. B.; Zuckermann, R. N., Sequence Programmable Peptoid Polymers for Diverse Materials Applications. *Adv. Mater.* **2015,** *27* (38), 5665-5691.

67. Sun, J.; Zuckermann, R. N., Peptoid Polymers: A Highly Designable Bioinspired Material. *ACS Nano* **2013,** *7* (6), 4715-4732.

68. Rosales, A. M.; Segalman, R. A.; Zuckermann, R. N., Polypeptoids: a model system to study the effect of monomer sequence on polymer properties and self-assembly. *Soft Matter* **2013,** *9* (35), 8400-8414.

69. Fetsch, C.; Flecks, S.; Gieseler, D.; Marschelke, C.; Ulbricht, J.; van Pée, K.-H.; Luxenhofer, R., Self-Assembly of Amphiphilic Block Copolypeptoids with C2-C5 Side Chains in Aqueous Solution. *Macromolecular Chemistry and Physics* **2015,** *216* (5), 547-560.

70. Sanii, B.; Kudirka, R.; Cho, A.; Venkateswaran, N.; Olivier, G. K.; Olson, A. M.; Tran, H.; Harada, R. M.; Tan, L.; Zuckermann, R. N., Shaken, Not Stirred: Collapsing a Peptoid Monolayer To Produce Free-Floating, Stable Nanosheets. *Journal of the American Chemical Society* **2011,** *133* (51), 20808-20815.

71. Mannige, R. V.; Haxton, T. K.; Proulx, C.; Robertson, E. J.; Battigelli, A.; Butterfoss, G. L.; Zuckermann, R. N.; Whitelam, S., Peptoid nanosheets exhibit a new secondary-structure motif. *Nature* **2015,** *526* (7573), 415-420.

72. Robertson, E. J.; Battigelli, A.; Proulx, C.; Mannige, R. V.; Haxton, T. K.; Yun, L.; Whitelam, S.; Zuckermann, R. N., Design, Synthesis, Assembly, and Engineering of Peptoid Nanosheets. *Accounts of Chemical Research* **2016,** *49* (3), 379-389.

73. Sun, J.; Jiang, X.; Lund, R.; Downing, K. H.; Balsara, N. P.; Zuckermann, R. N., Self-assembly of crystalline nanotubes from monodisperse amphiphilic diblock copolypeptoid tiles. *Proceedings of the National Academy of Sciences* **2016,** *113* (15), 3954-3959.

74. Jiang, X.; Sun, J.; Zuckermann, R.; Downing, K. H.; Balsara, N., Morphology Study of Phosphonated Peptoid Block Copolymer. *Microsc. Microanal.* **2016,** *22* (S3), 1926-1927.

75. Sun, J.; Teran, A. A.; Liao, X.; Balsara, N. P.; Zuckermann, R. N., Nanoscale Phase Separation in Sequence-Defined Peptoid Diblock Copolymers. *Journal of the American Chemical Society* **2013,** *135* (38), 14119-14124.

76. Goddard, E. D.; Turro, N. J.; Kuo, P. L.; Ananthapadmanabhan, K. P., Fluorescence probes for critical micelle concentration determination. *Langmuir* **1985,** *1* (3), 352-355.

77. Livesey, A. K.; Brochon, J. C., Analyzing the Distribution of Decay Constants in Pulse-Fluorimetry Using the Maximum Entropy Method. *Biophysical Journal* **1987,** *52* (5), 693-706.

78. Arnold, O.; Bilheux, J. C.; Borreguero, J. M.; Buts, A.; Campbell, S. I.; Chapon, L.; Doucet, M.; Draper, N.; Ferraz Leal, R.; Gigg, M. A.; Lynch, V. E.; Markvardsen, A.; Mikkelson, D. J.; Mikkelson, R. L.; Miller, R.; Palmen, K.; Parker, P.; Passos, G.; Perring, T. G.; Peterson, P. F.; Ren, S.; Reuter, M. A.; Savici, A. T.; Taylor, J. W.; Taylor, R. J.; Tolchenov, R.; Zhou, W.; Zikovsky, J., Mantid—Data analysis and visualization package for neutron scattering and μ SR experiments. *Nuclear Instruments and Methods in Physics Research Section A: Accelerators, Spectrometers, Detectors and Associated Equipment* **2014,** *764* (Supplement C), 156-166.

79. Gupta, S.; Camargo, M.; Stellbrink, J.; Allgaier, J.; Radulescu, A.; Lindner, P.; Zaccarelli, E.; Likos, C. N.; Richter, D., Dynamic phase diagram of soft nanocolloids. *Nanoscale* **2015,** *7* (33), 13924-34.

80. Pedersen, J. S.; Svaneborg, C.; Almdal, K.; Hamley, I. W.; Young, R. N., A Small-Angle Neutron and X-ray Contrast Variation Scattering Study of the Structure of Block Copolymer Micelles: Corona Shape and Excluded Volume Interactions. *Macromolecules* **2003,** *36* (2), 416-433.

81. Yang, Y.; Mijalis, A. J.; Fu, H.; Agosto, C.; Tan, K. J.; Batteas, J. D.; Bergbreiter, D. E., Reversible Changes in Solution pH Resulting from Changes in Thermoresponsive Polymer Solubility. *Journal of the American Chemical Society* **2012,** *134* (17), 7378-7383.

82. Gupta, S.; Camargo, M.; Stellbrink, J.; Allgaier, J.; Radulescu, A.; Lindner, P.; Zaccarelli, E.; Likos, C. N.; Richter, D., Dynamic phase diagram of soft nanocolloids. *Nanoscale* **2015,** *7* (33), 13924-13934.

83. Stubenrauch, K.; Voets, I.; Fritz-Popovski, G.; Trimmel, G., pH and ionic strength responsive polyelectrolyte block copolymer micelles prepared by ring opening metathesis polymerization. *Journal of Polymer Science Part A: Polymer Chemistry* **2009,** *47* (4), 1178-1191.

84. Mendes, E.; Schädler, V.; Marques, C. M.; Lindner, P.; Wiesner, U., Electrostatics in the self-assembly of macromolecular surfactants. *Europhys. Lett.* **1997,** *40* (5), 521.

85. Kunz, D.; Thurn, A.; Burchard, W., Dynamic light scattering from spherical particles. *Colloid and Polymer Science* **1983,** *261* (8), 635-644.

86. Helmstedt, M.; Schäfer, H., Determination of sizes of spherical particles, prepared by dispersion polymerization of methyl methacrylate in non-aqueous medium, by analysis of the particle scattering and autocorrelation functions. *Polymer* **1994,** *35* (16), 3377-3383.

87. Hirzinger, B.; Helmstedt, M.; Stejskal, J., Light scattering studies on core–shell systems: determination of size parameters of sterically stabilized poly(methylmethacrylate) dispersions. *Polymer* **2000,** *41* (8), 2883-2891.

88. Tande, B. M.; Wagner, N. J.; Mackay, M. E.; Hawker, C. J.; Jeong, M., Viscosimetric, Hydrodynamic, and Conformational Properties of Dendrimers and Dendrons. *Macromolecules* **2001,** *34* (24), 8580-8585.

89. Schneider, F.; Balaceanu, A.; Feoktystov, A.; Pipich, V.; Wu, Y.; Allgaier, J.; Pyckhout-Hintzen, W.; Pich, A.; Schneider, G. J., Monitoring the Internal Structure of Poly(N-vinylcaprolactam) Microgels with Variable Cross-Link Concentration. *Langmuir* **2014,** *30* (50), 15317-15326.

90. Lund, R.; Willner, L.; Stellbrink, J.; Radulescu, A.; Richter, D., Role of Interfacial Tension for the Structure of PEP−PEO Polymeric Micelles. A Combined SANS and Pendant Drop Tensiometry Investigation. *Macromolecules* **2004,** *37* (26), 9984-9993.

91. Bekhradnia, S.; Diget, J. S.; Zinn, T.; Zhu, K.; Sande, S. A.; Nyström, B.; Lund, R., Charged Star Diblock Copolymers in Dilute Solutions: Synthesis, Structure, and Chain Conformations. *Macromolecules* **2015,** *48* (8), 2637-2646.

92. Amann, M.; Willner, L.; Stellbrink, J.; Radulescu, A.; Richter, D., Studying the concentration dependence of the aggregation number of a micellar model system by SANS. *Soft Matter* **2015,** *11* (21), 4208-4217.

93. Kowalski, P. S.; Bhattacharya, C.; Afewerki, S.; Langer, R., Smart Biomaterials: Recent Advances and Future Directions. *ACS Biomaterials Science & Engineering* **2018,** *4* (11), 3809-3817.

94. Zhou, Q.; Zhang, L.; Yang, T.; Wu, H., Stimuli-responsive polymeric micelles for drug delivery and cancer therapy. *Int J Nanomedicine* **2018,** *13*, 2921-2942.

95. Nair, H. A.; Singh Rajawat, G.; Nagarsenker, M. S., Chapter 8 - Stimuli-responsive micelles: A nanoplatform for therapeutic and diagnostic applications. In *Drug Targeting and Stimuli Sensitive Drug Delivery Systems*, Grumezescu, A. M., Ed. William Andrew Publishing: 2018; pp 303-342.

96. Borisov, O. V.; Zhulina, E. B., Morphology of Micelles Formed by Diblock Copolymer with a Polyelectrolyte Block. *Macromolecules* **2003,** *36* (26), 10029-10036.

97. Förster, S.; Abetz, V.; Müller, A. E., Polyelectrolyte Block Copolymer Micelles. In *Polyelectrolytes with Defined Molecular Architecture II*, Schmidt, M., Ed. Springer Berlin Heidelberg: 2004; Vol. 166, pp 173-210.

98. Hales, K.; Pochan, D. J., Using polyelectrolyte block copolymers to tune nanostructure assembly. *Current Opinion in Colloid & Interface Science* **2006,** *11* (6), 330-336.

99. Mai, Y.; Eisenberg, A., Self-assembly of block copolymers. *Chemical Society Reviews* **2012,** *41* (18), 5969-5985.

100. Strandman, S.; Zarembo, A.; Darinskii, A. A.; Löflund, B.; Butcher, S. J.; Tenhu, H., Self-assembling of star-like amphiphilic block copolymers with polyelectrolyte blocks. Effect of pH. *Polymer* **2007,** *48* (24), 7008-7016.

101. Fernyhough, C.; Ryan, A. J.; Battaglia, G., pH controlled assembly of a polybutadiene-poly(methacrylic acid) copolymer in water: packing considerations and kinetic limitations. *Soft Matter* **2009,** *5* (8), 1674-1682.

102. Sternhagen, G. L.; Gupta, S.; Zhang, Y.; John, V.; Schneider, G. J.; Zhang, D., Solution Self-Assemblies of Sequence-Defined Ionic Peptoid Block Copolymers. *Journal of the American Chemical Society* **2018,** *140* (11), 4100-4109.

103. Burkhardt, M.; Martinez-Castro, N.; Tea, S.; Drechsler, M.; Babin, I.; Grishagin, I.; Schweins, R.; Pergushov, D. V.; Gradzielski, M.; Zezin, A. B.; Müller, A. H. E., Polyisobutylene-block-poly(methacrylic acid) Diblock Copolymers: Self-Assembly in Aqueous Media. *Langmuir* **2007,** *23* (26), 12864-12874.

104. Wu, C. W.; Sanborn, T. J.; Zuckermann, R. N.; Barron, A. E., Peptoid Oligomers with α-Chiral, Aromatic Side Chains: Effects of Chain Length on Secondary Structure. *Journal of the American Chemical Society* **2001,** *123* (13), 2958-2963.

105. Wu, C. W.; Sanborn, T. J.; Huang, K.; Zuckermann, R. N.; Barron, A. E., Peptoid Oligomers with α-Chiral, Aromatic Side Chains: Sequence Requirements for the Formation of Stable Peptoid Helices. *Journal of the American Chemical Society* **2001,** *123* (28), 6778-6784.

106. Utku, Y.; Dehan, E.; Ouerfelli, O.; Piano, F.; Zuckermann, R. N.; Pagano, M.; Kirshenbaum, K., A peptidomimetic siRNA transfection reagent for highly effective gene silencing. *Molecular BioSystems* **2006,** *2* (6-7), 312-317.

107. Maayan, G.; Ward, M. D.; Kirshenbaum, K., Folded biomimetic oligomers for enantioselective catalysis. *Proceedings of the National Academy of Sciences* **2009,** *106* (33), 13679.

108. Huang, M. L.; Shin, S. B. Y.; Benson, M. A.; Torres, V. J.; Kirshenbaum, K., A Comparison of Linear and Cyclic Peptoid Oligomers as Potent Antimicrobial Agents. *ChemMedChem* **2012,** *7* (1), 114-122.

109. Lee, C.-U.; Smart, T. P.; Guo, L.; Epps, T. H.; Zhang, D., Synthesis and Characterization of Amphiphilic Cyclic Diblock Copolypeptoids from N-Heterocyclic Carbene-Mediated Zwitterionic Polymerization of N-Substituted N-Carboxyanhydride. *Macromolecules* **2011,** *44* (24), 9574-9585.

110. Doriti, A.; Brosnan, S. M.; Weidner, S. M.; Schlaad, H., Synthesis of polysarcosine from air and moisture stable N-phenoxycarbonyl-N-methylglycine assisted by tertiary amine base. *Polymer Chemistry* **2016,** *7* (18), 3067-3070.

111. Lytle, T. K.; Chang, L.-W.; Markiewicz, N.; Perry, S. L.; Sing, C. E., Designing Electrostatic Interactions via Polyelectrolyte Monomer Sequence. *ACS Central Science* **2019,** *5* (4), 709-718.

112. Cabral, H.; Miyata, K.; Osada, K.; Kataoka, K., Block Copolymer Micelles in Nanomedicine Applications. *Chemical reviews* **2018,** *118* (14), 6844-6892.

APPENDIX A. COPYRIGHT RELEASE

PERMISSION/LICENSE IS GRANTED FOR YOUR ORDER AT NO CHARGE

This type of permission/license, instead of the standard Terms & Conditions, is sent to you because no fee is being charged for your order. Please note the following:

- Permission is granted for your request in both print and electronic formats, and translations.
- If figures and/or tables were requested, they may be adapted or used in part.
- Please print this page for your records and send a copy of it to your publisher/graduate school.
- Appropriate credit for the requested material should be given as follows: "Reprinted (adapted) with permission from (COMPLETE REFERENCE CITATION). Copyright (YEAR) American Chemical Society." Insert appropriate information in place of the capitalized words.
- One-time permission is granted only for the use specified in your request. No additional uses are granted (such as derivative works or other editions). For any other uses, please submit a new request.

If credit is given to another source for the material you requested, permission must be obtained from that source.

BACK CLOSE WINDOW

RightsLink®

Home | Create Account | Help

Title:	Peptoids and Polypeptoids at the Frontier of Supra- and Macromolecular Engineering
Author:	Niklas Gangloff, Juliane Ulbricht, Thomas Lorson, et al
Publication:	Chemical Reviews
Publisher:	American Chemical Society
Date:	Feb 1, 2016

LOGIN

If you're a copyright.com user, you can login to RightsLink using your copyright.com credentials.

Already **a RightsLink user** or want to learn more?

PERMISSION/LICENSE IS GRANTED FOR YOUR ORDER AT NO CHARGE

This type of permission/license, instead of the standard Terms & Conditions, is sent to you because no fee is being charged for your order. Please note the following:

- Permission is granted for your request in both print and electronic formats, and translations.
- If figures and/or tables were requested, they may be adapted or used in part.
- Please print this page for your records and send a copy of it to your publisher/graduate school.
- Appropriate credit for the requested material should be given as follows: "Reprinted (adapted) with permission from (COMPLETE REFERENCE CITATION). Copyright (YEAR) American Chemical Society." Insert appropriate information in place of the capitalized words.
- One-time permission is granted only for the use specified in your request. No additional uses are granted (such as derivative works or other editions). For any other uses, please submit a new request.

If credit is given to another source for the material you requested, permission must be obtained from that source.

BACK | CLOSE WINDOW

Royal Society of Chemistry LICENSE TERMS AND CONDITIONS

Jul 05, 2019

This is a License Agreement between Garrett Sternhagen ("You") and Royal Society of Chemistry ("Royal Society of Chemistry") provided by Copyright Clearance Center ("CCC"). The license consists of your order details, the terms and conditions provided by Royal Society of Chemistry, and the payment terms and conditions.

All payments must be made in full to CCC. For payment instructions, please see information listed at the bottom of this form.

License Number	4622641454828
License date	Jul 05, 2019
Licensed content publisher	Royal Society of Chemistry
Licensed content title	Chemical Society reviews
Licensed content date	Jan 1, 1972
Type of Use	Thesis/Dissertation
Requestor type	Academic institution
Format	Print, Electronic
Portion	chart/graph/table/figure
Number of charts/graphs/tables/figures	1
The requesting person/organization is:	Garrett Sternhagen
Title or numeric reference of the portion(s)	Figure 2
Title of the article or chapter the portion is from	Large-pore ordered mesoporous materials templated from non-Pluronic amphiphilic block copolymers
Editor of portion(s)	N/A
Author of portion(s)	Yonghui Deng, Jing Wei, Zhenkun Sun and Dongyuan Zhao
Volume of serial or monograph.	42
Issue, if republishing an article from a serial	9
Page range of the portion	4056
Publication date of portion	19th October 2012
Rights for	Main product
Duration of use	Life of current edition
Creation of copies for the disabled	yes
With minor editing privileges	no
For distribution to	Worldwide
In the following language(s)	Original language of publication
With incidental promotional	no

use	
The lifetime unit quantity of new product	Up to 499
Title	SEQUENCE-DEFINED IONIC PEPTOID BLOCK COPOLYMERS: SYNTHESIS AND SOLUTION SELF-ASSEMBLY
Institution name	Louisiana State University
Expected presentation date	Dec 2019
Total (may include CCC user fee)	0.00 USD
Terms and Conditions	

TERMS AND CONDITIONS

The following terms are individual to this publisher:

None

Other Terms and Conditions:

STANDARD TERMS AND CONDITIONS

1. Description of Service; Defined Terms. This Republication License enables the User to obtain licenses for republication of one or more copyrighted works as described in detail on the relevant Order Confirmation (the "Work(s)"). Copyright Clearance Center, Inc. ("CCC") grants licenses through the Service on behalf of the rightsholder identified on the Order Confirmation (the "Rightsholder"). "Republication", as used herein, generally means the inclusion of a Work, in whole or in part, in a new work or works, also as described on the Order Confirmation. "User", as used herein, means the person or entity making such republication.

2. The terms set forth in the relevant Order Confirmation, and any terms set by the Rightsholder with respect to a particular Work, govern the terms of use of Works in connection with the Service. By using the Service, the person transacting for a republication license on behalf of the User represents and warrants that he/she/it (a) has been duly authorized by the User to accept, and hereby does accept, all such terms and conditions on behalf of User, and (b) shall inform User of all such terms and conditions. In the event such person is a "freelancer" or other third party independent of User and CCC, such party shall be deemed jointly a "User" for purposes of these terms and conditions. In any event, User shall be deemed to have accepted and agreed to all such terms and conditions if User republishes the Work in any fashion.

3. Scope of License; Limitations and Obligations.

3.1 All Works and all rights therein, including copyright rights, remain the sole and exclusive property of the Rightsholder. The license created by the exchange of an Order Confirmation (and/or any invoice) and payment by User of the full amount set forth on that document includes only those rights expressly set forth in the Order Confirmation and in these terms and conditions, and conveys no other rights in the Work(s) to User. All rights not expressly granted are hereby reserved.

3.2 General Payment Terms: You may pay by credit card or through an account with us payable at the end of the month. If you and we agree that you may establish a standing account with CCC, then the following terms apply: Remit Payment to: Copyright Clearance Center, 29118 Network Place, Chicago, IL 60673-1291. Payments Due: Invoices are payable upon their delivery to you (or upon our notice to you that they are available to you for downloading). After 30 days, outstanding amounts will be subject to a service charge of 1-1/2% per month or, if less, the maximum rate allowed by applicable law. Unless otherwise specifically set forth in the Order Confirmation or in a separate written agreement signed by CCC, invoices are due and payable on "net 30" terms. While User may exercise the rights licensed immediately upon issuance of the Order Confirmation, the license is automatically revoked and is null and void, as if it had never been issued, if complete payment for the

RightsLink®

Home | Account Info | Help

Title:	Solution Self-Assemblies of Sequence-Defined Ionic Peptoid Block Copolymers
Author:	Garrett L. Sternhagen, Sudipta Gupta, Yueheng Zhang, et al
Publication:	Journal of the American Chemical Society
Publisher:	American Chemical Society
Date:	Mar 1, 2018

Logged in as:
Garrett Sternhagen
LOGOUT

PERMISSION/LICENSE IS GRANTED FOR YOUR ORDER AT NO CHARGE

This type of permission/license, instead of the standard Terms & Conditions, is sent to you because no fee is being charged for your order. Please note the following:

- Permission is granted for your request in both print and electronic formats, and translations.
- If figures and/or tables were requested, they may be adapted or used in part.
- Please print this page for your records and send a copy of it to your publisher/graduate school.
- Appropriate credit for the requested material should be given as follows: "Reprinted (adapted) with permission from (COMPLETE REFERENCE CITATION). Copyright (YEAR) American Chemical Society." Insert appropriate information in place of the capitalized words.
- One-time permission is granted only for the use specified in your request. No additional uses are granted (such as derivative works or other editions). For any other uses, please submit a new request.

BACK | CLOSE WINDOW

RightsLink®

Home | Create Account | Help

Title: Tuning Cationic Block Copolymer Micelle Size by pH and Ionic Strength

Author: Dustin Sprouse, Yaming Jiang, Jennifer E. Laaser, et al

Publication: Biomacromolecules

Publisher: American Chemical Society

Date: Sep 1, 2016

LOGIN

If you're a copyright.com user, you can login to RightsLink using your copyright.com credentials.

Already a RightsLink user or want to learn more?

PERMISSION/LICENSE IS GRANTED FOR YOUR ORDER AT NO CHARGE

This type of permission/license, instead of the standard Terms & Conditions, is sent to you because no fee is being charged for your order. Please note the following:

- Permission is granted for your request in both print and electronic formats, and translations.
- If figures and/or tables were requested, they may be adapted or used in part.
- Please print this page for your records and send a copy of it to your publisher/graduate school.
- Appropriate credit for the requested material should be given as follows: "Reprinted (adapted) with permission from (COMPLETE REFERENCE CITATION). Copyright (YEAR) American Chemical Society." Insert appropriate information in place of the capitalized words.
- One-time permission is granted only for the use specified in your request. No additional uses are granted (such as derivative works or other editions). For any other uses, please submit a new request.

If credit is given to another source for the material you requested, permission must be obtained from that source.

BACK | CLOSE WINDOW

APPENDIX B. SUPPLEMENTAL INFORMATION FOR CHAPTER 2

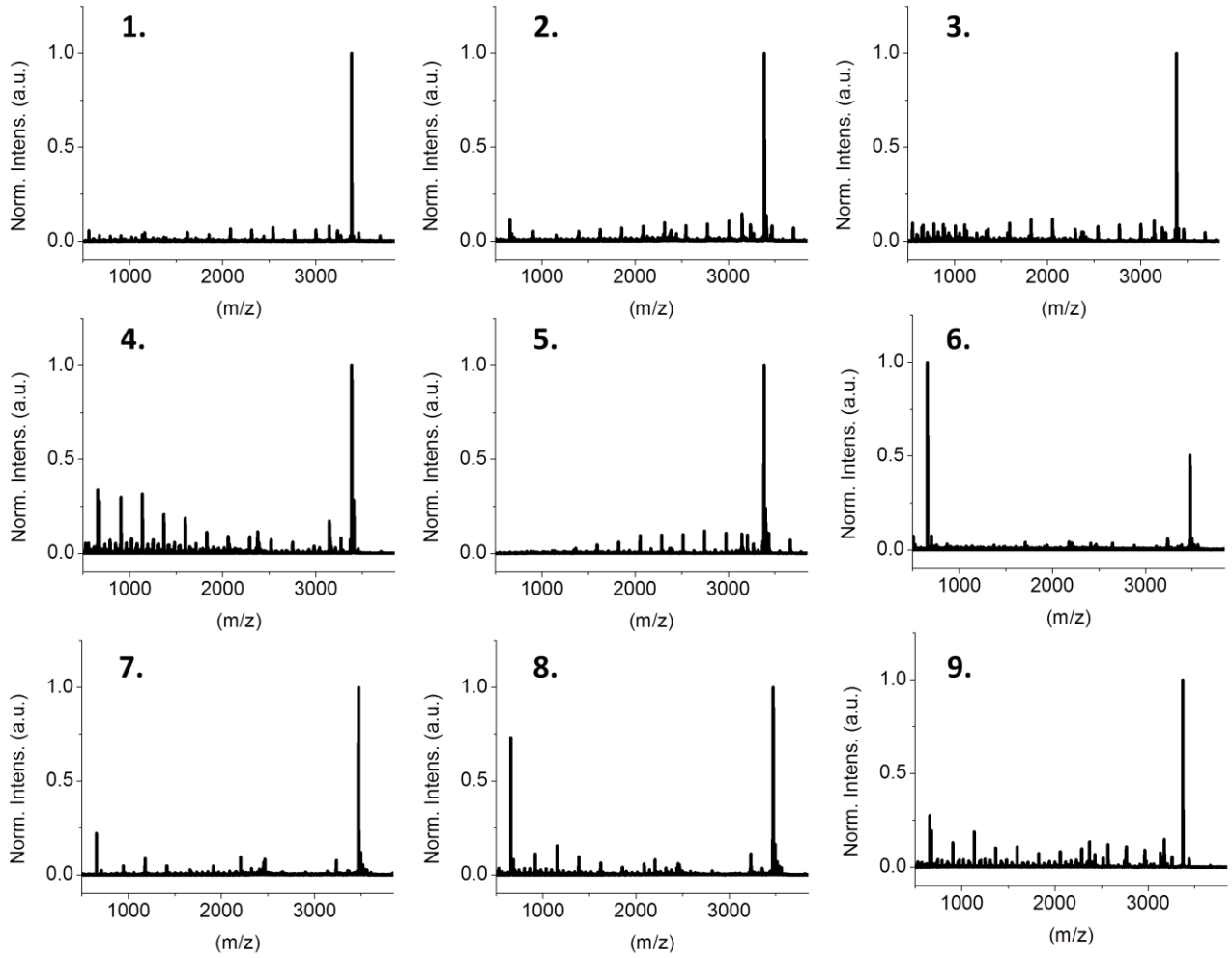

Figure S2.1. MALDI-TOF MS spectra of sequence-defined peptoid block copolymers (Sequence 1-9, Figure 2.1B) obtained by the sub-monomer method.

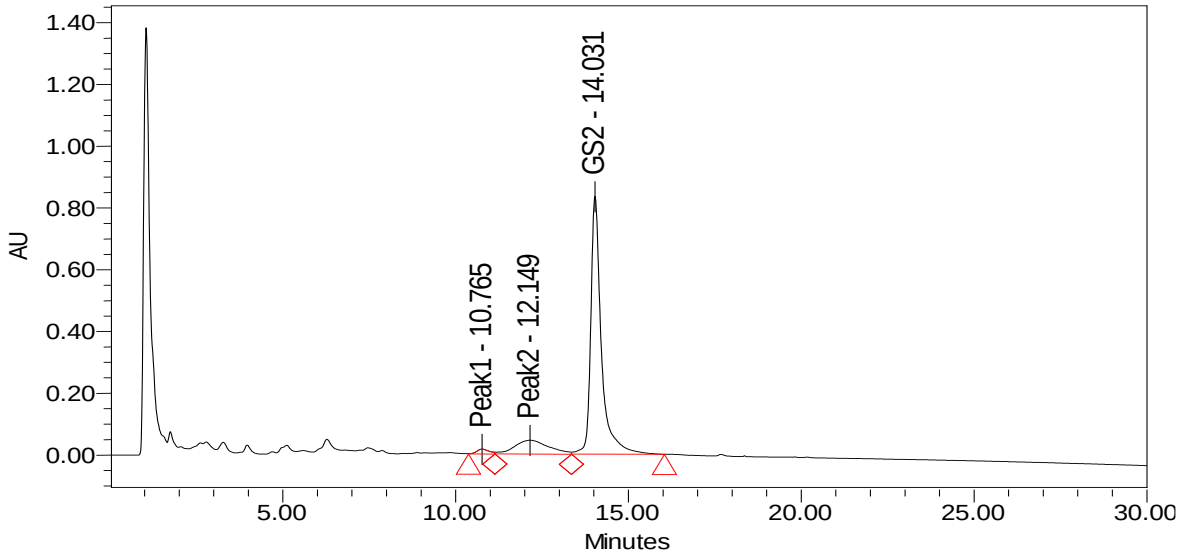

Figure S2.2. Representative HPLC chromatogram of a sequence-defined peptoid block copolymer (Sequence #2, Table 2.1). The major peak at 14.0 min corresponds to the full length peptoids polymer, with deletion impurities at lower elution times (12.1 and 10.8 min).

Table S2.1. Experimentally determined exact molecular weights of various sequence-defined peptoid block copolymers (Sequence 1-9, Figure 2.1B) by the MALDI-TOF MS analysis, the calculated exact molecular weights based on molecular formula and the sample purity level based on HPLC analysis.

Sequence #	Molecular Formula		Calc. (m/z)	Found (m/z)	Purity Level (%)
1	C162H297N26O47Na	$[M+Na]^+$	3383.163	3382.380	94
2	C162H297N26O47Na	$[M+Na]^+$	3383.163	3383.449	84
3	C162H297N26O47Na	$[M+Na]^+$	3383.163	3382.457	95
4	C162H297N26O47Na	$[M+Na]^+$	3383.163	3383.078	93
5	C162H297N26O47Na	$[M+Na]^+$	3383.163	3382.493	92
6	C162H291N26O49Na2K	$[M+Na+Na+K]^+$	3471.05	3471.493	93
7	C162H291N26O49Na2K	$[M+Na+Na+K]^+$	3471.05	3470.384	89
8	C162H291N26O49Na2K	$[M+Na+Na+K]^+$	3471.05	3466.326	90
9	C162H300N26O46	$[M+Na]^+$	3369.183	3369.304	82

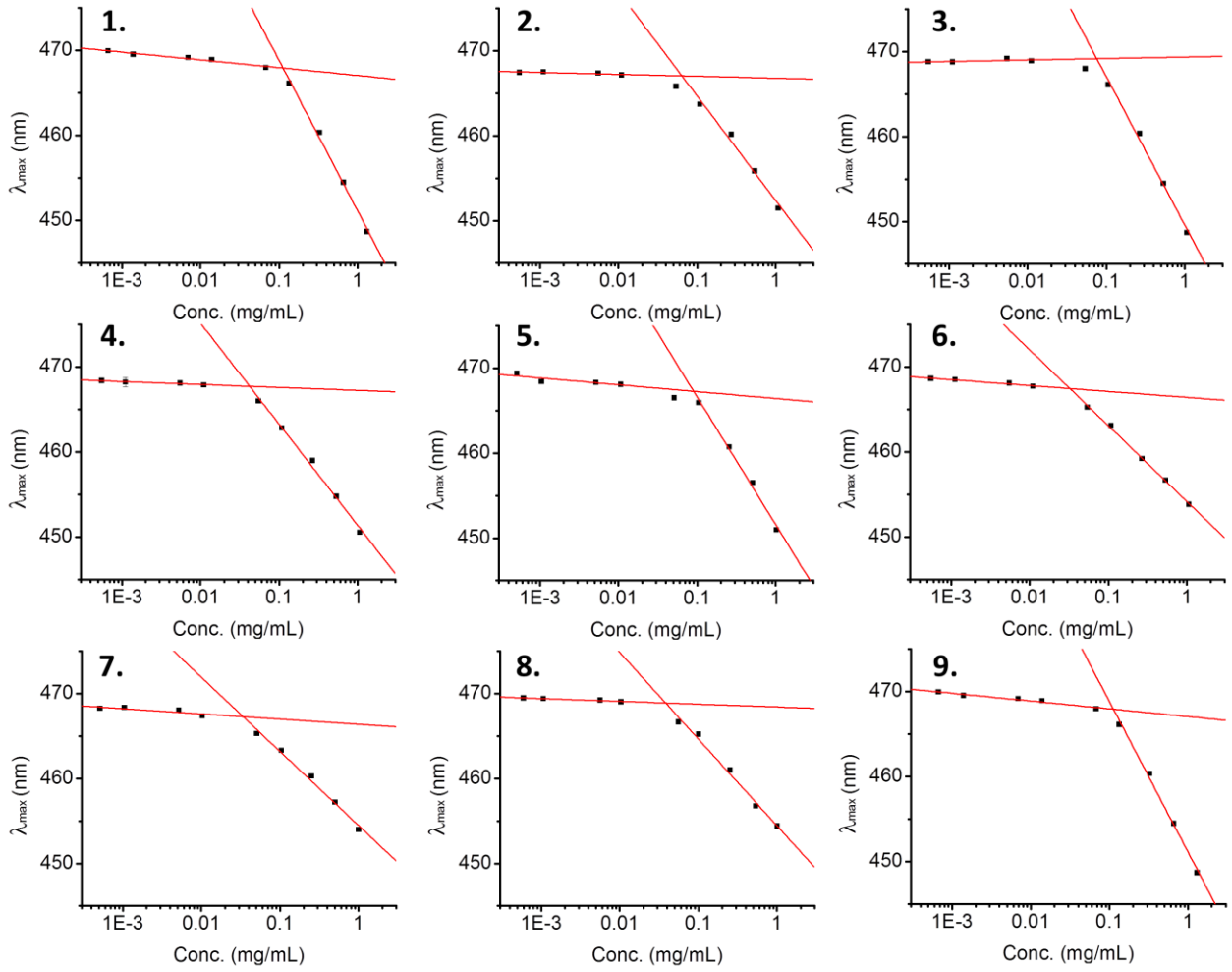

Figure S2.3. The plots of the UV absorption wavelength at the maximal intensity for pyrene-1-carboxaldehyde versus polymer concentration for various sequence-defined peptoid block copolymers (Sequence 1-9, Figure 2.1) to determine the critical micellar concentration (CMC).

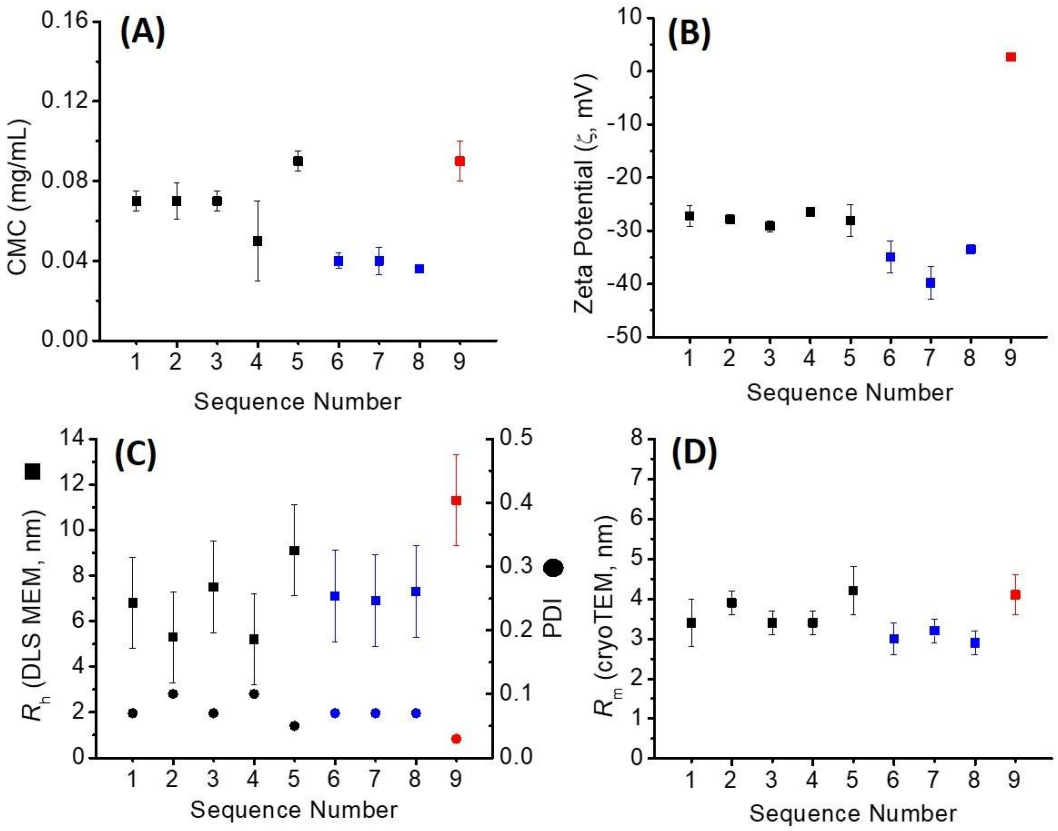

Figure S2.4. (A) critical micellar concentrations (CMC), (B) zeta-potentials (ζ), (C) hydrodynamic radius (R_h) and polydispersity determined by DLS-MEM analysis, and (D) micellar radius determined by CryoTEM analysis of various sequence-defined peptoid block copolymers (Sequence 1-9, Figure 2.1) in dilute aqueous solution (pH = 9). Shown above are the singly charged system in black, triply charged in blue and the neutral in red.

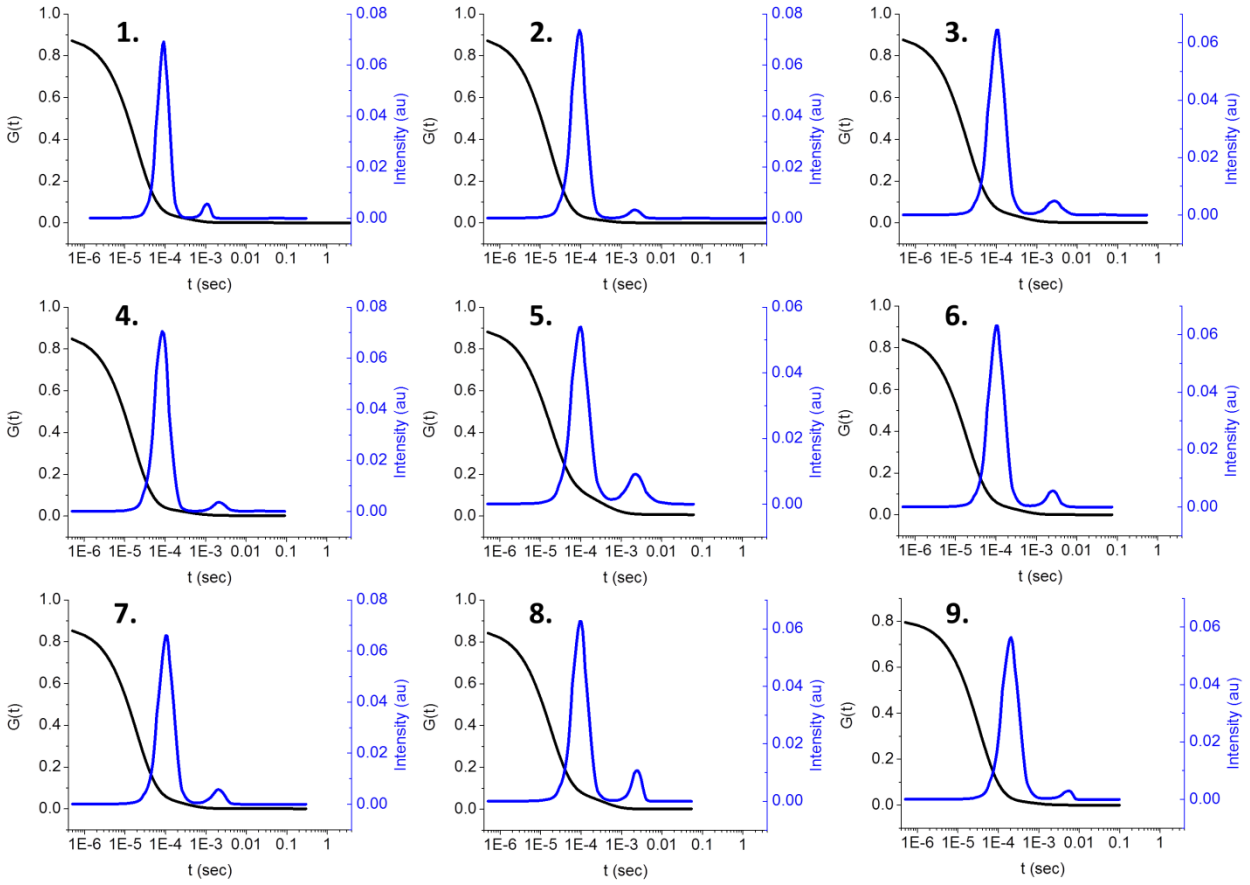

Figure S2.5. DLS data of various sequence-defined peptoid block copolymers (Sequence 1-9, Figure 2.1) in dilute aqueous solution (5 mg/mL, pH 9).

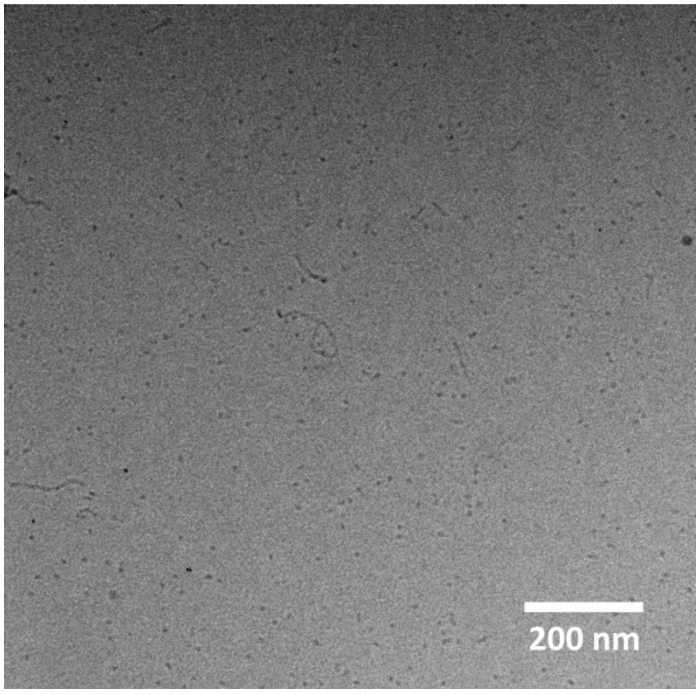

Figure S2.6. CryoTEM images showing the spherical micelles with occasional worm-like micelles present in the dilute aqueous solution of charge-neutral peptoid block copolymer micelles (Sequence 9, Figure 2.1).

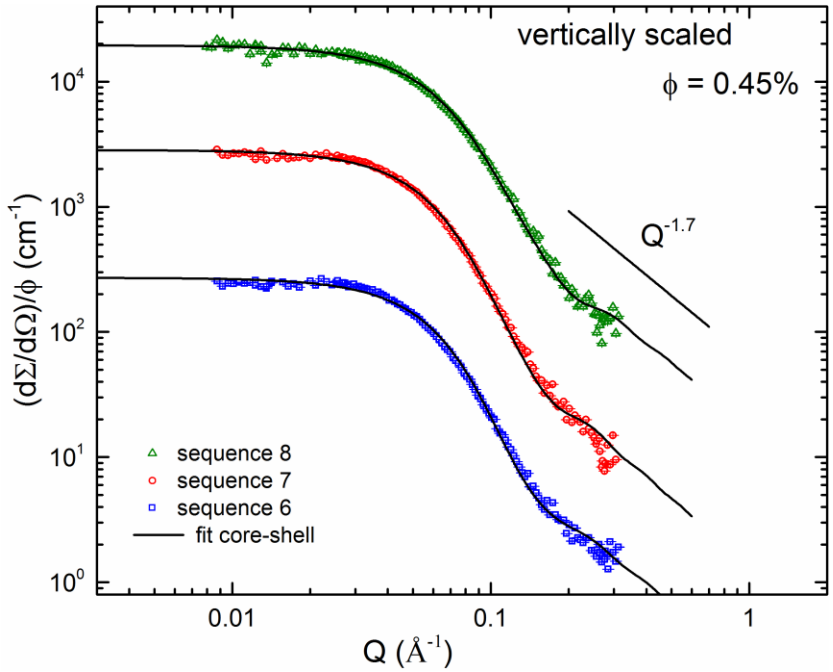

Figure S2.7. SANS data and analysis of the micellar solutions of sequence-defined peptoid block copolymers bearing three ionic monomers (Sequence 6-8, Figure 2.1) in 0.45 vol% D_2O (pH 9). Pictured are the fitted data for the triply charged peptoid block copolymer series and the data vertically scaled by a constant for clarity.

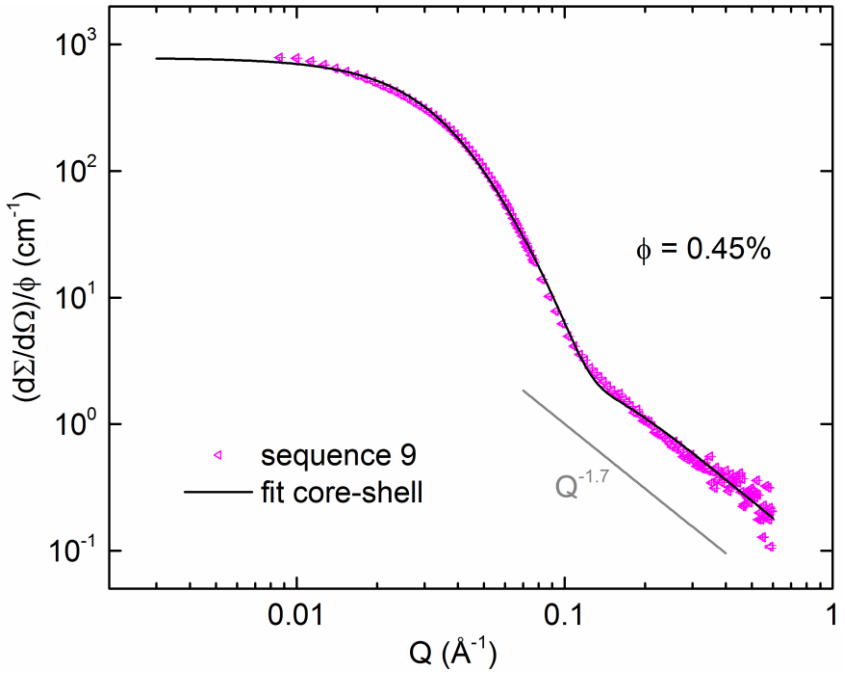

Figure S2.8. SANS data and analysis of the micellar solutions of neutral sequence-defined peptoid block copolymer (Sequence 9, Figure 2.1) in 0.45 vol% D_2O (pH 9).

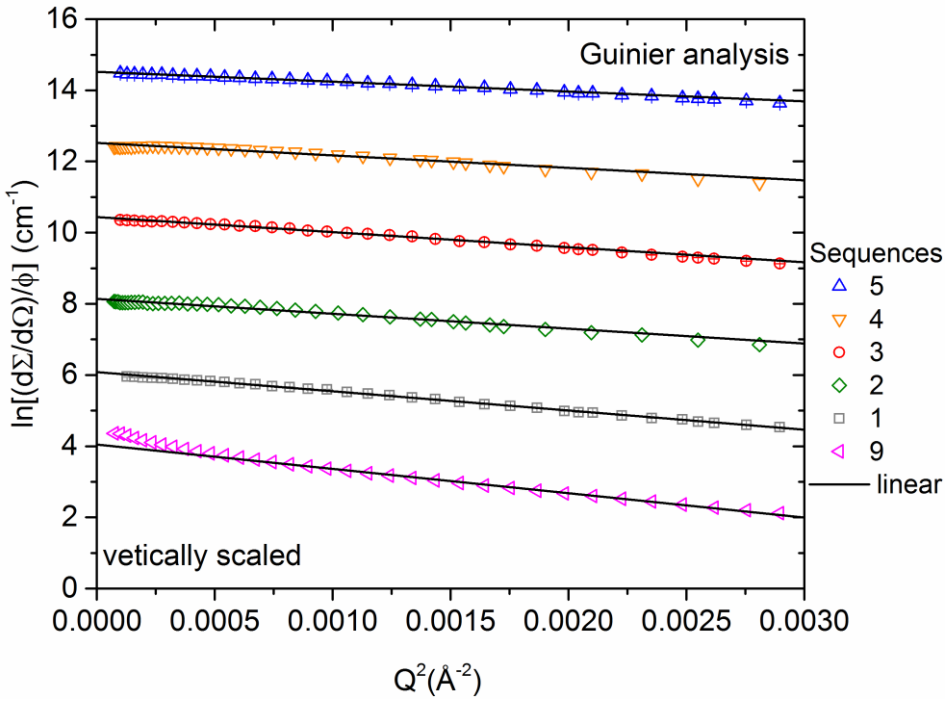

Figure S2.9. Gunier plot analysis of SANS data in the *q* range selected based on the criteria of $R_g \cdot q_{max} << 1$ for the singly charged peptoid block copolymer micelles (Sequence 1-5, Table 2.1) and charge-neutral micelle (Sequence 9, Table 2.1).

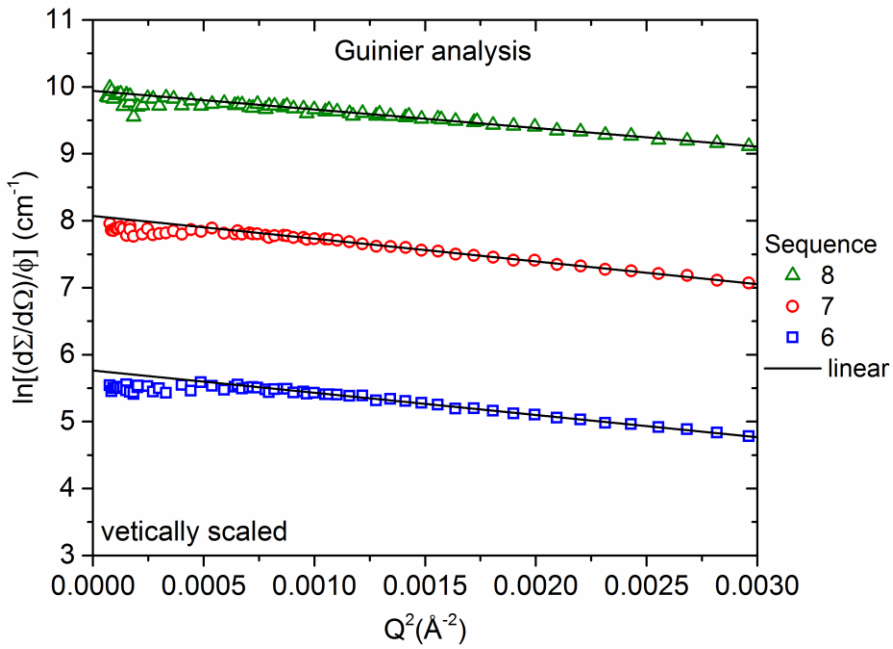

Figure S2.10. Gunier plot analysis of SANS data in the *q* range selected based on the criteria of $R_g \cdot q_{max} << 1$ for the triply charged peptoid block copolymer micelles (Sequence 6-8, Table 2.1).

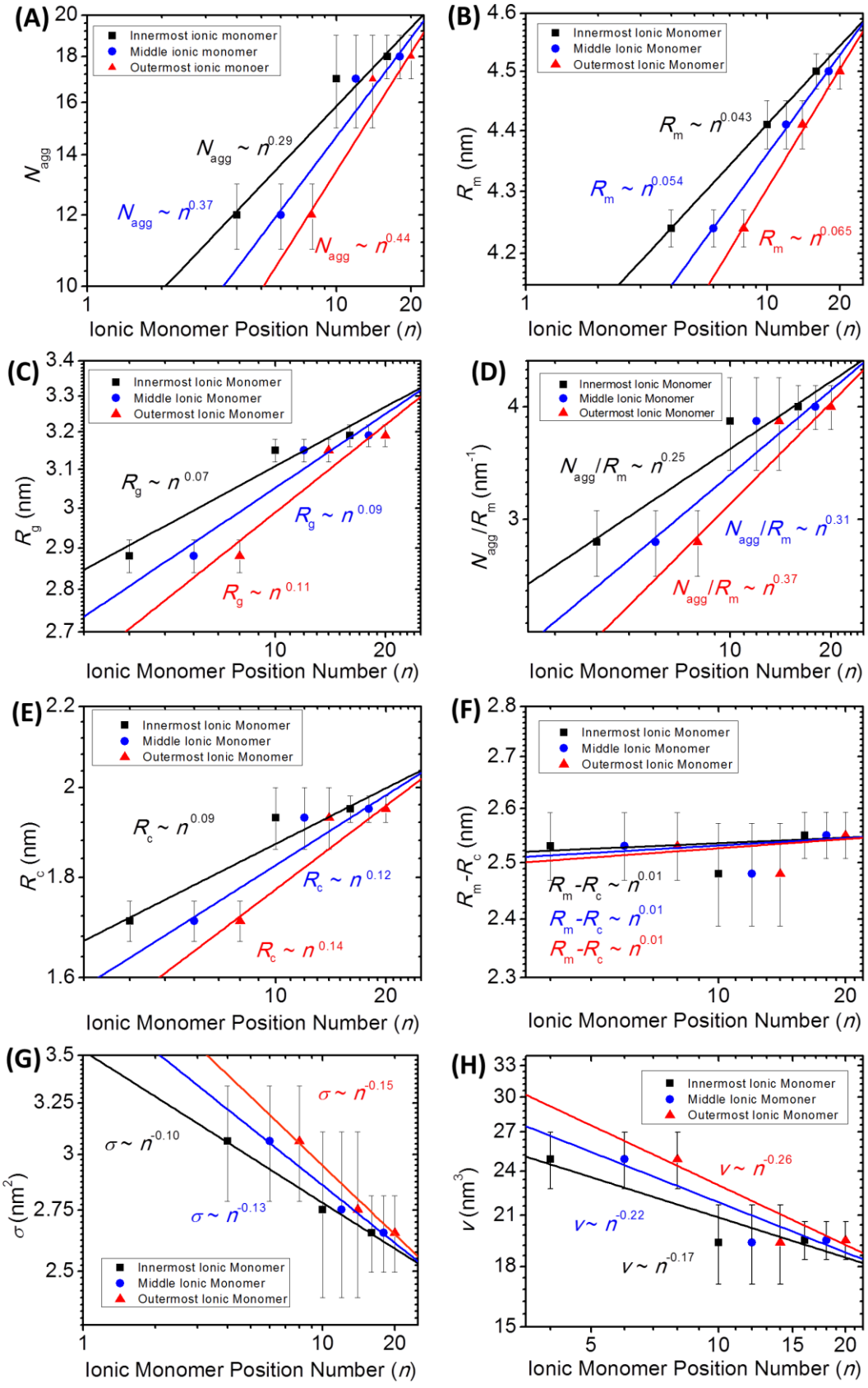
(A)
Innermost ionic monomer
Middle ionic monomer
Outermost ionic monoer
$N_{agg} \sim n^{0.29}$
$N_{agg} \sim n^{0.37}$
$N_{agg} \sim n^{0.44}$
N_{agg}
Ionic Monomer Position Number (n)
(B)
Innermost Ionic Monomer
Middle Ionic Monomer
Outermost Ionic Monomer
$R_m \sim n^{0.043}$
$R_m \sim n^{0.054}$
$R_m \sim n^{0.065}$
R_m (nm)
Ionic Monomer Position Number (n)
(C)
Innermost Ionic Monomer
Middle Ionic Monomer
Outermost Ionic Monomer
$R_g \sim n^{0.07}$
$R_g \sim n^{0.09}$
$R_g \sim n^{0.11}$
R_g (nm)
Ionic Monomer Position Number (n)
(D)
Innermost Ionic Monomer
Middle Ionic Monomer
Outermost Ionic Monomer
$N_{agg}/R_m \sim n^{0.25}$
$N_{agg}/R_m \sim n^{0.31}$
$N_{agg}/R_m \sim n^{0.37}$
N_{agg}/R_m (nm^{-1})
Ionic Monomer Position Number (n)
(E)
Innermost Ionic Monomer
Middle Ionic Monomer
Outermost Ionic Monomer
$R_c \sim n^{0.09}$
$R_c \sim n^{0.12}$
$R_c \sim n^{0.14}$
R_c (nm)
Ionic Monomer Position Number (n)
(F)
Innermost Ionic Monomer
Middle Ionic Monomer
Outermost Ionic Monomer
R_m-$R_c \sim n^{0.01}$
R_m-$R_c \sim n^{0.01}$
R_m-$R_c \sim n^{0.01}$
R_m-R_c (nm)
Ionic Monomer Position Number (n)
(G)
$\sigma \sim n^{-0.15}$
$\sigma \sim n^{-0.10}$
$\sigma \sim n^{-0.13}$
Innermost Ionic Monomer
Middle Ionic Monomer
Outermost Ionic Monomer
σ (nm^2)
Ionic Monomer Position Number (n)
(H)
Innermost Ionic Monomer
Middle Ionic Momoner
Outermost Ionic Monomer
$v \sim n^{-0.26}$
$v \sim n^{-0.22}$
$v \sim n^{-0.17}$
v (nm^3)
Ionic Monomer Position Number (n)

Figure S2.11. (A) Plots of the aggregation number (N_{agg}), (B) the micellar radius (R_m), (C) the radius of gyration (R_g) of the micelles, (D) the N_{agg}/R_m ratio, (E) the micellar core radius (R_c), (F) the micellar corona size (R_m-R_c), (G) the core-corona interfacial area per polymer chain (σ) and (H) the corona volume occupied per polymer chain (v) versus the ionic monomer position number (n) for the triply charged peptoid block copolymer series. The position number is defined as the ionic monomer number along the hydrophilic segment counted by starting from the junction of the hydrophilic and hydrophobic segments. For the triply charged series, the position number is considered for the ionic monomer at either the innermost (■), middle (●) or outermost position (▲) away from the junction of the hydrophilic and hydrophobic segments.

APPENDIX C. SUPPLEMENTAL INFORMATION FOR CHAPTER 3

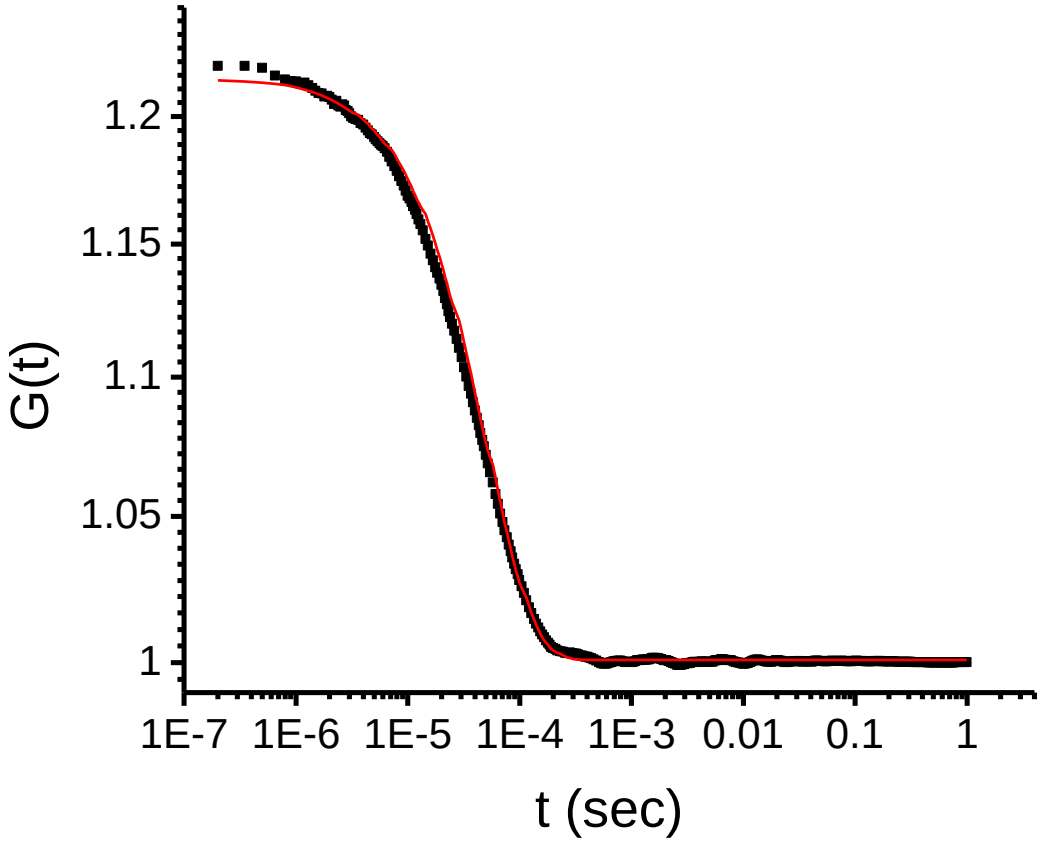

Figure S3.1. Representative correlation function from dynamic light scattering measurement of sequence defined ionic peptoid block copolymer. Experimental data is plotted in black, with the cumulants fitting in red.

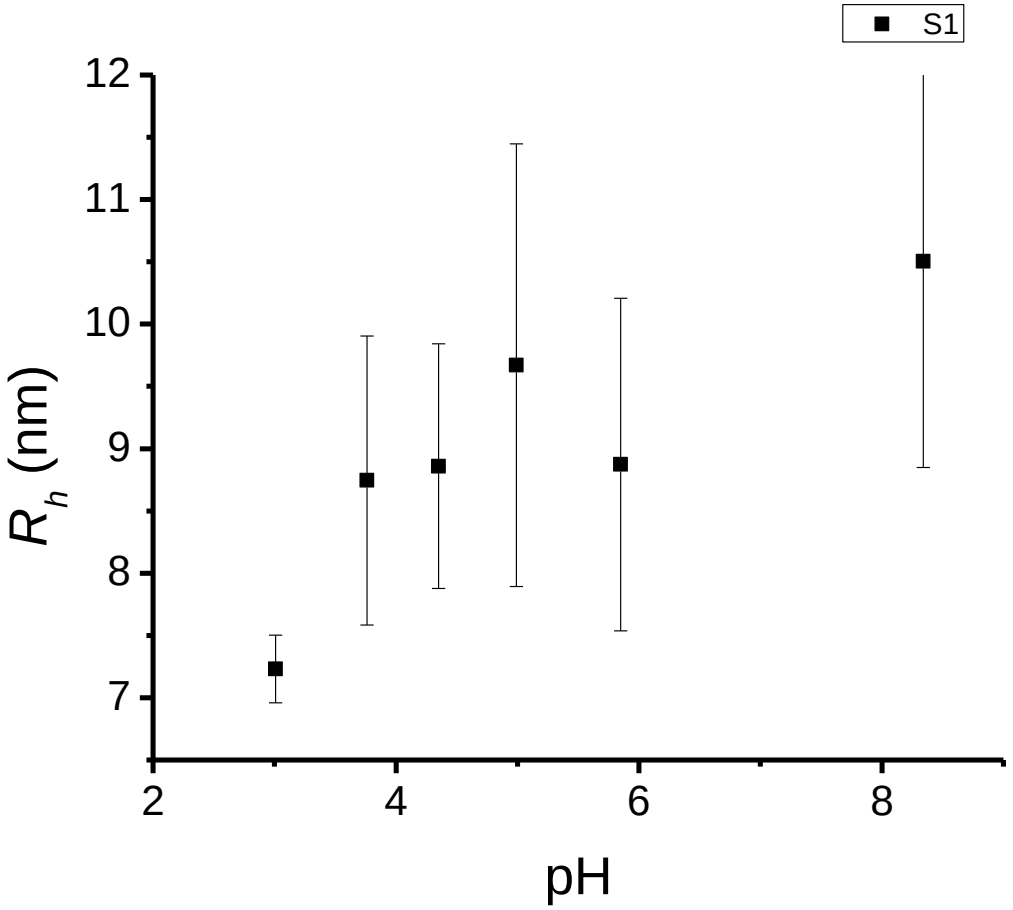

Figure S3.2. Plot of R_h vs solution pH for sample 1.

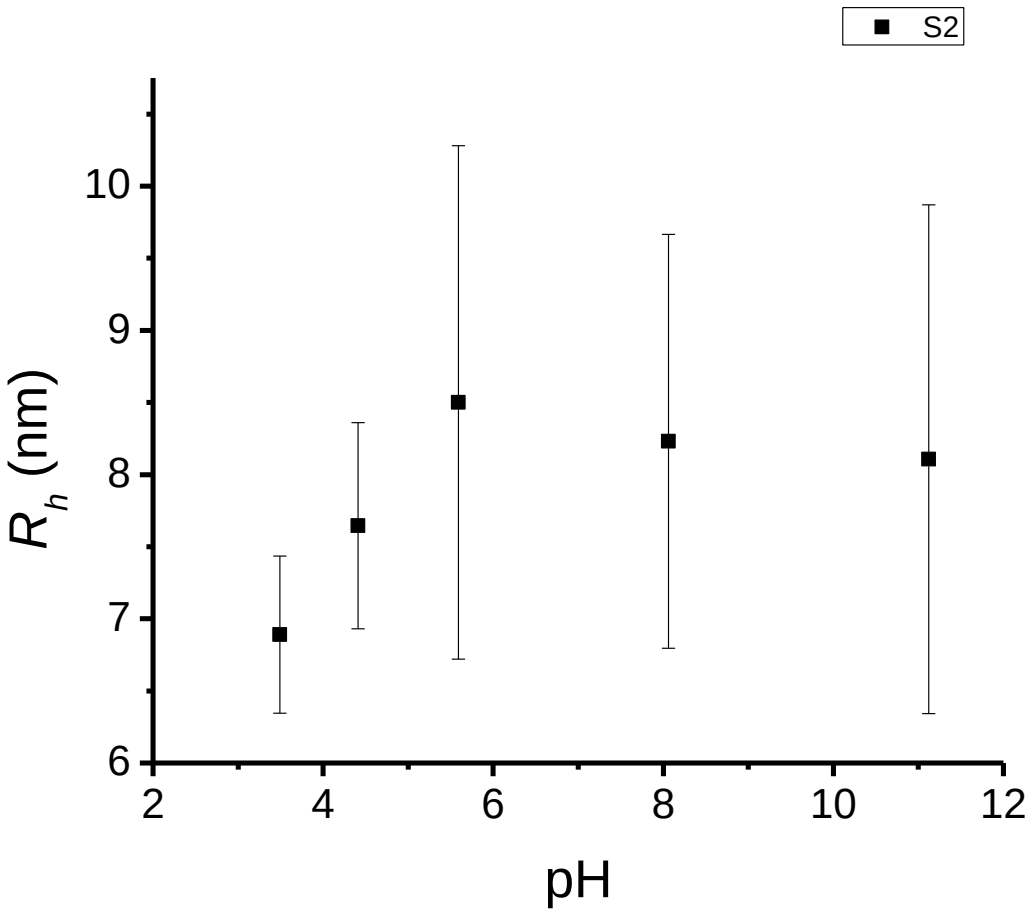

Figure S3.3. Plot of R_h vs solution pH for sample 2.

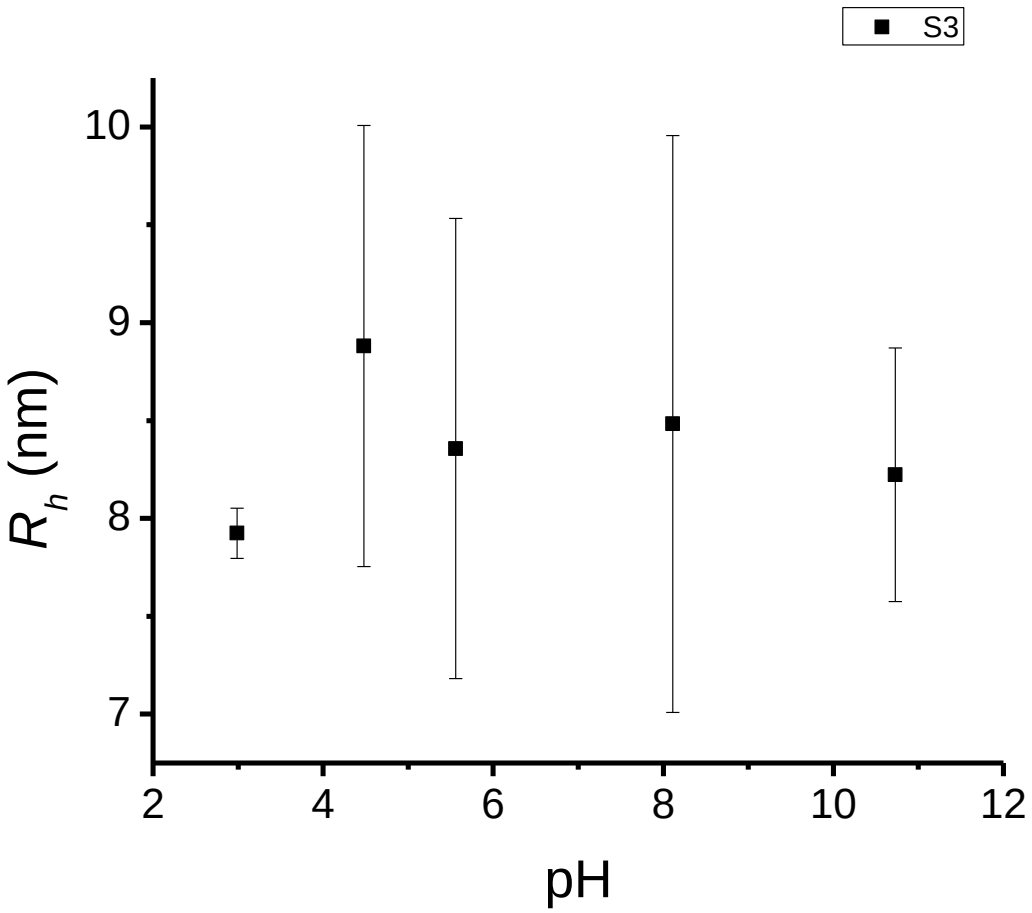

Figure S3.4. Plot of R_h vs solution pH for sample 3.

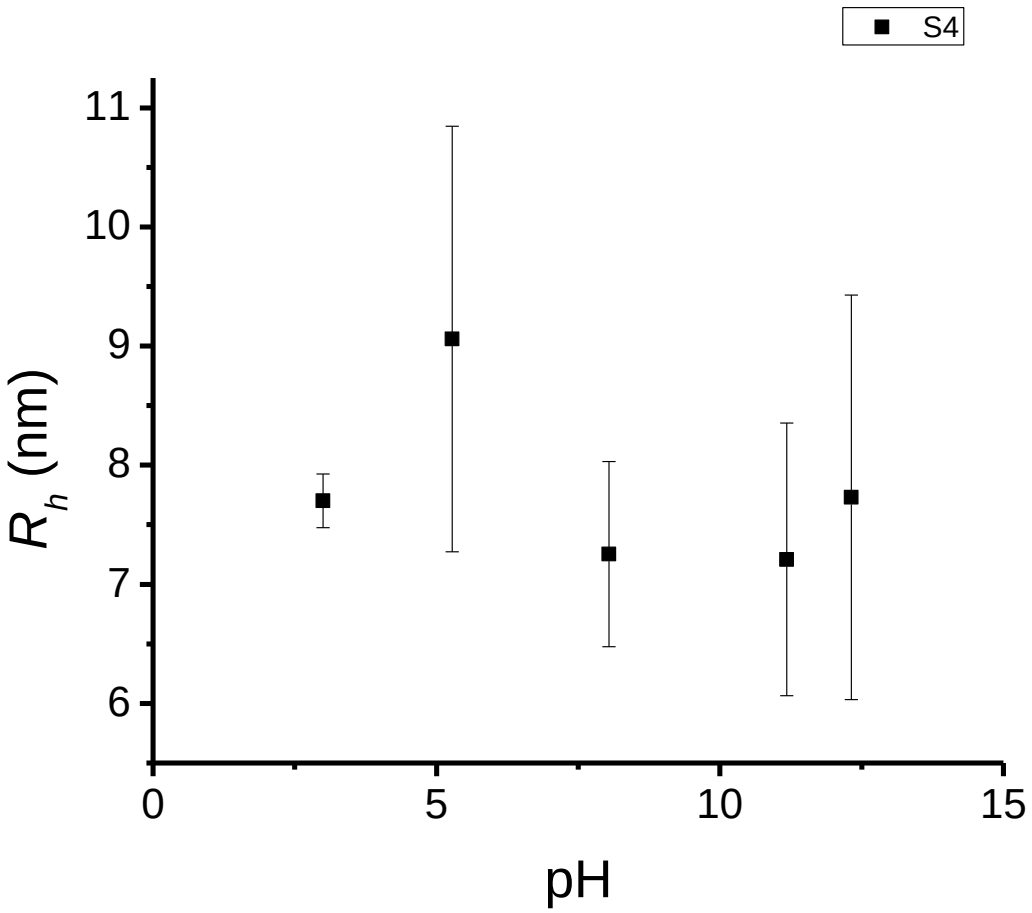

Figure S3.5. Plot of R_h vs solution pH for sample 4.

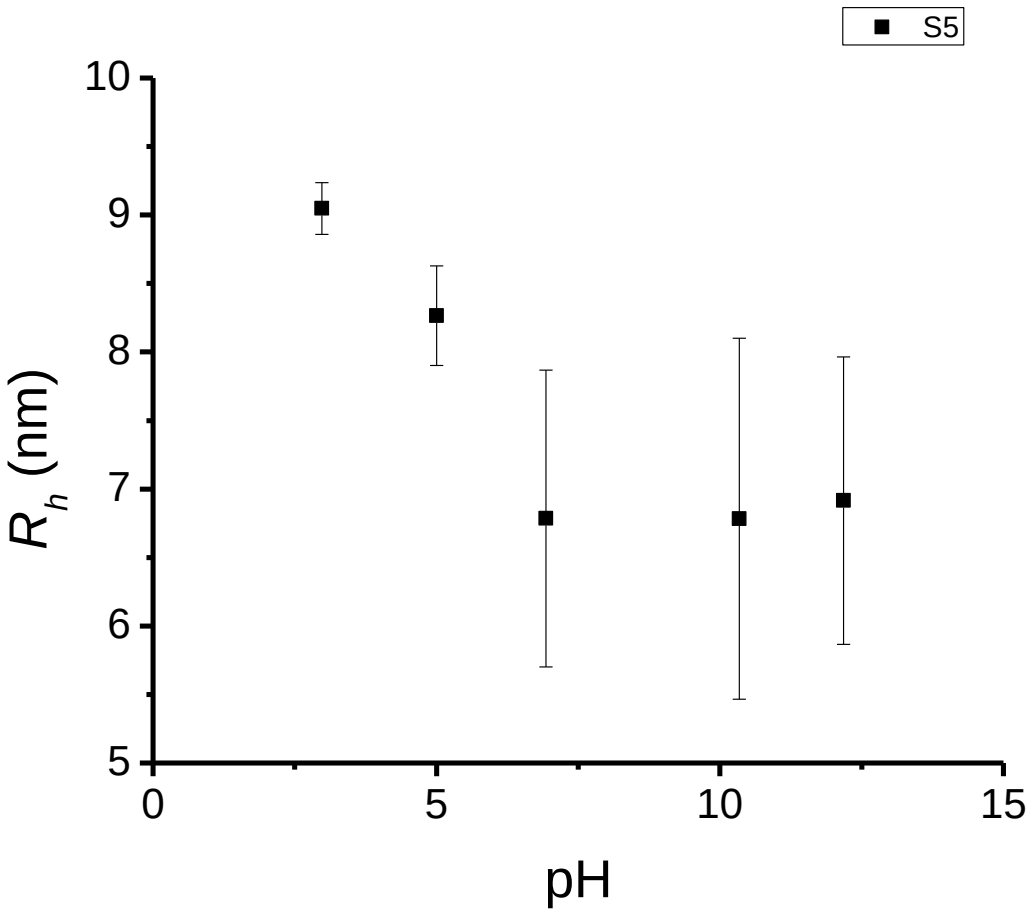

Figure S3.6. Plot of R_h vs solution pH for sample 5.

Table S3.1. Measured pH and R_h values for sequence-defined ionic peptoid block copolymers (Figure 3.2) in aqueous solution.

Sequence #	pH	R_h (nm)	error (nm)	Sequence #	pH	R_h (nm)	error (nm)
1	3.01	7.2	0.3				
	3.76	8.7	1.2				
	4.35	8.9	1.0				
	4.99	9.7	1.8				
	5.85	8.9	1.3				
	8.34	10.5	1.7				
2	3.49	6.9	0.5	4	3.00	7.7	0.2
	4.41	7.6	0.7		5.28	9.1	1.8
	5.59	8.5	1.8		8.04	7.3	0.8
	8.06	8.2	1.4		11.18	7.2	1.1
	11.12	8.1	1.8		12.32	7.7	1.7
3	2.99	7.9	0.1	5	2.98	9.0	0.2
	4.48	8.9	1.1		5.00	8.3	0.4
	5.56	8.4	1.2		6.93	6.8	1.1
	8.11	8.5	1.5		10.34	6.8	1.3
	10.73	8.2	0.6		12.18	6.9	1.0

APPENDIX D. SUPPLEMENTAL INFORMATION FOR CHAPTER 4

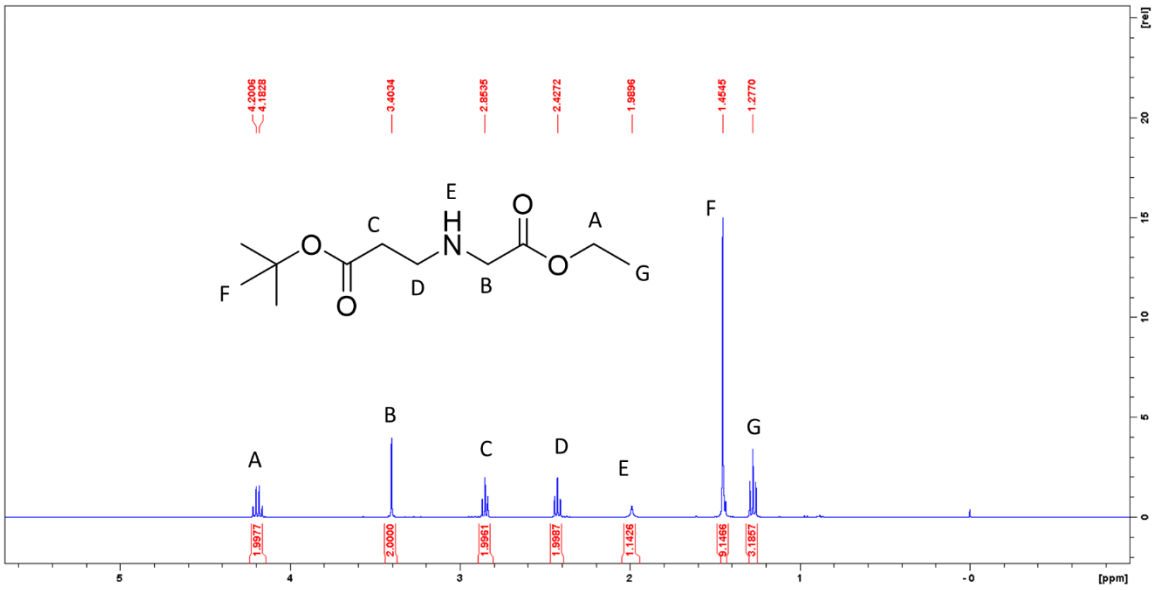

Figure S4.1. ^{1}H NMR spectrum of compound **1**.

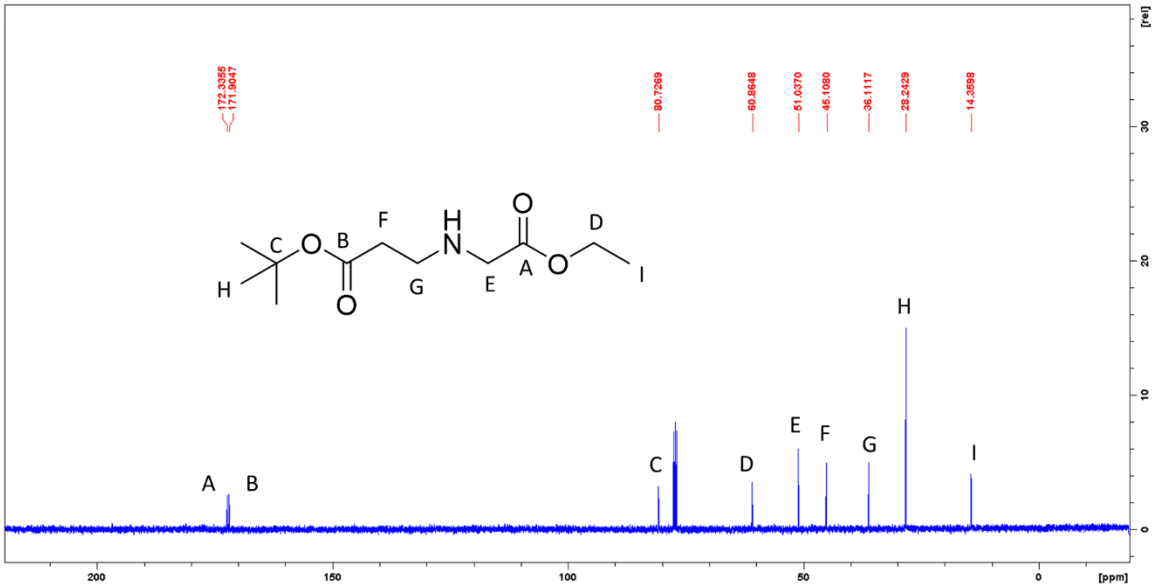

Figure S4.2. ^{13}C NMR spectrum of compound **1** in $CDCl_3$.

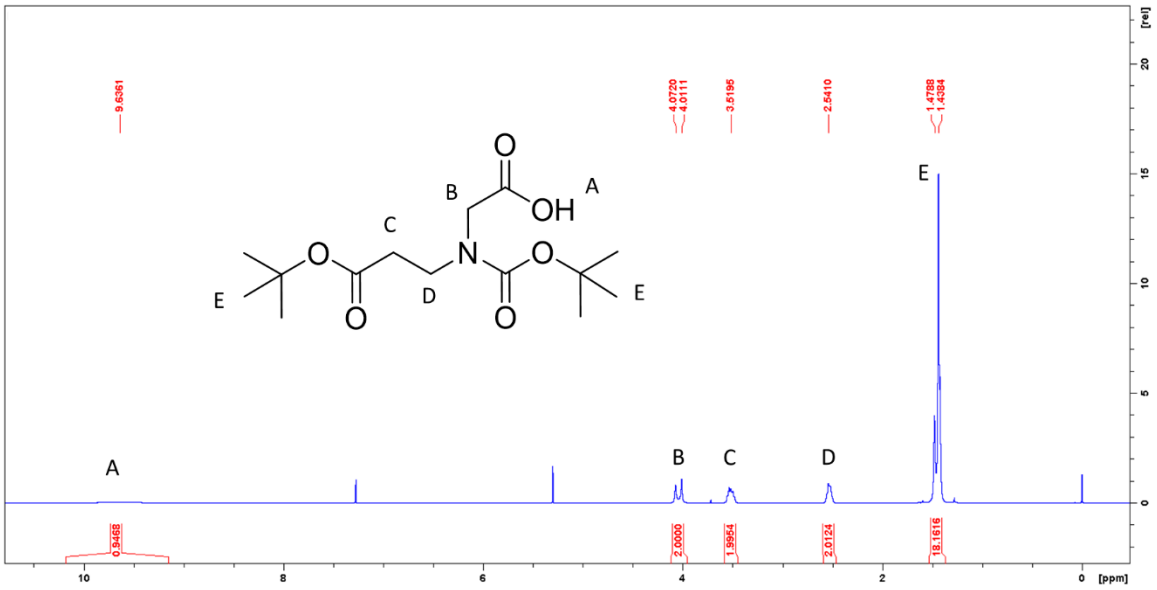

Figure S4.3. ^{1}H NMR spectrum of compound **2** in $CDCl_3$.

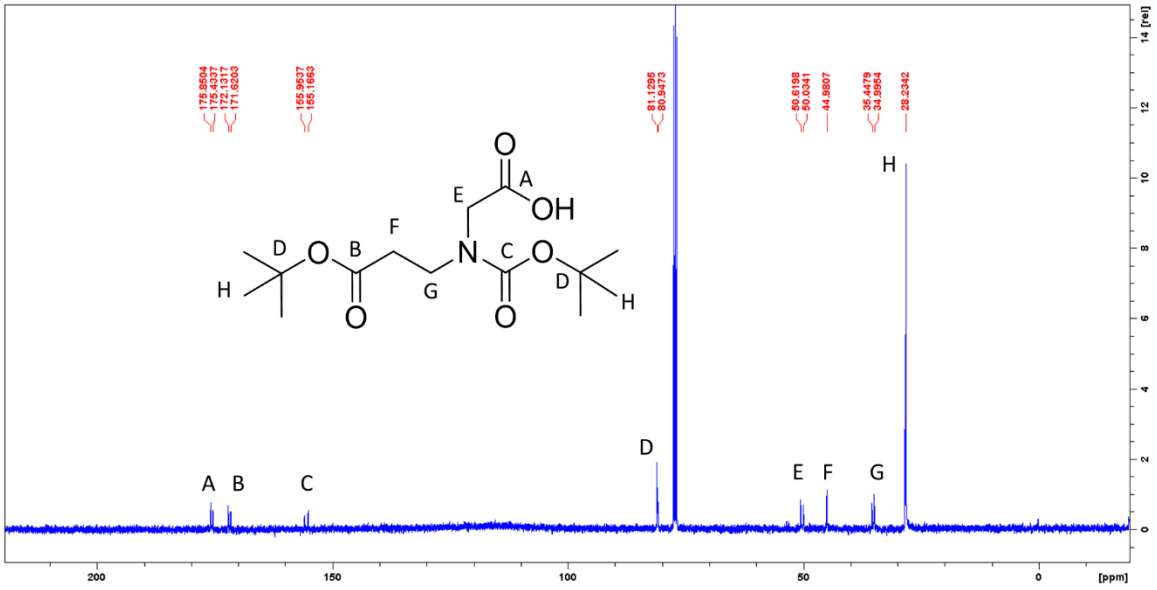

Figure S4.4. ^{13}C NMR spectrum of compound **2** in $CDCl_3$.

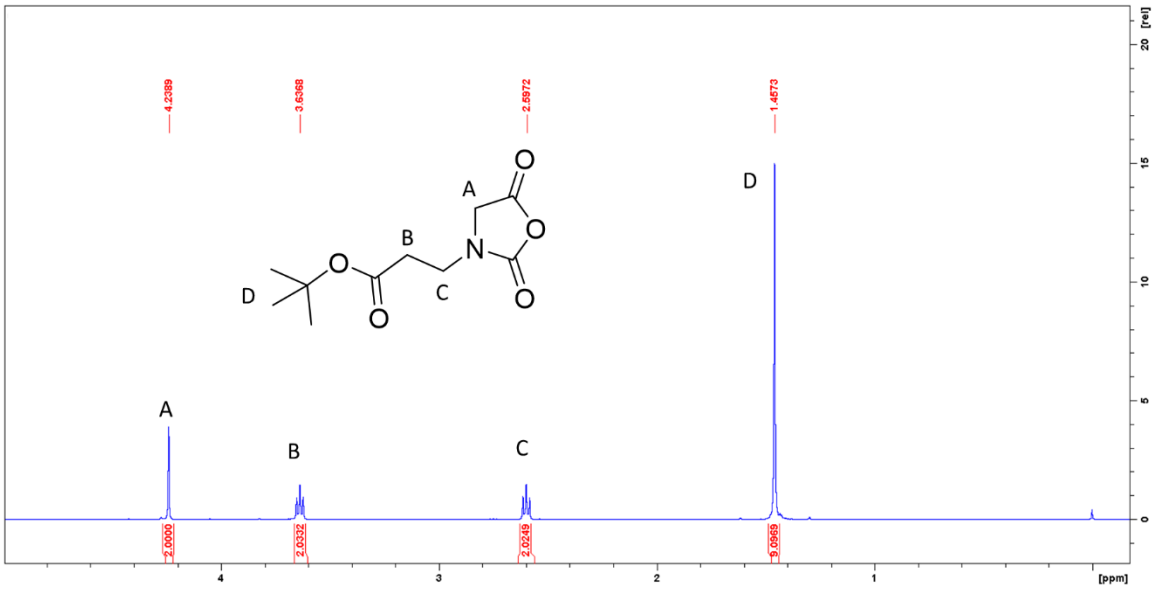

Figure S4.5. ^{1}H NMR of compound **M1** in $CDCl_3$.

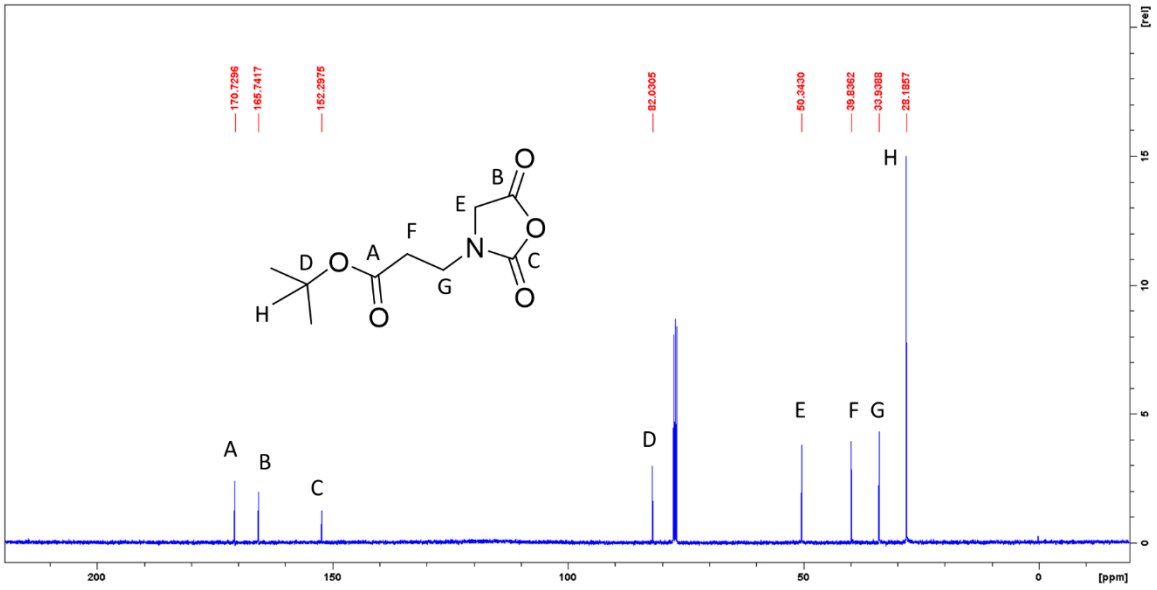

Figure S4.6. ^{13}C NMR spectrum of compound **M1** in $CDCl_3$.

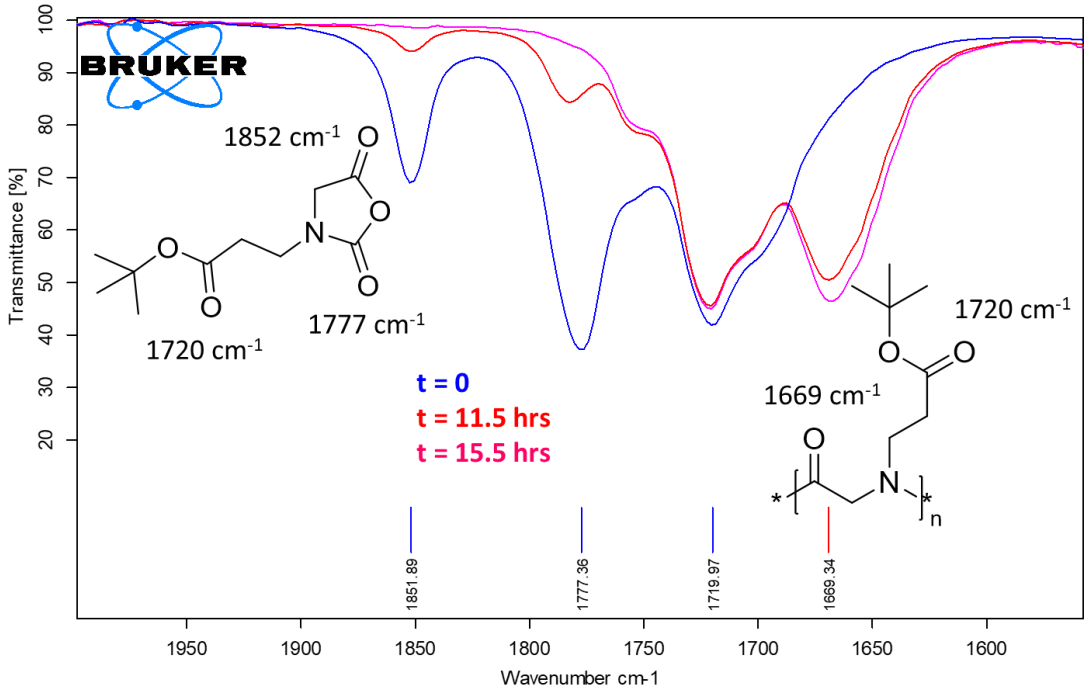

Figure S4.7. Polymerization of COE-NCA tracked by FTIR spectroscopy. I = benzylamine. M_o = 0.5 M, $[M]_o$:$[I]_o$ = 400:1.

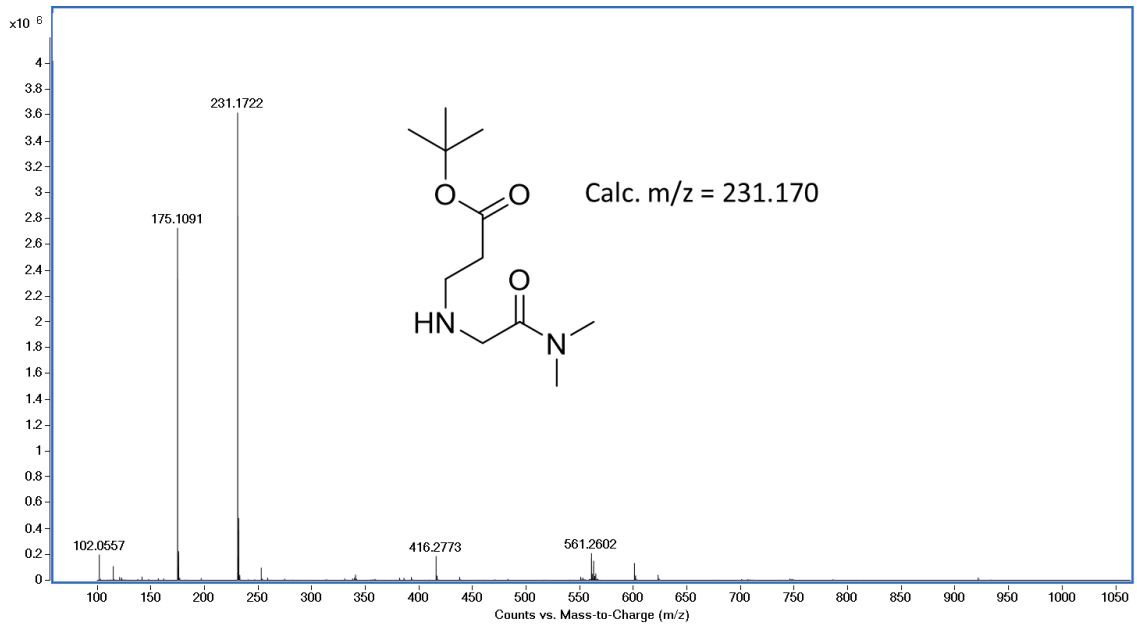

Figure S4.8. ESI-MS spectrum of tert-butyl 3-[[2-(dimethylamino)-2-oxoethyl]amino]propanoate **3**.

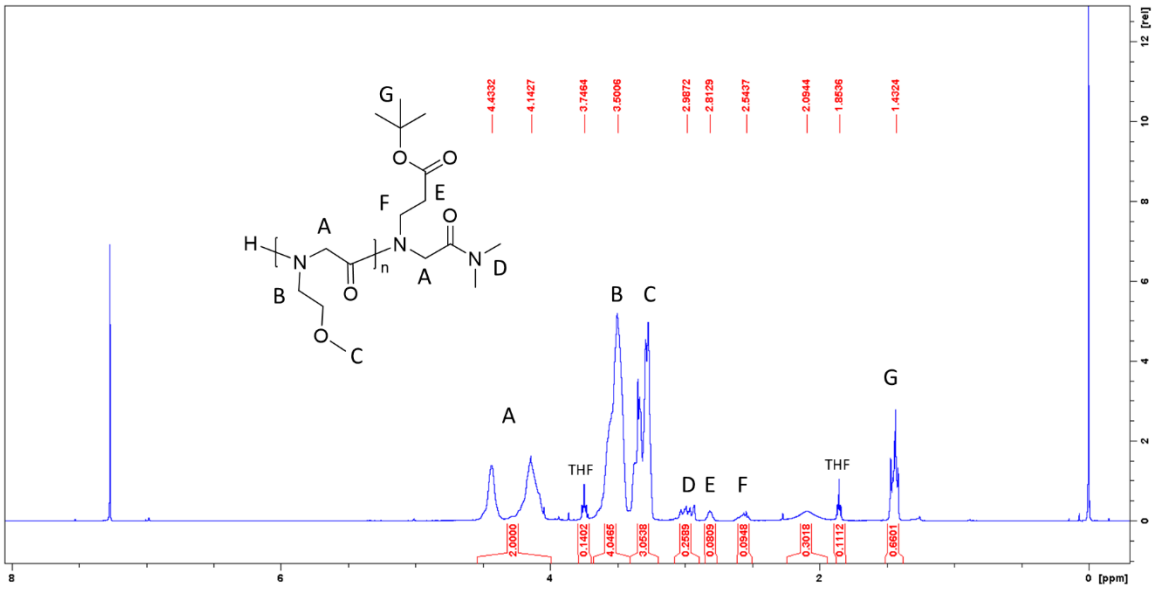

Figure S4.9. ^{1}H NMR spectrum of polymer **4** in $CDCl_3$.

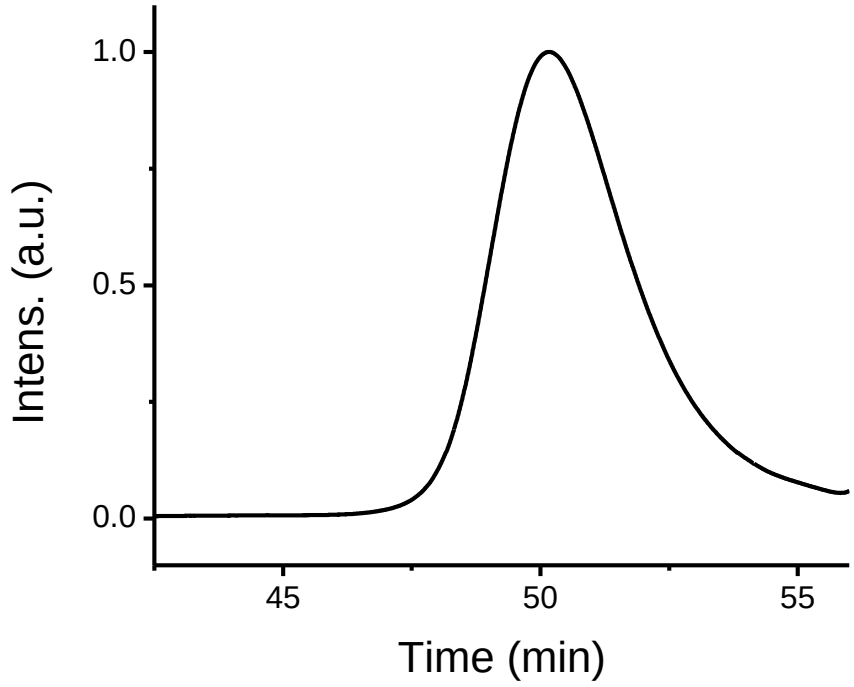

Figure S4.10. GPC chromatogram of polymer **4**.

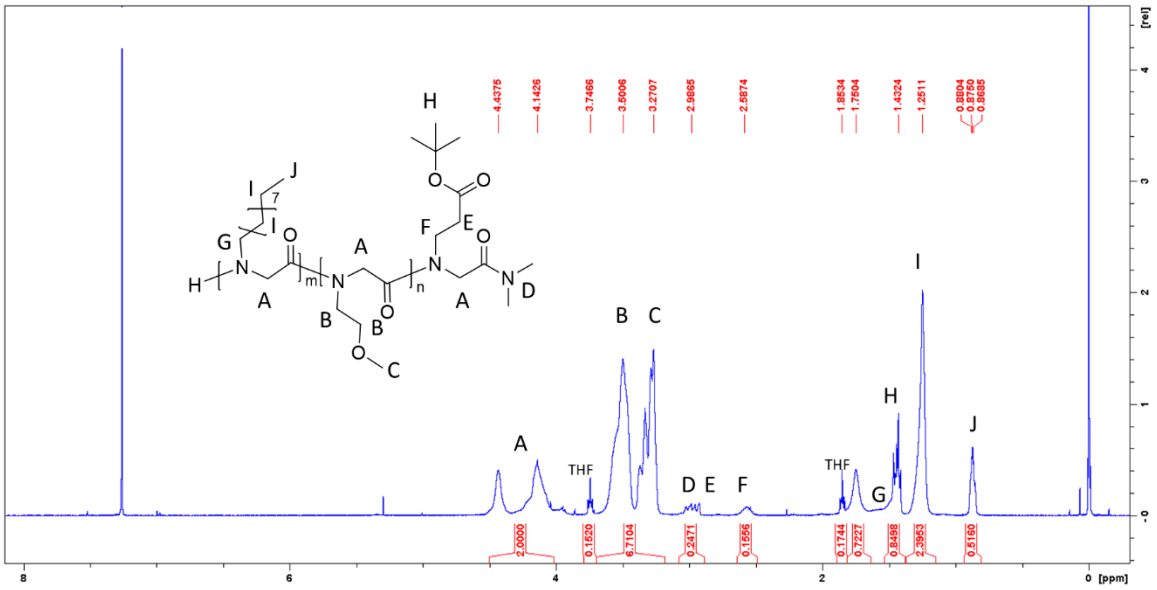

Figure S4.11. ^{1}H NMR spectrum of polymer **5** in $CDCl_3$.

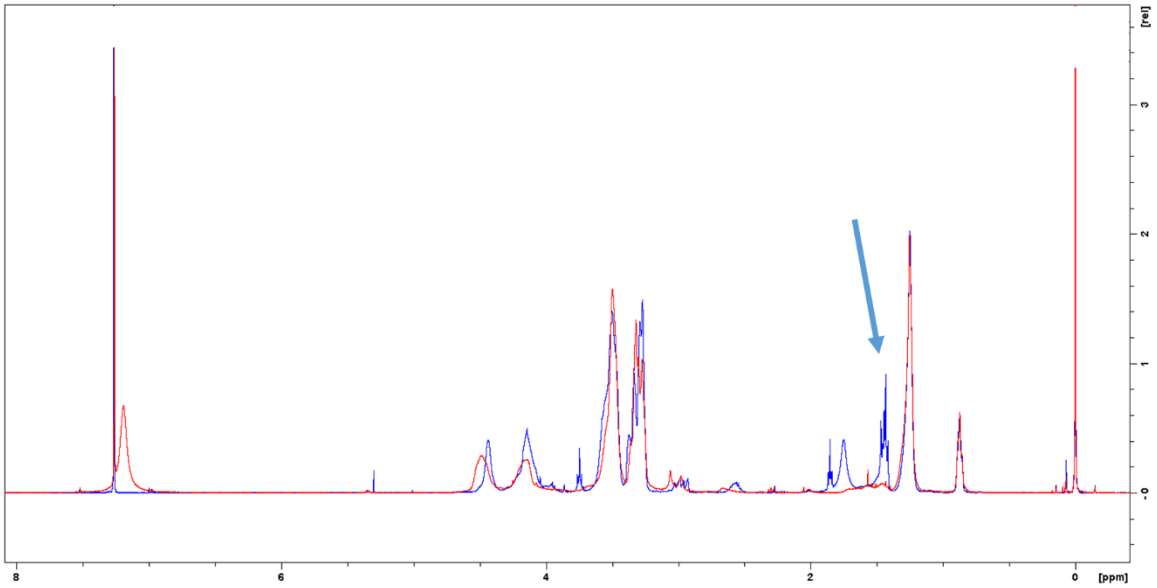

Figure S4.12. ^{1}H NMR spectra of polymer **5** in blue before treatment with TFA and polymer **6** in red after treatment with TFA, in $CDCl_3$.

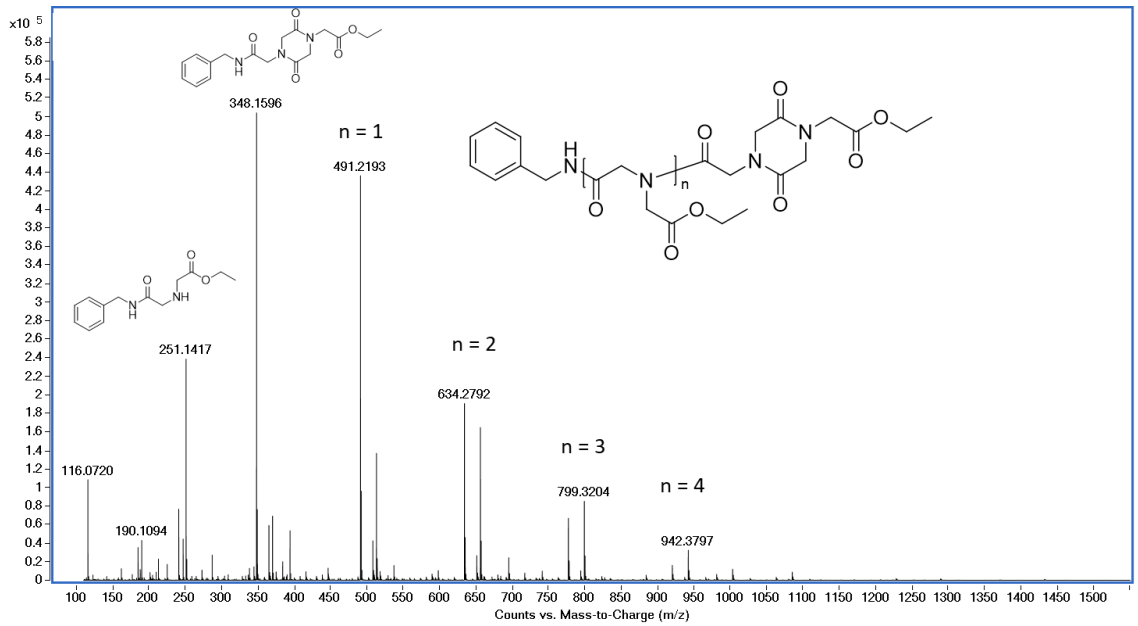

Figure S4.13. ESI-MS spectrum of observed diketopiperazine formation, terminating polymerization.

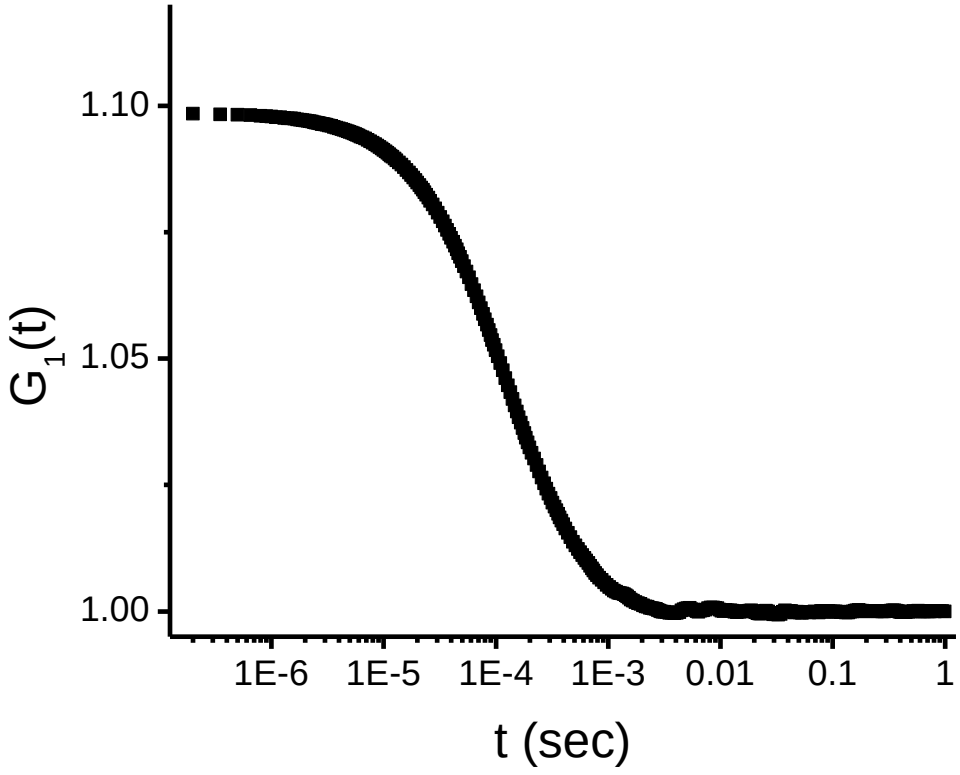

Figure S4.14. Correlation function measured for polymer **7** in water (0.5 wt%) at pH = 9. Cumulants fit showed R_h = 32±2 nm, R^2= 0.99.

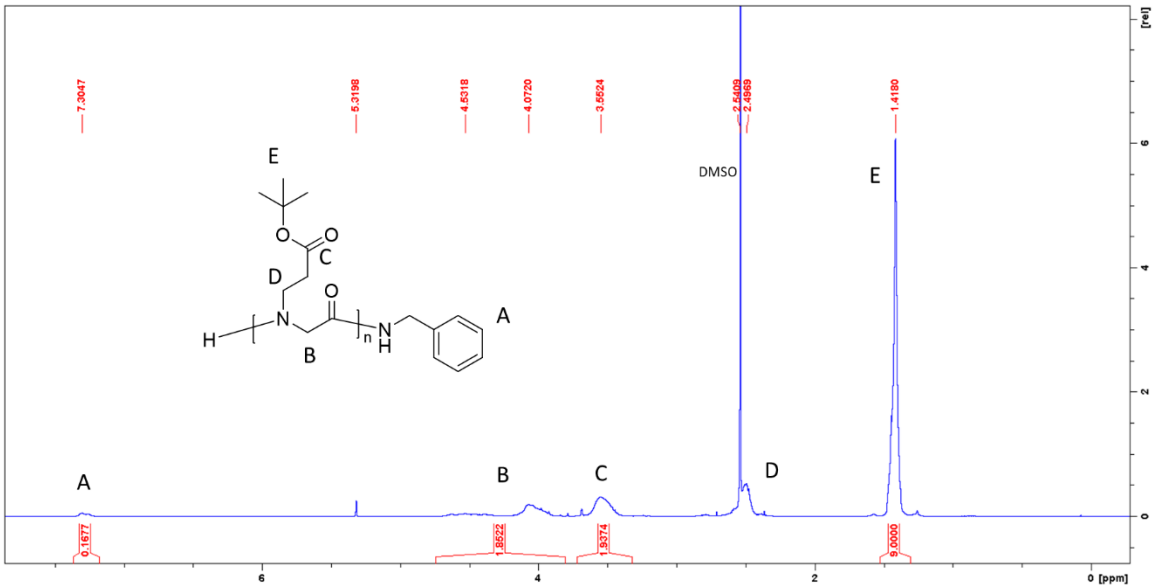

Figure S4.15. Representative ^{1}H-NMR of poly(N-2-t-butoxycarboxyethyl glycine) in CD_2Cl_2. Integration of end group phenyl protons at 7.18-7.37 ppm and the polymer sidechain t-butyl protons at 1.31-1.53 ppm yield a polymer DP = 29.8.

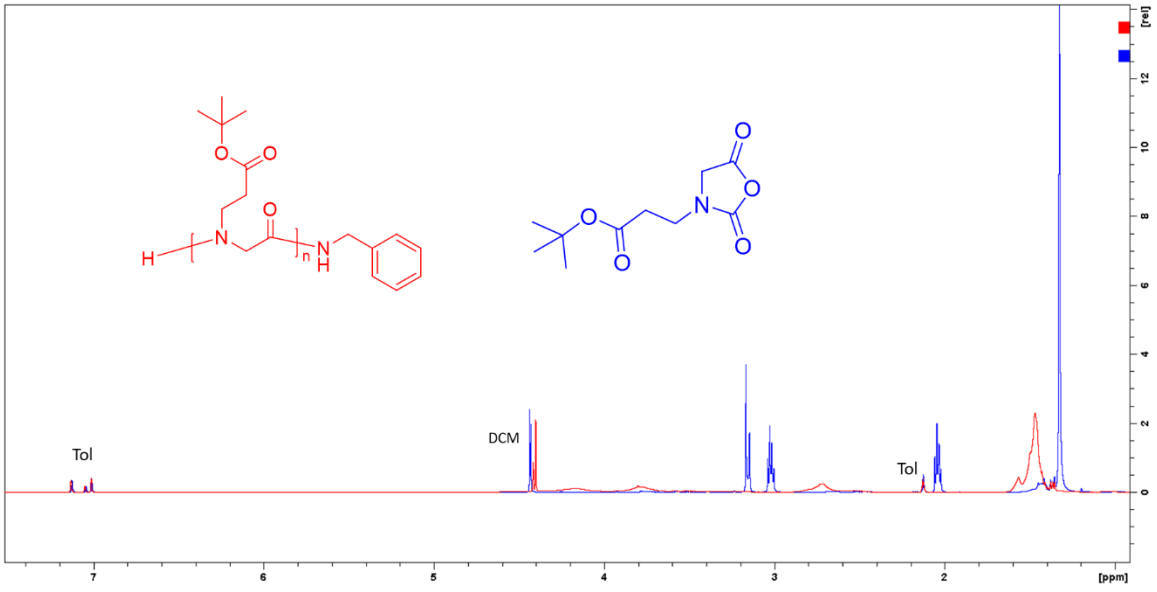

Figure S4.16. Representative 1H-NMR of kinetics measurement at 0.5 M in Tol-d8 and 23 °C. Initial spectrum at t= 2 min is shown in blue, with the final polymer spectrum in red. Conversion was calculated by integration of monomer peak (δ = 2.04 ppm) and comparison with the polymer (δ = 2.88-2.31 ppm).

VITA

Garrett Sternhagen was born and raised in Appleton, WI. He received his Bachelor of Science degree in Biochemistry and German from the University of Wisconsin – Stevens Point in 2012, where he pursued undergraduate research in polymer science under Professor John Droske. Garrett joined the research lab of Professor Donghui Zhang in 2013 to begin graduate research at Louisiana State University. His research interests include the relationship between material structure and function, and the synthesis of well-defined polymers. Garrett plans to graduate with his Ph.D. degree in Chemistry in December 2019.